Multiphysically Coupled Modelling of Polymer-based Materials

Vom Promotionsausschuss der
Technischen Universität Hamburg-Harburg
zur Erlangung des akademischen Grades
Doktor-Ingenieur (Dr.-Ing.)
genehmigte Dissertation

von
Jana Wilmers

aus
Bochum

2016

Gutachter der Dissertation:
Prof. Dr.-Ing. Swantje Bargmann, Technische Universität Hamburg-Harburg
Prof. Dr. (Tekn.) Ragnar Larsson, Chalmers University of Technology

Datum der Disputation: 23. November 2016

Vorsitzender des Prüfungsausschusses:
Prof. Dr.-Ing. Dr. h.c. Stefan Heinrich, Technische Universität Hamburg-Harburg

Acknowledgments

First of all, I thank my advisor Prof. Swantje Bargmann, not only for giving me the opportunity to work on this thesis as part of her group at the Helmholtz-Zentrum Geesthacht but especially for her invaluable support and guidance over the past four years. I am incredibly grateful for her patience, motivation and the knowledge she shared in numerous discussions both directly on the research presented in this thesis as well as on all the "little" things related to it, from proposal writing to always keeping your priorities straight.

Furthermore, I want to thank Prof. Ragnar Larsson for agreeing to be the second reviewer of this thesis and his active interest in the topic and insightful questions. I also thank Prof. Stefan Heinrich for being chairman of the examination committee.

I'm grateful to past and present members of the Simulation of Solids and Structures group at HZG and the Institute of Continuum Mechanics and Material Mechanics at TUHH, especially Edgar Husser, Jan-Eike Schnabel, Konrad Schneider, Ingo Scheider and Dirk Steglich, and our colleagues of other groups at HZG for scientific discussions, advice and the best working climate one could wish for.

Special thanks is owed to Nadiia Mameka, Jürgen Markmann and Tobias Kitzler for countless discussions on (and explanations of) electrochemistry. Andrew McBride for help and guidance in implementing interface elasticity and him and Prof. Daya Reddy for a pleasant and productive stay at the University of Cape Town. Prof. Nobutada Ohno, Dai Okumura and Fumiko Asada for being incredibly gracious hosts at Nagoya University who made me feel welcome and taught me a lot.

Last but not least, I would like to thank friends and colleagues who all contributed to this thesis in their own way, from insights into computational mechanics over fuelling my caffeine addiction to preventing me from ending this whole endeavour in a climbing accident long before submission. Baran, Benjamin, Dirk, Edgar, Fredie, Henry, Ingo, Jan, Jeong-Yun, Jürgen, Kaixiong, Katrin, Konrad, Lars, Mamun, Michi, Nadiia, Nam, Natalia, Nora, Paul, Paula, Sebastian, Sebastian, Shan, Songyun, Tobias, Xiaowei, thank you for making the my four years in Geesthacht so enjoyable in and outside the office.

Multiphysically Coupled Modelling of Polymer-based Materials

Jana Wilmers

Abstract

The multiphysically coupled modelling and numerical simulation of mass transport in polymeric materials is investigated. Coupled behaviour arises in these materials due to molecular interactions of the polymer chains with the transported particles or fluids. Due to these interactions, mass transport in polymers is often associated with large deformations and significant changes of the mechanical behaviour that, in turn, may lead to cracking and failure. On the other hand, this behaviour can be utilised deliberately, for example for microstructuring or in smart materials. Thus, a detailed understanding of the processes involved is necessary.

In this thesis, a model for multiphysically coupled mass transport in the framework of nonlinear continuum mechanics is developed. The governing equations describing two different example cases, namely, anomalous Case II diffusion and electroactive polymers, are derived from fundamental balance principles and equipped with suitable constitutive equations. For the description of Case II diffusion, a novel relation for the diffusion flux is developed that accounts for the delayed kinetics resulting from the molecular interactions and, thus, allows to describe the characteristic transport behaviour during Case II diffusion. To accurately model the processes occurring in composites of nanoporous metals filled with different types of electroactive polymers, the interface elasticity theory is extended to chemoelectromechanical coupling, yielding a framework that allows to describe deformation, electrostatics and charge carrier transport and their interactions in the bulk material and on the metal/polymer interface.

These models are subsequently implemented into a finite element code and numerical studies are carried out to elucidate the models' capabilities and provide insight into the coupled nature of the investigated phenomena.

Multiphysikalisch gekoppelte Modellierung von Polymer-Materialien

Zusammenfassung

In dieser Arbeit werden die multiphysikalisch gekopplete Modellierung und numerische Simulation von Massentransportphänomenen in Polymer-Materialien untersucht. In diesen Materialien tritt gekoppeltes Verhalten aufgrund von molekularen Wechselwirkungen zwischen den Polymerketten und den transportierten Partikeln oder Fluiden auf. Aufgrund dieser Wechselwirkungen geht Massentransport in Polymeren häufig mit großen Deformationen und signifikanten Änderungen des mechanischen Verhaltens einher, die wiederum zur Bildung von Rissen und zum Materialversagen führen können. Andererseits ist es möglich dieses gekoppelte Verhalten bewusst auszunutzen, zum Beispiel in der Mikrostrukturierung oder in so genannten Intelligenten Werkstoffen. Daher ist es wichtig, ein tiefes Verständnis der grundlegenden Prozesse zu erlangen.

In der vorliegenden Arbeit wird ein kontinuumsmechanisches Modell für multiphysikalisch gekoppelten Massentransport entwickelt. Die grundlegenden Gleichungen, die das Verhalten von zwei ausgesuchten Beispielfällen, nämlich Case II-Diffusion und elektroaktiven Polymeren, beschreiben, werden dabei aus physikalischen Bilanzen abgeleitet und mit geeigneten Konstitutivgleichungen ergänzt. Zur Beschreibung der anormalen Case II-Diffusion wird ein neuartiges Diffusionsgesetz hergeleitet, das die verzögerte Transportkinetik, die aus den molekularen Wechselwirkungen resultiert, berücksichtigt und es so ermöglicht, das charakteristische Verhalten der Case II diffusion zu beschreiben. Um die Prozesse, die in Kompositen von nanoporösen Metallen mit elektroaktiven Polymeren ablaufen, abzubilden, wird die Grenzflächenelastizitätstheorie auf chemoelektromechanische Kopplung erweitert. So wird ein grundlegendes Modell entwickelt, das es erlaubt, Deformation, Elektrostatik, Ladungsträgertransport und ihre Interaktionen sowohl im Volumen als auch auf der Metall/Polymer-Grenzfläche zu beschreiben. Diese Modelle werden weiterhin in einen Finite Elemente-Code implementiert, mit dem numerische Studien durchgeführt werden, um die Möglichkeiten der entwickelten Modelle zu untersuchen und Einsichten in die gekoppelte Natur der untersuchten Phänomene zu erlangen.

Contents

List of Figures

List of Tables

Nomenclature

Continuum mechanics

α	thermal expansion coefficient	[1/K]
$\boldsymbol{n}$,$\boldsymbol{N}$	normal vectors to the surfaces $\partial\Omega$ and $\partial\Omega_0$, respectively	[–]
$\boldsymbol{v}$	velocity	[m/s]
δ	variation of the diffusion coefficient with concentration	
K	thermal conductivity	[W/(m · K)]
$\boldsymbol{b}$	specific body force vector	[N/kg]
$\mathcal{B}, \mathcal{B}_0$	body in the current and reference configuration, respectively	
$\boldsymbol{F}$	deformation gradient $\boldsymbol{F}(\boldsymbol{X}, t) := \mathrm{Grad}\, \boldsymbol{\varphi}(\boldsymbol{X}, t)$	[–]
$\boldsymbol{C}$	right Cauchy-Green deformation tensor $\boldsymbol{C} = \boldsymbol{F}^T \cdot \boldsymbol{F}$	[–]
$\overset{3}{\boldsymbol{\varepsilon}}$	Levi-Civita symbol	
$\boldsymbol{\sigma}$	Cauchy stress tensor	[Pa]
η	specific entropy	[J/K]
$\mathcal{E}$	total energy of a system	[J]
ε	specific internal energy	[J/kg]
Γ_0	dissipation density	[W/(K · m^3)]
J	Jacobi determinant $J = \det \boldsymbol{F}$	[–]
Ω, Ω_0	control volume in the current and reference configuration, respectively	
$\boldsymbol{\varphi}$	motion mapping between configurations	
$\boldsymbol{P}$	first Piola-Kirchhoff stress tensor	[Pa]
$\boldsymbol{Q}$	heat flux	[W/m^2]
ρ,ρ_0	mass density with respect to the current and reference configuration, respectively	[kg/m^3]
r	specific heat supply	[W/kg]
T	absolute temperature	[K]
t	time	[s]
$\boldsymbol{u}$	displacement vector	[m]
$\boldsymbol{x}, \boldsymbol{X}$	position vector in the current and reference configuration, respectively	[m]

Diffusion

β	ratio of Young's moduli of glassy and rubber-like polymer	[–]
χ^{FH}	Flory-Huggins interaction parameter	[–]
C_p	specific heat capacity	[J/(kg · K)]
c_0	concentration with respect to the reference configuration	[kg/m^3]
c_0^{eq}	equilibrium concentration with respect to the reference configuration	[kg/m^3]
De	Deborah number	[–]

$\boldsymbol{D}$	diffusion coefficient	$[\mathrm{m}^2/\mathrm{s}]$
η	specific entropy	$[\mathrm{J}/(\mathrm{kg}\cdot\mathrm{K})]$
η^{mix}	specific entropy of mixing	$[\mathrm{J}/(\mathrm{kg}\cdot\mathrm{K})]$
ε	specific enthalpy	$[\mathrm{J}/\mathrm{kg}]$
φ^{mix}	specific enthalpy of mixing	$[\mathrm{J}/\mathrm{kg}]$
E_A	activation energy	$[\mathrm{J}/\mathrm{mol}]$
ΔG^{mix}	specific Gibbs energy of mixing	$[\mathrm{J}/\mathrm{kg}]$
$\boldsymbol{H}_{\mathrm{eff}}$	combined contribution of diffusion and heat flux to system's entropy	$[\mathrm{W}/(\mathrm{K}\cdot\mathrm{m}^2)]$
ΔH^{mix}	specific enthalpy of mixing	$[\mathrm{J}/\mathrm{kg}]$
H_{eff}	combined sources of entropy from diffusion and heat	$[\mathrm{W}/(\mathrm{K}\cdot\mathrm{m}^3)]$
$\boldsymbol{J}$	diffusion flux with respect to the reference configuration	$[\mathrm{kg}/(\mathrm{m}^2\cdot\mathrm{s})]$
k_B	Boltzmann constant, $k_B = 1.380649\cdot 10^{-23}$ J/K	$[\mathrm{J}/\mathrm{K}]$
λ	Lamé parameter	$[\mathrm{Pa}]$
μ	Lamé parameter	$[\mathrm{Pa}]$
μ^{mix}	specific chemical potential of the mixture	$[\mathrm{J}/\mathrm{kg}]$
m	mass	$[\mathrm{kg}]$
ν_s	volume fraction of solvent	$[-]$
n	number of chain segments per polymer molecule	$[-]$
N_p	number of polymer molecules	$[-]$
N_s	number of solvent molecules	$[-]$
ψ	specific Helmholtz free energy	$[\mathrm{J}/\mathrm{kg}]$
$\boldsymbol{Q}_{\mathrm{eff}}$	combined contribution of diffusion and heat flux to internal energy	$[\mathrm{W}/\mathrm{m}^2]$
Q_{eff}	combined contribution of mass and heat sources to internal energy	$[\mathrm{W}/\mathrm{m}^2]$
ρ_0^s	mass density of the solvent with respect to the reference configuration	$[\mathrm{kg}/\mathrm{m}^3]$
R	gas constant, $R = 8.3144598$ J/(mol · K)	$[\mathrm{J}/(\mathrm{mol}\cdot\mathrm{K})]$
ΔS^{mix}	specific enthropy of mixing	$[\mathrm{J}/(\mathrm{kg}\cdot\mathrm{K})]$
τ	relaxation time	$[\mathrm{s}]$
τ_c	relaxation time for the concentration	$[\mathrm{s}]$
τ_j	relaxation time for the diffusion flux	$[\mathrm{s}]$
T_g	glass transition temperature	$[\mathrm{K}]$
V_0	reference volume	$[\mathrm{m}^3]$
W	mass source density	$[\mathrm{kg}/(\mathrm{m}^2\cdot\mathrm{s})]$

Electroelasticity

$\boldsymbol{d}, \boldsymbol{D}$	current and nominal electric displacement field vector	$[\mathrm{C}/\mathrm{m}^2]$
$\boldsymbol{b}, \boldsymbol{B}$	current and nominal magnetic induction field vector	$[\mathrm{V}\cdot\mathrm{s}/\mathrm{m}^2]$
$\boldsymbol{e}, \boldsymbol{E}$	current and nominal electric field vector	$[\mathrm{V}/\mathrm{m}]$
$\boldsymbol{h}, \boldsymbol{H}$	current and nominal magnetic field vector	$[\mathrm{C}/(\mathrm{s}\cdot\mathrm{m})]$
$\boldsymbol{m}, \boldsymbol{M}$	current and nominal magnetisation vector	$[\mathrm{C}/(\mathrm{s}\cdot\mathrm{m})]$
$\boldsymbol{p}, \boldsymbol{P}$	current and nominal electric polarisation vector	$[\mathrm{C}/\mathrm{m}^2]$
c_0^i	concentration of species i with respect to reference configuration	$[\mathrm{mol}/\mathrm{m}^3]$

ε_0	vacuum permittivity, $\varepsilon_0 = 8.854188 \cdot 10^{-12}$ F/m	[F/m]
ε_r	relative permittivity	[−]
F	Faraday constant, $F = 96,485.33$ C/mol	[C/mol]
$\boldsymbol{i}, \boldsymbol{I}$	flux of electric charges, i.e., the current density, with respect to the current and reference configuration, respectively	[C/(m^2 · s)]
$\boldsymbol{J}^i$	flux of species i with respect to reference configuration	[mol/(m^2 · s)]
μ^{mix}	chemical potential of mixing	[J/mol]
μ_0	vacuum permeability, $\mu_0 = 1.256637 \cdot 10^{-6}$ V s/(A m)	[V · s/(A · m)]
μ_r	relative permeability	[−]
η^{mix^i}	specific enthropy of mixing	[J/(mol · K)]
Φ	electric potential	[V]
φ^{mix^i}	specific enthalpy of mixing	[J/mol]
q	total charge density in the current configuration	[C/m^3]
q^b	density of bound charges	[C/m^3]
q^f	density of free charges	[C/m^3]
r_a	rate of salt association	[1/s]
r_d	rate of salt dissociation	[1/s]
W^i	sources of species i with respect to reference configuration	[mol/(m^3 · s)]
χ	electric susceptibility	[−]
z	valence of an ion	[−]

1 Introduction

In this thesis, the multiphysically coupled modelling and numerical simulation of mass transport in polymers and polymer-based composites is investigated. As polymers are made up of long, entangled molecule chains that differ in their chemical composition and the degree of crosslinking between the chains, their properties strongly depend on chemical forces and interactions. The mechanical behaviour of polymers, thus, varies with their chemical structure from liquid-like states in, e.g., polyionic liquids over highly deformable elastomers to rigid and brittle thermosets. However, they all are light-weight and during production easily formable. This and the possibilty to adjust their behaviour by modification of the chemical structure makes polymers an interesting starting point for the development of new and so-called smart materials.

Smart polymers are used in a variety of fields, for example in lithography or optics and, especially, in the field of biomedical applications [3] due to their biocompatibility. Here, the functional behaviour of the materials can be stimulated externally, e.g., through electric fields, or naturally through body temperature or changes in pH. Examples of biomedical applications of smart polymers include, among others, controlled drug delivery, bioseparators or heat-activated self-tightening thread for stitches.

Another important type of smart polymers exhibits "active" behaviour, i.e., a reversible deformation of the material due to, e.g., a thermal or electrical stimulus. Polymers exhibiting the latter, i.e., translation of electric energy into deformation and vice versa, are called electroactive polymers. These have in the last years received a lot of attention in applications such as micropumps, tactile displays, or biomimetic actuators [11]. There are various mechanisms through which such electromechanically coupled behaviour arises, some of which are based on electrostatic forces associated with electrical polarisation of the material while others depend on mass transport within the polymer.

In fact, mass transport of fluids or particles within polymers often results in coupled behaviour due to physical and chemical interactions on the molecular scale. Most commonly, the uptake and transport of fluids results in significant swelling as the polymer network expands. This swelling can be utilised in actuators, particularly in the case of stimuli-responsive hydrogels which will react to external stimuli with considerable volume changes. This change in dimension evidently involves a change in mechanical properties as the molecule network is extended and the solvent interacts chemically and physically with the polymer molecules. The influence of these molecular interactions is especially visible in Case II diffusion, a type of anomalous transport behaviour in which solvent uptake induces a transition from the glassy to a rubber-like state. This significant change in the mechanical behaviour is, furthermore, associated with the formation of a sharp diffusion front and macroscopic swelling.

Understanding the processes involved in solvent transport and the arising coupled effects is essential not only to utilise it in smart materials but also to prevent failure in technical

applications due to the uptake of fluids from the environment that might lead to cracking or significant changes in the material properties.

Modelling such processes starts with the description of the transport. There are multiple factors influencing the transport kinetics such as available free volume, molecular interactions between fluid and medium or the fluid mobility. However, the most important factor affecting any kind of transport is the driving force that provides the incentive to change the current state of the system. This driving force arises from gradients of physical fields such as temperature, concentration or electric potential. These gradients are energetically unfavourable and, thus, result in behaviour that aims to balance the gradients. In any system, multiple kinds of gradients might be present that influence the fluid and their combined effects result in a macroscopic flux of the fluid or particles through the polymer medium.

While the type of driving force and the effect the transport has on the overall system may be very different for different polymers, the underlying physical principles governing the behaviour tend to be similar. This is utilised in this thesis, which aims to develop physically motivated models for the multiphysically coupled behaviour in polymers by examining the fundamental balance principles which govern the physics of the phenomenon. The models are formulated in the framework of non-linear continuum mechanics and solved numerically using the finite element method. In developing the models, care is taken to formulate the governing equations as generally as possible to ensure that no aspect of the phenomenon is missed in modelling. Furthermore, such a general framework allows to identify parallels and general principles of multiphysically coupled behaviour, thus, adding to the understanding of the phenomena under investigation.

This modelling approach based on fundamental physical principles is employed in describing two different examples of multiphysically coupled mass transport in polymers and the similarities in the description are pointed out. In contrast to highly specific or phenomenological models, this approach allows to take insight into the mechanisms of the coupling and can conveniently be extended or adjusted to describe other coupled phenomena.

Modelling of multiphysical behaviour

Multiphysical coupling is observed whenever different physical processes occur simultaneously, interacting with and influencing each other. This is, in fact, the case for almost all technical processes and naturally occurring phenomena. One typical and very illustrative example of such a multiphysically coupled process is metal forming in which the imposed plastic deformation is partly dissipated into heat that is transported through the metal and, in turn, induces thermal deformation of the metal. Furthermore, both deformation and temperature may affect the metal's crystal structure and, therefore, its heat conduction and deformation behaviour.

Fully resolving all occurring physical processes and their interactions is, however, highly complex. Therefore, for many classical engineering problems it is standard procedure to focus on only one of the processes, neglecting the others to simplify the description. Often, this simplification is sufficient to achieve meaningful results. In modern material design, however, multiphysically coupled phenomena have been gaining interest especially in the development of so-called "smart materials" which have properties that can be purposefully and reversibly altered by an external stimulus, i.e., they exhibit coupled behaviour that is utilised

to functionalise the material. As practically any physical field can interact with any other field resulting in a multitude of coupled effects, a variety of specialised smart materials such as, for example, thermoelectrica or piezoelectrica, photochromic materials or shape memory alloys exists. The mechanisms responsible for the characteristic coupled behaviour are as diverse as the possible applications and not in all cases well understood.

Particularly for the development of new materials and their implementation as "smart" parts, it is necessary to be able to theoretically describe their behaviour. Imagine, for example, an actuator used as a robotic clamping device. To be able to control the device's motion, a model describing how the external stimulus is translated into deformation is necessary. Furthermore, a general theoretical description of the physical processes at work is needed to understand the behaviour and develop and tune new materials.

Such multiphysically coupled modelling is based on the identification and description of the individual fields involved, such as deformation and temperature in the above example of metal forming. The coupled nature of these phenomena yields partial differential equations for the individual fields that are in turn functions of the other field variables. For some of these problems, analytic models can be established that can be solved exactly but are unfortunately only able to describe very simple cases, e.g., certain simple geometries. More general models of multiphysically coupled phenomena require a numerical solution based on discretisation schemes such as the finite element method or finite differences. The coupled nature and non-linearity of the resulting system manifests in large systems that are computationally expensive and call for a careful numerical and computational treatment.

Structure of the thesis

In the following, two distinct examples of multiphysically coupled mass transport in polymers are examined, namely Case II diffusion and electroactive polymers. As the common basis for both models, the underlying continuum mechanical principles are summarised in Chapter 2. There, the kinematics and balance equations used to model thermomechanical problems are introduced. Subsequently, these fundamental principles are utilised and extended to model the two example systems.

In Chapter 3, the Case II diffusion phenomenon is investigated. After an overview of the nature of the phenomenon and the current state of the art in modelling, a diffusion law accounting for the anomalous diffusion kinetics is developed. This diffusion law is then incorporated into a thermoelasticity framework to model the fully coupled behaviour. Numerical examples allowing insight into the nature of the coupling are provided.

The second example which is presented in Chapter 4 are electroactive polymers. First, different mechanisms of charge carrier transport and electromechanical coupling as well as their description are discussed. Subsequently, an extension of interface elasticity theory is established which in the following is utilised to model the dominant interface modification effects in nanoscale metal/ion-conducting polymer composites. The presentation of this model is again concluded with numerical studies of such composites.

Finally, in Chapter 5, the work is summarised and discussed. Furthermore, an outlook on potential extensions and future work is given.

2 Continuum mechanics

Continuum mechanics is used to model the behaviour of bodies in response to external loads which can be, among others, mechanical or thermal in nature. This behaviour is described using kinematic measures, which will be introduced in this chapter. Furthermore, the physical laws governing the material's behaviour, i.e., the balance laws and the fundamental principles of constitutive material modelling are summarised in the following. A more extensive description can be found, e.g., in the textbooks [61, 66, 119].

2.1 Kinematics

In continuum mechanics, a body $\mathcal{B}$ is described by a continuous distribution of material particles $X(\boldsymbol{x}, t)$ uniquely defined by their position in space $\boldsymbol{x}$ at a time t. The body is bounded by the surface $\partial\mathcal{B}$. At a time $t = 0$, this body is in the so-called *reference configuration* denoted by $\mathcal{B}_0$ which is typically load-free and is chosen for convenience of the analysis. In response to applied loads, the body deforms into the so-called *current configuration* which can be described using a motion function $\boldsymbol{\varphi}(\boldsymbol{X}, t)$ which maps the reference position $\boldsymbol{X}$ of every particle to their current position $\boldsymbol{x}$ as depicted in Fig. 2.1.

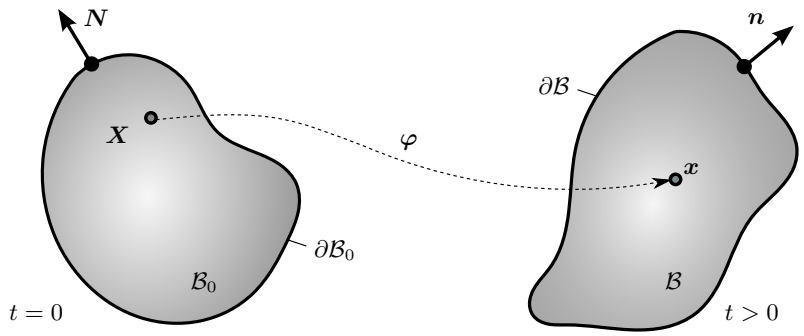

Figure 2.1: Schematic representation of the relationship between reference and current configuration. A continuum body occupying the reference configuration $\mathcal{B}_0$ is mapped to the current configuration $\mathcal{B}$ by the motion $\boldsymbol{\varphi}$.
Figure adapted from [142].

Based on these different states or configurations, one can differentiate between two descriptions of continuum mechanical problems, i.e., the *Langrangian* or *material* setting and the *Eulerian* or *spatial* setting. The Langrangian setting is commonly used in solid mechanics and describes the problem in terms of the material particles and considers their movement over time. In contrast, the Eulerian setting describes the fields in terms of a point in space $\boldsymbol{x}$ at time t. This setting is preferred in fluid mechanics where it is usually difficult (and of no interest) to define a specific reference configuration.

The motion $\boldsymbol{\varphi}$ connecting the spatial and material settings is a one-to-one mapping. With it, it is possible to define other parameters that simplify the description of the body's deformation and changes in its shape. One fundamental deformation measurement is the deformation gradient $\boldsymbol{F}$ defined by

$$\boldsymbol{F}(\boldsymbol{X}, t) := \operatorname{Grad} \boldsymbol{\varphi}(\boldsymbol{X}, t)\,, \tag{2.1}$$

where $\operatorname{Grad} \bullet$ denotes the gradient in space with respect to the reference configuration. A gradient with respect to the current configuration would be denoted by $\operatorname{grad} \bullet$. This way of differentiating the setting by using capital and lower case letters is employed in the whole thesis.

The determinant of the deformation gradient is referred to as the Jacobi determinant $J := \det \boldsymbol{F}$ and describes the volume change of a particle. As the motion $\boldsymbol{\varphi}$ is invertible, $J(\boldsymbol{X}) \neq 0$. Furthermore, J has to be positive to prevent self-penetration of the body. That is, the Jacobi determinant has to obey

$$J > 0 \tag{2.2}$$

and a volume preserving motion yields $J = 1$.

The deformation gradient describes both rotation and deformation. For the context of mechanics, it is convenient to define a deformation measure that is independent of any rotations because these do not induce stresses in a body. One possible rotation-independent deformation measure that is used throughout this thesis is the right Cauchy-Green deformation tensor $\boldsymbol{C}$ defined by

$$\boldsymbol{C} = \boldsymbol{F}^T \cdot \boldsymbol{F}\,. \tag{2.3}$$

These relations and parameters form the framework in which deformation and motion of a body are described. Which deformations occur, however, has to be calculated from field equations that are derived from physical balance equations and constitutive relations.

2.2 Fundamental balance equations

The physical laws governing the behaviour of a deformable body are universal balance equations that are independent of the material at hand. For any given physical field, a balance equation can be established as a special case of the so-called *general volume balance*. This general volume balance describes the change of the physical field f over time due to fluxes, sources and production within a body.

For any closed control volume Ω_0 in a body $\mathcal{B}_0$, the evolution of a physical quantity f can, thus, be described by an integral relation

$$\frac{\mathrm{D}}{\mathrm{D}t} \int_{\Omega_0} f \,\mathrm{d}V = -\int_{\partial\Omega_0} \boldsymbol{g} \cdot \boldsymbol{N} \,\mathrm{d}A + \int_{\Omega_0} h \,\mathrm{d}V + \int_{\Omega_0} \hat{f} \,\mathrm{d}V\,, \tag{2.4}$$

where $\boldsymbol{g}$ denotes the density of the fluxes over the boundary $\partial\Omega_0$ where an outflux is positive, h is the source density and $\hat{f}$ is the production density of f. Note that f here is a scalar but the general volume balance can be formulated for any tensor quantity. For a conserved

quantity such as mass or energy, the production vanishes in an isolated system[1]. This holds for any control volume Ω_0 inside $\mathcal{B}_0$, while for the isolated system $\mathcal{B}_0$ as a whole, the right hand side of Eq. (2.4) vanishes.

A multiphysically coupled problem is governed by the balances of mass, linear momentum, angular momentum, energy and entropy. As these balances form the basis for any continuum mechanical modelling, they are briefly introduced in the following. For more information on the derivation in the material and spatial setting, the reader is referred to continuum mechanics textbooks, e.g., [66].

2.2.1 Balance of mass

In Newtonian physics, mass cannot be produced or destroyed. Furthermore, for most mechanical problems, no sources from which mass is supplied or sinks in which it is absorbed exist.[2] In most mechanical systems it is assumed that the mass of the control volume does not change during deformation, thus, the balance equation for the mass density with respect to the reference configuration ρ_0 is given by

$$\frac{\mathrm{D}}{\mathrm{D}t}\int_{\Omega_0}\rho_0\,\mathrm{d}V = 0\,. \tag{2.5}$$

The mass of the system is given by $m = \int_{\Omega_0}\rho_0\,\mathrm{d}V$ and as Eq. (2.5) states that mass is conserved during any deformation, the mass is the same in the material and spatial setting at any time:

$$m = \int_{\Omega_0}\rho_0\,\mathrm{d}V = \int_{\Omega}\rho\,\mathrm{d}v\,. \tag{2.6}$$

Using the pull-back of a volume element from the spatial to the material setting $J^{-1}\,\mathrm{d}v = \mathrm{d}V$, this expression is equal to

$$\int_{\Omega_0}\left[\rho_0 - \rho J\right]\,\mathrm{d}V = 0\,. \tag{2.7}$$

For an arbitrary volume V, this global expression can be localised yielding

$$\rho_0 = \rho J\,. \tag{2.8}$$

This classical formulation of the balance of mass holds for closed systems in which the control volume is defined by the material occupying it. However, when considering mass transport within such a system, e.g., diffusion within a solid, the balance of mass for the diffusing species i has to account for flux into and out of the control volume and sources W, yielding

$$\frac{\mathrm{D}}{\mathrm{D}t}\int_{\Omega_0}\rho_0^i\,\mathrm{d}V = -\int_{\partial\Omega_0}\boldsymbol{J}^i\cdot\boldsymbol{N}\,\mathrm{d}A + \int_{\Omega_0}W\,\mathrm{d}V\,. \tag{2.9}$$

[1] An isolated system is one that does not interact with its surroundings.

[2] In multi-phase systems, the balances for the different phases may have source terms representing, e.g., chemical reactions, describing the transfer of mass from one phase to the other. The balance for the complete mass of the system, however, remains source-free.

Here, $\boldsymbol{J}^i$ denotes the mass flux and $\boldsymbol{N}$ is the normal vector of the control volume's surface.

In the reference configuration, the volume is time-independent, thus the order of differentiation and integration can be readily exchanged in Eq. (2.9) and localisation exploiting the divergence theorem gives

$$\dot{\rho}_0^i = -\mathrm{Div}\, \boldsymbol{J}^i + W\,, \tag{2.10}$$

where the superimposed dot $\dot{\bullet}$ denotes a time derivative and Div is the divergence operator with respect to the reference configuration.

2.2.2 Balance of linear momentum

The balance of linear momentum states that the momentum only changes due to external forces, i.e,

$$\frac{\mathrm{D}}{\mathrm{D}t}\int_{\Omega_0} \rho_0 \dot{\boldsymbol{u}}\,\mathrm{d}V = \int_{\partial\Omega_0} \boldsymbol{P}\cdot\boldsymbol{N}\,\mathrm{d}A + \int_{\Omega_0} \rho_0 \boldsymbol{b}\,\mathrm{d}V\,. \tag{2.11}$$

Here, $\dot{\boldsymbol{u}}$ is the time derivative of the displacement $\boldsymbol{u} = \boldsymbol{x} - \boldsymbol{X}$, i.e., a velocity. The right hand side of Eq. (2.11) is the sum of body forces $\rho_0\boldsymbol{b}$ such as gravity that act on the volume and forces acting on the surface. These surface forces are expressed by a stress tensor and the normal vector to the surface $\boldsymbol{N}$ according to the Cauchy theorem. In the material setting, this stress is the first Piola-Kirchhoff stress tensor $\boldsymbol{P}$, which correlates the force acting in the spatial setting to the area in the material setting.

With that, the local form of the balance of linear momentum is given by

$$\rho_0 \ddot{\boldsymbol{u}} = \mathrm{Div}\boldsymbol{P} + \rho_0 \boldsymbol{b}\,. \tag{2.12}$$

2.2.3 Balance of angular momentum

Changes in the angular momentum result from the torque exerted by the body and surface forces presented in Section 2.2.2. Thus, the balance of angular momentum reads

$$\frac{\mathrm{D}}{\mathrm{D}t}\int_{\Omega_0} \rho_0 \boldsymbol{x}\times\dot{\boldsymbol{u}}\,\mathrm{d}V = \int_{\partial\Omega_0} \boldsymbol{x}\times\boldsymbol{P}\cdot\boldsymbol{N}\,\mathrm{d}A + \int_{\Omega_0} \rho_0 \boldsymbol{x}\times\boldsymbol{b}\,\mathrm{d}V\,. \tag{2.13}$$

Applying the divergence theorem and inserting the momentum balance Eq. (2.12) into the resulting expression reduces this to the localised form of the balance of angular momentum

$$\boldsymbol{0} = \overset{3}{\boldsymbol{\varepsilon}} : \left[\boldsymbol{F}\cdot\boldsymbol{P}^T\right]\,, \tag{2.14}$$

where $\overset{3}{\boldsymbol{\varepsilon}}$ is the Levi-Civita symbol. This system of equations has to be satisfied pointwise and is only satisfied if $\boldsymbol{P}\cdot\boldsymbol{F}^T = \boldsymbol{F}\cdot\boldsymbol{P}^T$, i.e., the first Piola-Kirchhoff stress tensor is in general not symmetric but its contraction with the deformation gradient is. More importantly, the balance of angular momentum states that the stress in the spatial configuration, the Cauchy stress $\boldsymbol{\sigma}$, is symmetric[3], as it is connected with $\boldsymbol{P}$ by $\boldsymbol{P} = J\boldsymbol{\sigma}\cdot\boldsymbol{F}^{-T}$.

[3] This also follows from examining the balance of angular momentum in the spatial configuration.

2.2.4 Balance of energy

The first law of thermodynamics postulates the conservation of energy, stating that the energy $\mathcal{E}$ of a closed system only changes due to the mechanical work it performs and heat it generates. The energy of a system consists of the internal energy and the kinetic energy:

$$\mathcal{E} = \int_{\Omega_0} \left[\rho_0 \varepsilon + \frac{1}{2} \rho_0 \dot{\boldsymbol{u}} \cdot \dot{\boldsymbol{u}} \right] \mathrm{d}V \,. \tag{2.15}$$

Here, ε denotes the specific internal energy.

Thus, the energy balance is given by

$$\begin{aligned} \frac{\mathrm{D}}{\mathrm{D}t} \int_{\Omega_0} \left[\rho_0 \varepsilon + \frac{1}{2} \rho_0 \dot{\boldsymbol{u}} \cdot \dot{\boldsymbol{u}} \right] \mathrm{d}V = & \underbrace{\int_{\partial\Omega_0} \dot{\boldsymbol{u}} \cdot \boldsymbol{P} \cdot \boldsymbol{N} \, \mathrm{d}A + \int_{\Omega_0} \rho_0 \dot{\boldsymbol{u}} \cdot \boldsymbol{b} \, \mathrm{d}V}_{\text{mechanical power}} \\ & \underbrace{- \int_{\partial\Omega_0} \boldsymbol{Q} \cdot \boldsymbol{N} \, \mathrm{d}A + \int_{\Omega_0} \rho_0 r \, \mathrm{d}V}_{\text{thermal power}} \,, \end{aligned} \tag{2.16}$$

where $\boldsymbol{Q}$ is the heat flux and r is the specific heat supply.

Keeping in mind that the volume of Ω_0 is constant in time, employing the divergence theorem yields the localised form of the energy balance:

$$\rho_0 \dot{\varepsilon} + \rho_0 \dot{\boldsymbol{u}} \cdot \ddot{\boldsymbol{u}} = \dot{\boldsymbol{u}} \operatorname{Div} \boldsymbol{P} + \boldsymbol{P} : \operatorname{Grad} \dot{\boldsymbol{u}} - \operatorname{Div} \boldsymbol{Q} + \rho_0 \dot{\boldsymbol{u}} \cdot \boldsymbol{b} + \rho_0 r \,. \tag{2.17}$$

This expression includes both the kinetic and the internal energy of the system which can be separated by introduction of the balance of the kinetic energy that results from the scalar product of the velocity $\dot{\boldsymbol{u}}$ with the balance of linear momentum Eq. (2.12):

$$\rho_0 \dot{\boldsymbol{u}} \cdot \ddot{\boldsymbol{u}} = \dot{\boldsymbol{u}} \operatorname{Div} \boldsymbol{P} + \rho_0 \dot{\boldsymbol{u}} \cdot \boldsymbol{b} \,. \tag{2.18}$$

Subtracting this expression from the total energy balance yields the balance of internal energy

$$\rho_0 \dot{\varepsilon} = \boldsymbol{P} : \dot{\boldsymbol{F}} - \operatorname{Div} \boldsymbol{Q} + \rho_0 r \,, \tag{2.19}$$

stating that the internal energy of a closed system arises from heat flux and heat sources, as well as from a mechanical term, the stress power $\boldsymbol{P} : \dot{\boldsymbol{F}}$.

2.2.5 Balance of entropy

Following the standard procedure outlined before, the balance of entropy reads

$$\frac{\mathrm{D}}{\mathrm{D}t} \int_{\Omega_0} \rho_0 \eta \, \mathrm{d}V = - \int_{\partial\Omega_0} \boldsymbol{G} \cdot \boldsymbol{N} \, \mathrm{d}A + \int_{\Omega_0} G \, \mathrm{d}V + \int_{\Omega_0} \Gamma_0 \, \mathrm{d}V \,. \tag{2.20}$$

For the entropy flux $\boldsymbol{G}$ and the source density G, commonly a-priori assumptions are made relating them to the heat flux and heat supply according to:

$$\boldsymbol{G} = \frac{\boldsymbol{Q}}{T} \qquad \text{and} \qquad G = \frac{\rho_0 r}{T} \,,$$

where T denotes the absolute temperature. However, other formulations are possible if further effects have to be accounted for, cf. Section 3.3.1.

Furthermore, the second law of thermodynamics states that the entropy production or dissipation density Γ_0 is never negative. Thus, the localised form of the balance of entropy can be written as the general entropy imbalance

$$\rho_0 \dot{\eta} + \operatorname{Div} \boldsymbol{G} - G \geq 0 \,. \tag{2.21}$$

2.3 Material modelling

The kinematic and governing equations introduced in Sections 2.1 and 2.2 form a general framework describing the thermomechanically coupled behaviour of a continuum body. This framework is so far material-independent and underdetermined.

Thus, further equations are needed to fully determine the system. These are called constitutive relations and describe the behaviour of a specific material. To be physically sound, these constitutive relations have to obey a few general principles that pose restrictions on the form the equations can take. In summary, these principles state that the constitutive relations are a-priori functions of all process variables (*equipresence*) and the present state of a particle is fully determined by past and present states (*determinism*) of the particle and its neighbourhood, not the whole body (*local action*). Furthermore, the constitutive equations have to be invariant to changes of the observer (*material objectivity*) and have to reflect material symmetries (*material invariance*). Moreover, the constitutive relations cannot violate the balance equations and the second law of thermodynamics (*admissibility*).

The latter requirement is ensured by evaluating the entropy imbalance Eq. (2.21) to pose further restrictions on the form of the constitutive equations. However, as of now, there is no consensus on how this evaluation has to be carried out and different approaches exist. In this thesis, the principle of Coleman-Noll [27] based on the Clausius-Duhem inequality is used. Further details on this and other entropy principles can be found in the literature, e.g., in [73, 119, 123].

3 Case II diffusion

Diffusion is a form of mass transport within a medium based on the random thermal movement of molecules. Despite the fact that an individual molecule moves without preference for any direction, in total, a flux from regions of high concentration towards regions of low concentration arises, leading eventually to perfect mixing of two substances. This is due to the fact that, statistically speaking, more molecules leave high concentration areas than enter them. The resulting macroscopic mass flux can, thus, be described as being driven by a negative concentration gradient[1].

This concentration-driven macroscopic transport is classically described by Fick's laws. These, however, only describe the kinetics of an unhindered mass transport due to a concentration gradient, while it has become apparent that especially in polymers a variety of diffusion kinetics can be observed due to interactions of the solvent molecules with the polymer chains. Because of these interactions, delays in the diffusion kinetics may occur as well as changes in the polymeric base material such as plasticisation or macroscopic swelling.

Understanding and modelling the mechanisms involved in such multiphysically coupled diffusion processes in polymers is a field of great research interest, as is evident from a wide variety of models proposed in the literature which, however, mostly deal with a phenomenological description or the modelling of special cases. In this chapter, a special case of hindered, that is *anomalous*, diffusion, the so-called Case II diffusion is examined. Case II diffusion exhibits distinct diffusion kinetics with a sharp front and macroscopic swelling. These may cause crazing and catastrophic failure and, thus, be undesirable. On the other hand, there exist many applications in which this characteristic behaviour is used deliberately, e.g., for non-destructive microstructuring [108]. Other possible applications include photoresists [96], membranes [71] and controlled release drugs [86, 114]. This wide range of possible applications calls for a deep understanding of the processes and mechanisms of Case II diffusion.

In the following, an overview about the phenomenon of Case II diffusion and previous modelling approaches is presented. Subsequently, a diffusion law accounting for the anomalous kinetics is developed. In Section 3.3, this new model is included in a fully coupled system of diffusion/deformation/heat conduction.

This chapter has in parts been published by Wilmers and Bargmann in [141] and [142].

3.1 State of the art: Case II diffusion in solid polymers

The term Case II diffusion was coined by Alfrey et al. in 1966 [1]. There exists a large number of earlier experimental works, e.g. [30, 31, 65, 102], describing deviation from Fickian behaviour for diffusion of comparatively small molecules in glassy polymers and the sharp

[1] In fact, the driving force for diffusion is a gradient in the chemical potential. However, for most processes this correlates with the concentration gradient and modelling of diffusion is, therefore, usually based on concentration gradients, see Section 3.2. An example for the few systems in which the concentration analogy is invalid is spinodal decomposition.

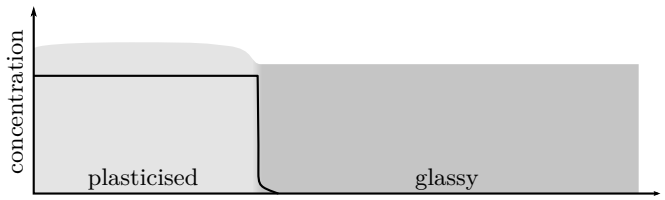

Figure 3.1: Sketch of sharp diffusion front and swelling during Case II diffusion. Swelling only occurs in the plasticised region. Ahead of the sharp front, a small Fickian precursor is visible.

diffusion fronts and large swelling accompanying it. Based on their own experimental work, Alfrey et al. introduced Case II diffusion as a limiting case for extremely non-Fickian behaviour and gave the first systematic description of the process.

The anomalous nature of Case II diffusion is based on the fact that in glassy polymers, almost no free volume is available for diffusion of a solvent. However, a suitable solvent may interact with the polymer to cause plasticisation, i.e., a localised transition from the glassy into the rubber-like state in which diffusion is unhindered. This relaxation takes place at a finite rate that is significantly slower than that of the unhindered diffusion. Therefore, the relaxation hinders solvent uptake and is the rate-controlling process.

This imbalance is responsible for the occurrence of several characteristic phenomena during Case II diffusion [1], compare also Fig. 3.1:

1. Almost no diffusion or solvent uptake is possible in the glassy regions ahead of the current relaxation region. Thus, a sharp front forms between the plasticised and the glassy region of the polymer.

2. The relaxation allows the polymer chains to rearrange to accommodate the solvent. This results in considerable macroscopic swelling accompanying the uptake and transport of the solvent.

3. Behind the front, i.e., in the plasticised region, the maximum concentration and an equilibrium state of swelling are established instantaneously compared to the time of relaxation and, thus, the front velocity.

4. The front moves with constant velocity that is independent of time and concentration, because the relaxation time does not depend on either quantity. In combination with 3., this translates to mass uptake kinetics that are linear in time.

5. Small amounts of solvent are able to diffuse within the free volume within the glassy polymer. This may be visible in the so-called Fickian precursor of varying size occurring ahead of the front.

6. The desorption process follows Fickian diffusion kinetics, because no further relaxation is necessary. This, furthermore, also means that the swelling remains after desorption as the polymer returns to the glassy state.

None of these characteristics *alone* are conclusive for the identification of Case II behaviour and other kinds of anomalous diffusion may exhibit some of the characteristic features of Case II diffusion, as anomalous diffusion always occurs because of a delay in the diffusion

due to interaction of the solvent with the polymer network. Transition from one kind of anomalous behaviour to the other, therefore, is smooth and different types may be difficult to distinguish. The wide range of possible diffusion behaviour can be characterised by the mass uptake over time $m(t)$ using the relation

$$\frac{m(t)}{m^{\mathrm{eq}}} = k\, t^n \,. \tag{3.1}$$

Here, the mass is normalised by the mass of solvent incorporated in the polymer at equilibrium m^{eq} and k is a proportionality constant. For Case II diffusion, the exponent n takes the value of 1, while for Fickian diffusion it is equal to 0.5. Other types of anomalous diffusion behaviour fall in the range $0.5 < n < 1$ and occur in systems in which relaxation and diffusion time are of the same order[2].

The ratio of relaxation rate to unhindered diffusion velocity determines the kind of diffusive behaviour a given polymer-penetrant system exhibits. To illustrate this relation, Vrentas et al. [133, 134] introduced the diffusional Deborah number De as a parameter to characterise diffusion behaviour. The Deborah number is defined as

$$De = \frac{\tau}{t_c} \,, \tag{3.2}$$

where τ denotes the relaxation time and t_c is the characteristic unhindered diffusion time. For Case II diffusion $De > 1$, indicating the dominating nature of relaxation.

Both, the relaxation time and the diffusion speed, depend on different factors such as steric effects, the polarity of the molecules involved or thermal and mechanical history [33]. Of these parameters, the most prominent one is temperature, which dominates any diffusion process as molecular motion of the solvent and the polymer is thermally activated. Furthermore, temperature is also an important factor determining whether the polymer is in the glassy or rubber-like state. Thus, a variety of diffusion types may be observed in any given polymer/solvent system [69]. In general, for temperatures well above the glass transition temperature T_g of the mixture, Fickian diffusion occurs in an amorphous polymer, while below T_g, anomalous and Case II behaviour are observed.

Since the first systematic description of Case II diffusion, numerous experimental studies have been carried out, observing Case II behaviour in different polymers, including the widely used poly(methyl methacrylate) [71, 116] and polystyrene [101, 126], among others [49, 70, 108]. In addition to these experimental works, there has been considerable effort in the development of a theoretical model describing Case II diffusion. There are two general approaches to modelling the characteristic Case II behaviour, based on either the description of the mechanical behaviour and its influence on the transport or on reproduction of the diffusion kinetics. Surprisingly, the latter approach that focusses solely on the transport is less often employed and mostly in phenomenological approaches, such as [20]. The work presented in [20] is based on a separation of the diffusive flux into a sum of different contributions, that each have their own relaxation time. This model qualitatively describes transport with Fickian and Case II as well as the intermediate anomalous behaviour. An earlier but similiar phenomenologic approach is presented in [104], where the power law Eq. (3.1) is modified to

[2] Note that these values for the exponent n are only valid for diffusion in a slab. The effects of other geometries on the power law Eq. (3.1) have been investigated in [109, 110].

describe anomalous diffusion behaviour as a superposition of Fickian and Case II diffusion. In [57], a more phyiscally motivated approach is chosen, using dual-mode sorption to account for the molecular interactions responsible for front formation.

Earlier models focus more on the deformation behaviour and its coupling to the diffusive flux. The first extensive modelling approach in this direction was published by Thomas and Windle [121, 122]. This model considers the osmotic pressure caused by solvent uptake as being responsible for the viscous response of the polymer. Durning et al. [41] used the Maxwell viscoelastic model instead of the viscous one suggested by Thomas and Windle and derived a model for differential sorption from thermodynamical considerations that incorporates the Thomas-Windle model as a special case for small Deborah numbers [55]. These models are limited to one spatial dimension and do not account for the influence of external mechanical forces or deformation. Wu et al. [144] extended Durning's model to integral sorption under assumption of ideal mixing and small deformations. Further examples for models describing anomalous and Case II diffusion kinetics are presented in the review papers [13, 33] and references therein.

A thorough model of Case II diffusion has to account for the characteristic transport kinetics as well as the strong coupling of concentration and deformation that is responsible for the swelling. Furthermore, it is well known that the diffusion behaviour in polymers strongly depends on temperature [40] as do the plasticisation and the mechanical properties of the polymer.

Such a more general, multiphysically coupled formulation of Case II diffusion was first introduced by Govindjee and Simo [60] in 1993. They propose a physically-motivated continuum mechanical framework explicitly for Case II diffusion, coupling concentration and displacement. The model accounts for the viscoelastic material response as well as for the large deformations occurring during Case II diffusion. It is shown to be able to reproduce the characteristics of Case II diffusion for the example of a traction free slab. McBride et al. [94, 95, 118] extended the Govindjee-Simo model by coupling it to thermomechanics, establishing a general framework describing non-Fickian diffusion that can be specialised for Case II by an appropriate formulation of the Helmholtz free energy. However, no specification of the form of the Helmholtz free energy or other constitutive equations is presented for this model.

The strong coupling and the steep profiles in stresses and concentrations are sources of possible instabilities in numerical simulations of Case II diffusion. Therefore, particular care has to be put into the numerical treatment and concurrently few thorough numerical studies are to be found in the literature. In [145], Wu et al. describe a finite difference scheme for simulations of the method introduced in [144]. This approach is reviewed by Vijalapura et al. in [130, 131] and deficiencies in the solution procedure are addressed. Furthermore, Vijalapura et al. propose a numerical procedure for the solution of Govindjee and Simo's method [60]. For spatial discretisation, a finite element approach is used and an adaptive finite difference scheme is formulated with great rigour for time discretisation. This implementation, however, is restricted to the quasi-static case which does not fully meet the requirements of the large deformations seen during Case II diffusion.

There are numerous other numerical studies concerning other types of coupling of mass transport and deformation in polymers. For example, Wang et al. [137] follow the works of Govindjee and Simo [60] and McBride et al. [95] to include viscoelastic behaviour into the modelling of polymeric gels and present examples of numerical simulations. However, their

work does not concern anomalous diffusion. Similarily, in [7], the coupling of diffusion and large deformations is modelled and simulated without consideration of anomalous behaviour, and in [36] the influence of stresses on the diffusion behaviour is investigated. A recent contribution regarding the coupling between large deformations in amorphous polymers and temperature is presented in [4, 5]. These coupled models are derived from thermodynamic considerations and can be applied to the description of typical phenomena known from hydrogel processing, e.g., buckling of thin films [86]. However, they are based on classical Fickian diffusion and not all of the choices in the description of the mechanical behaviour in hydrogels are also valid for the polymeric glasses which exhibit Case II diffusion.

Thus, in the following, a diffusion law accounting for the molecular interactions influencing the solvent transport is developed and after numerical studies illustrating the suitability of the developed transport description, it is coupled to thermomechanic behaviour based on the general set of equations presented in [94].

3.2 Modelling diffusion

An extensive introduction to the mathematical description of diffusion processes is presented in [29]. In the following, a short overview of the classical description using Fick's laws is given before a model for anomalous Case II diffusion is developed and studied numerically.

3.2.1 Fickian diffusion

Fick's laws were published in 1855 [48] based on experimental observations. They introduce the concentration gradient as the driving force for the diffusive flux $\boldsymbol{J}$. This constitutive relation for the diffusion flux is referred to as Fick's 1$^{\text{st}}$ law and is given by

$$\boldsymbol{J}(\boldsymbol{X},t) = -\boldsymbol{D}(\boldsymbol{X}) \cdot \operatorname{Grad} c_0(\boldsymbol{X},t)\,. \tag{3.3}$$

Here, $\boldsymbol{D}$ denotes the second order diffusion coefficient tensor which is the material parameter describing the diffusivity of the solvent in the medium. Large values of $\boldsymbol{D}$ denote a fast solvent transport. The concentration c_0 is the current mass of solvent per volume of the undeformed medium, i.e., the polymer, in the reference configuration. This measure is readily available from experiments. Fick's 1$^{\text{st}}$ law is formally identical to Fourier's law of heat conduction [53] which stands to reason as heat conduction is based on the same thermal movement on the molecular scale.

Fick's 2$^{\text{nd}}$ law is in fact the mass balance of the diffusing species Eq. (2.9) in its localised form without sources:

$$\frac{\partial c_0}{\partial t} = -\operatorname{Div} \boldsymbol{J}. \tag{3.4}$$

Inserting the constitutive equation (3.3) into this mass balance yields the diffusion law

$$\dot{c}_0 = \operatorname{Div}\left(\boldsymbol{D} \cdot \operatorname{Grad} c_0\right). \tag{3.5}$$

This diffusion law is well suited to describe most classical diffusion phenomena despite the fact that it is parabolic and, thus, unphysical as it assumes information propagation at infinite

speed. Furthermore, Fickian diffusion cannot account for any of the described characteristics of anomalous diffusion. There have been numerous approaches to address these shortcomings, e.g., by introduction of a concentration dependence of the diffusion coefficient [91]. However, none of these phenomenological approaches are able to accurately capture the unique kinetics of Case II diffusion. Thus, a new constitutive model for the diffusion flux $\boldsymbol{J}$ in Case II diffusion is needed.

3.2.2 A diffusion law for Case II diffusion

Most of the existing constitutive models for Case II diffusion are based on summation of different diffusion laws to fit the Case II behaviour or by describing the solvent uptake as dependent on diffusivity and viscosity values of the material. This, however, does not account for the dependence of the Case II mechanism on molecular interactions and the resulting relaxation processes in the polymer. In the following, a constitutive model is proposed that focusses on these molecular interactions and accounts for the wave-like transport kinetics known from experimental studies.

Such a wave-like transport cannot be described using a parabolic equation such as Fick's law but requires a hyperbolic model. Introduction of hyperbolic-like equations is an established approach in modelling of non-classical heat conduction, cf., e.g., the extensive reviews [78, 79]. The first, and probably most well known, of these approaches was published independently by Maxwell [92], Cattaneo [21] and Vernotte [129] who introduced "thermal inertia" in form of a relaxation time to Fourier heat conduction, yielding a hyperbolic model with finite propagation speed. Similar results are achieved by employing a dual-phase-lag approach which was originally developed to describe microstructural effects during rapid heating which result in wave-like heat conduction [107, 124, 125]. This approach has also been transferred to mass transport problems in [25] to account for deviations from classical Fickian transport due to the occurrence of chemical reactions.

The dual-phase-lag approach is based on interpreting processes occurring on the microscale as the source of a delayed response on the macroscopic scale. This concept is an accurate description of the processes occurring during Case II behaviour: Solvent transport is hindered by interactions of the solvent with the polymer molecules and the induced relaxation of the polymer network, which macroscopically results in the formation of the sharp wave-front and non-classical kinetics. Thus, the dual-phase-lag approach is chosen as the basis for developing the constitutive equation for Case II diffusion in this thesis.

The delay or lag due to molecular interactions is captured by introducing retardation times to Fick's 1$^{\text{st}}$ law, Eq. (3.3):

$$\boldsymbol{J}(\boldsymbol{X}, t+\tau_j) = -\boldsymbol{D}(\boldsymbol{X}) \cdot \operatorname{Grad} c_0(\boldsymbol{X}, t+\tau_c)\,. \tag{3.6}$$

Here, $\tau_j \geq 0$ denotes the delay in the flux due to the relaxation of the polymer and $\tau_c \geq 0$ is the delay in formation of the concentration gradient due to interactions of the solvent molecules with the polymer network during transport. These relaxation times are intrinsic properties of a given polymer/solvent system.

Depending on the ratio τ_j/τ_c, the dual-phase-lag approach is able to model different types of transport. For $\tau_j = \tau_c = 0$, this model reduces to classical Fickian transport. In materials exhibiting Case II diffusion, the relaxation of the polymer is the rate-determining process,

thus, $\tau_j \gg \tau_c$. If the formation of the concentration gradient is not hindered at all, $\tau_c = 0$, and the dual-phase-lag model is identical to the Maxwell-Cattaneo-Vernotte approach applied to species diffusion.

Equation (3.6) is expanded using a Taylor series. Keeping in mind that a change of the unit system should not change the constitutive relations, terms that are quadratic in the retardation times are neglected. Thus, the first order approximation yields:

$$\boldsymbol{J}(\boldsymbol{X},t) + \tau_j \frac{\partial \boldsymbol{J}(\boldsymbol{X},t)}{\partial t} = -\boldsymbol{D}(\boldsymbol{X}) \cdot \operatorname{Grad} c_0(\boldsymbol{X},t) - \tau_c \boldsymbol{D}(\boldsymbol{X}) \cdot \frac{\partial \operatorname{Grad} c_0(\boldsymbol{X},t)}{\partial t} . \tag{3.7}$$

This expression alone only accounts for the occurrence of molecular interactions and polymer relaxation during transport. As detailed above, the relaxation is, however, associated with a glass transition that results in considerable changes in the mechanical and transport behaviour. These changes have to be reflected in the constitutive equation by choice of the material constants. In the glassy area ahead of the diffusion front, transport is severely hindered, resulting in a low value of the diffusion coefficient $\boldsymbol{D}$, while behind the front at high solvent concentrations, diffusion is much faster. Thus, the diffusion coefficient is concentration dependent.

The concentration dependence of $\boldsymbol{D}$ during anomalous diffusion has been experimentally investigated in [102] for different halocarbons in polystyrene and is shown to follow a relation $\boldsymbol{D}(c_0) = \overline{\boldsymbol{D}} \exp(\delta\,[c_0/c_0^{\mathrm{eq}} - 0.5])$, where the average diffusion coefficient $\overline{\boldsymbol{D}}$ and the parameter δ are constants for any polymer/solvent system at constant temperature and c_0^{eq} denotes the solvent concentration in equilibrium. This formulation of the concentration dependence is valid for different polymers, cf. [144].

Additionally, the diffusion coefficient also depends strongly on the temperature and deformation of the polymer. In modelling pure diffusion, both the temperature and the deformation are assumed to be constant. However, for the fully coupled model presented in Section 3.3, these effects cannot be neglected. So, for the sake of completeness and better comparability, temperature and deformation dependence are incorporated into the model here already. For comparison, in [141], the proposed diffusion model is presented with plain concentration dependence.

As the polymer in both states is homogeneous and isotropic, it is possible to reduce the diffusion coefficient to a position independent scalar measure. Hence, the complete expression for the diffusion coefficient is

$$D(c_0,T,J) = D_0\,[1-\nu_s]^2 \left[1 - 2\chi^{FH}\nu_s\right] \exp\left(-\frac{E_A}{RT} + \delta\left[\frac{c_0}{c_0^{\mathrm{eq}}} - 0.5\right]\right) . \tag{3.8}$$

Here, T is the temperature and J is the Jacobian determinant characterising the change in volume between the current and the undeformed reference configuration, cf. Section 2.

The deformation dependence of the diffusion coefficient is expressed using the current volume fraction of the solvent $\nu_s = \frac{V_s(t)}{V(t)} = \frac{c_0}{J\,\rho_0^s}$ relating the volume of the solvent present to the total volume of the mixture V with the solvent's density ρ_0^s. The factor D_0 and the non-dimensional Flory-Huggins parameter χ^{FH} are properties of the solvent/polymer system. Further details regarding the meaning of the Flory-Huggins parameter are given in Section 3.3. The temperature dependence of the diffusion coefficient is known to follow an Arrhenius relation with the activation energy E_A. This expression follows from free volume theory as

described in [40] and is here extended by a concentration dependent term that characterises the change in the diffusion coefficient upon relaxation with the parameter δ. This exponential description follows from experimental studies of different halocarbons in polystyrene [102] and is known to be applicable for different polymer/solvent systems exhibiting Case II diffusion [144].

Inserting these constitutive relations into the mass balance Eq. (3.4) yields the modified diffusion law

$$\dot{c}_0 + \tau_j \, \ddot{c} = \operatorname{Div}\left(D(c_0, T, J) \operatorname{Grad} c_0\right) + \tau_c \operatorname{Div}\left(D(c_0, T, J) \operatorname{Grad} \dot{c}_0\right). \tag{3.9}$$

This proposed diffusion law describes the concentration evolution during Case II diffusion. To solve it and carry out simulations of the behaviour, it needs to be supplemented with boundary and initial conditions that characterise the problem at hand. Thus, for Case II diffusion in a body $\mathcal{B}_0$, Eq. (3.9) has to be solved within the body while on its surface $\partial\mathcal{B}_0$, boundary conditions for the concentration or the fluxes are imposed according to

$$c_0(\boldsymbol{X}, t) = f(\boldsymbol{X}, t) \qquad \text{on } \partial\mathcal{B}_0^a \tag{3.10}$$

$$\boldsymbol{J}(\boldsymbol{X}, t) = \boldsymbol{g}(\boldsymbol{X}, t) \qquad \text{on } \partial\mathcal{B}_0^b = \partial\mathcal{B}_0 \setminus \partial\mathcal{B}_0^a \,. \tag{3.11}$$

This set of equations is completed by the initial conditions. As Eq. (3.9) includes a second order derivative in time, two initial conditions are required; one for the concentration and one for the first order time derivative.

3.2.3 Numerical treatment

The partial differential equations describing diffusion processes can in general only be solved numerically, e.g., using methods such as the finite element method (FEM). This approach is based on the discretisation of the solution domain into a set of finite sub-domains, the so-called elements. An extensive description of finite element methods is presented, for example, in the textbooks [146] and [15].

For time-dependent partial differential equations such as the diffusion laws Eq. (3.5) and Eq. (3.9), there are two possible strategies in treating them numerically, depending on the order of spatial and temporal discretisation, see, e.g., [34]. Using the Method of Lines, the spatial domain is discretised first, yielding a semi-discretised system of ordinary differential equations. Alternatively, the equations can be discretised in time first, resulting in a stationary partial differential equation for every time step. This approach is called Rothe's method. Rothe's method allows for the utilisation of adaptive meshes as every time step can be discretised in space independently of the discretisation employed in the previous step. Such adaptive meshes can be especially useful in capturing moving fronts such as the one occurring during Case II diffusion. However, solving problems with higher order time derivatives using Rothe's method would require the introduction of an additional field variable accounting for the first time derivative, thus, adding another degree of freedom and increasing computational effort significantly.

The Method of Lines, on the other hand, allows for a straight-forward treatment of higher order time derivatives as they occur in Eq. (3.9) and in the dynamic momentum balance describing the deformation behaviour of the material (see Section 3.3). As the number in field

variables in a fully-coupled problem is already high, in the following, the Method of Lines is applied in numerical studies of Fickian and Case II diffusion. For the spatial discretisation, finite elements are used. The resulting semi-discrete problem is then solved using a finite difference scheme in time.

Spatial discretisation using finite elements

By weighting the diffusion laws Eq. (3.5) for Fickian and Eq. (3.9) for Case II diffusion with a test function δc and integrating over the volume $\mathcal{B}_0$, the equations' weak forms are obtained:
Fick:

$$\int_{\mathcal{B}_0} \delta c\, \dot{c}_0 \,\mathrm{d}V = D \int_{\mathcal{B}_0} \delta c \,\mathrm{Div}\,(\mathrm{Grad}\, c_0)\,\mathrm{d}V \tag{3.12}$$

Case II:

$$\int_{\mathcal{B}_0} \delta c\,[\dot{c}_0 + \tau_j \ddot{c}_0]\,\mathrm{d}V = \int_{\mathcal{B}_0} \delta c\ [\mathrm{Div}\,(D(c_0)\mathrm{Grad}\, c_0) + \tau_c\,\mathrm{Div}\,(D(c_0)\mathrm{Grad}\,\dot{c}_0)]\,\mathrm{d}V\,. \tag{3.13}$$

Integrating these expressions by parts and utilising Gauß's theorem yields:
Fick:

$$\int_{\mathcal{B}_0} \delta c\, \dot{c}_0 \,\mathrm{d}V = -\,D \int_{\mathcal{B}_0} \mathrm{Grad}\,\delta c \cdot \mathrm{Grad}\, c_0 \,\mathrm{d}V + D \int_{\partial\mathcal{B}_0} \delta c\,\mathrm{Grad}\, c_0 \cdot \boldsymbol{N}\,\mathrm{d}A \tag{3.14}$$

Case II:

$$\begin{aligned}\int_{\mathcal{B}_0} \delta c\,[\dot{c}_0 + \tau_j \ddot{c}_0]\,\mathrm{d}V = &-\int_{\mathcal{B}_0} D(c_0)\mathrm{Grad}\,\delta c \cdot [\mathrm{Grad}\, c_0 + \tau_c\,\mathrm{Grad}\,\dot{c}_0]\,\mathrm{d}V \\ &+ \int_{\partial\mathcal{B}_0} D(c_0)\delta c\,[\mathrm{Grad}\, c_0 + \tau_c\,\mathrm{Grad}\,\dot{c}_0]\cdot\boldsymbol{N}\,\mathrm{d}A\,,\end{aligned} \tag{3.15}$$

with $\boldsymbol{N}$ denoting the normal vector on the surface $\partial\mathcal{B}_0$. Equations (3.14) and (3.15) form the basis of the finite element discretisation which employs a standard Bubnov-Galerkin approach, i.e., both the concentration c_0 and the test function δc are approximated with the same, here linear, functions N^i over the n nodes, according to

$$c_0 = \sum_{i=1}^{n} N^i\, c_{0i}\,, \qquad\qquad \delta c = \sum_{i=1}^{n} N^i\,\delta c_i\,.$$

For the gradients of the concentration and the test functions, the following approximations are applied

$$\mathrm{Grad}\, c_0 = \sum_{i=1}^{n} \mathrm{Grad}\, N^i\, c_{0i}\,, \qquad\qquad \mathrm{Grad}\,\delta c = \sum_{i=1}^{n} \mathrm{Grad}\, N^i\,\delta c_i\,.$$

Furthermore, the isoparametric concept is employed, so that the shape functions interpolating the geometry are equal to N^i, i.e., $\boldsymbol{X} = \sum_{i=1}^{n} N^i\,\boldsymbol{X}_i$.

Temporal integration using finite differences

The finite element discretisations of the diffusion laws yield a semi-discrete system of ordinary differential equations. This is integrated and solved using a finite difference time stepping scheme.

Hence, the time derivatives are approximated by a difference between discrete time steps t_j. These steps divide the time domain into intervals of width $\Delta t_j = t_{j+1} - t_j$. For a constant

Table 3.1: Material parameters for diffusion of toluene in polystyrene

	symbol	value	source
equilibrium concentration	c_0^{eq}	0.13 g/cm^3	[56]
mass density of the solvent	ρ_0^s	0.8669 g/cm^3	
diffusion coefficient factor	D_0	$4.50714 \cdot 10^8$ cm^2/min	[56]
Flory interaction parameter	χ^{FH}	0.133	[112]
activation energy	E_A	109 kJ/mol	[56]
variation parameter of concentration dependence	δ	5	
retardation time (flux)	τ_j	6732.45 min	†
retardation time (gradient)	τ_c	50 min	

† estimated from velocity values given in [56] using the Deborah number theory [134]

interval width Δt, the first and second order time derivatives are, thus, given by

$$\dot{c}_0(t^{j+1}) \approx \frac{c_0^{j+1} - c_0^j}{\Delta t} \quad \text{and} \quad \ddot{c}_0(t^{j+1}) \approx \frac{c_0^{j+1} - 2c_0^j + c_0^{j-1}}{\Delta t^2}\,, \tag{3.16}$$

respectively. As the approximation at the time step t^{j+1} is a function of t^{j+1}, the method applied here, the so-called "backward Euler" scheme, is implicit.

Implicit methods are used in this thesis because they are more stable for diffusion-type problems and often less prone to oscillations than explicit or mixed methods. However, implicit methods are computationally more costly as they require a non-linear solver.

Solution of the non-linear system of equations is carried out using the Newton-Raphson method in an in-house finite element code utilising the program library `deal.II` [9].

3.2.4 Numerical study of the proposed Case II diffusion law

In order to test the applicability of the proposed approach for modelling of Case II diffusion and to compare it to Fick's law, numerical simulations are carried out in the following. The diffusion of toluene in polystyrene is chosen as the example system considered here because it has been shown to exhibit Case II behaviour for small toluene concentrations [56] and is commonly used in experimental studies. Hence, material constants and characteristic values of the system are readily available in the literature. The parameters used in the numerical study are summarised in Table 3.1.

The same sample geometry as it is depicted in Fig. 3.2 is used in both, the simulation of Fickian and Case II diffusion. The cuboid has a length of 3 μm and is discretised using $75 \times 10 \times 10$ linear hexahedral elements. On one of the cuboid's small faces, a constant concentration c_0^{eq} is applied, modelling contact with a large reservoir of the solvent. Flux-free boundary conditions $\boldsymbol{J}(\boldsymbol{X}, t) = \boldsymbol{0}$ are imposed on all other surfaces.

For Case II diffusion, the relation for the concentration dependence of the diffusion coefficient Eq. (3.8) is employed at constant temperature $T = 298.15$ K and no deformation ($J = 1$). For Fickian diffusion, the constant diffusion coefficient at equilibrium concentration $D(c_0^{\text{eq}}) = 3.054 \cdot 10^{-10}$ cm^2/min is used, representing the unhindered transport in the completely plasticised polymer. Therefore, the Case II transport has a Deborah number of $De = 22.8$ with the characteristic time $t_c = {}^{l^2}/_{D(c_{\text{eq}})}$, and, thus, fulfils the criterion for Case II diffusion according to Eq. (3.2).

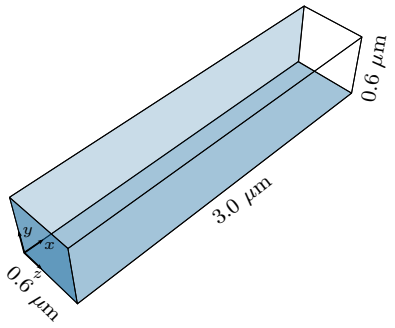

Figure 3.2: Geometry of the sample. On the front face (darkest colour), a constant concentration c_0^{eq} is imposed. On all other surfaces, zero flux boundary conditions are applied.
Figure adapted from [142].

Comparison of Fickian and Case II diffusion

Different types of diffusion behaviour may be defined by consideration of their mass uptake kinetics, cf. Eq. (3.1). In Fig. (3.3), the mass uptake arising from Fickian diffusion and the proposed Case II diffusion law are depicted. Fickian diffusion shows the expected proportionality to $\sqrt{t}$, while the uptake for Case II is clearly linear in time. In the beginning of Case II diffusion, an almost invisible deviation from the linear kinetics occurs while establishing the front.

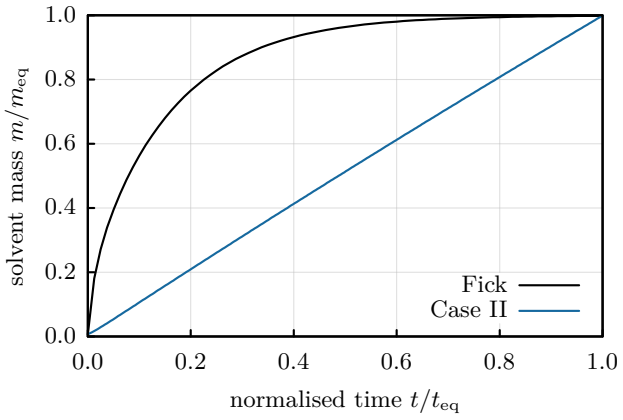

Figure 3.3: The mass uptake of Fickian and Case II diffusion over time. For better comparison, the solvent mass and time are normalised with respect to their equilibrium values. The mass uptake for Fickian diffusion is proportional to $\sqrt{t}$, whereas the proposed model for Case II transport accurately predicts linear uptake kinetics.

Beside the linear uptake kinetics, the most important characteristic of Case II diffusion is the sharp diffusion front. In Fig. 3.4, the concentration profiles for Fick and Case II over the whole length of the specimen are shown at three different time steps. From comparing the timescales, the different propagation speeds in Fickian and Case II diffusion are evident. Figure 3.4(a) shows the typical smooth curves caused by balancing the concentration difference between the two ends of the specimen.

For Case II diffusion, Fig. 3.4(b), the model predicts a sharp diffusion front for all time steps. Behind the front, only a negligible gradient is visible and this step-like concentration profile does not vary over time.

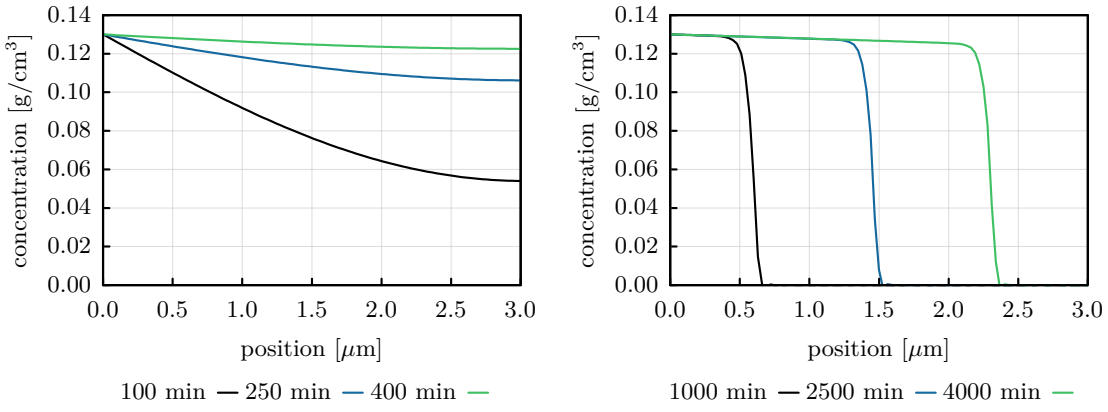

(a) Fickian diffusion

(b) Case II diffusion

Figure 3.4: Comparison of the concentration profiles arising during (a) Fickian and (b) Case II diffusion. Fickian diffusion exhibits smooth concentration gradients that flatten over time while the profiles during Case II diffusion uphold the characteristic front over time.

It is evident from the simulation results, that the proposed diffusion law Eq. (3.9) based on the dual-phase-lag approach is well suited to describe the characteristics of Case II diffusion. As seen in Fig. 3.3, the model exhibits the linear uptake kinetics described already by Alfrey [1] and observed experimentally, e.g., in [117, 120]. The concentration profiles depicted in Fig. 3.4(b) have the same distinct step-form with a sharp front as observed in experiments by Stamatialis and coworkers using microinterferometry [117]. For non-Case II anomalous diffusion these concentration profiles differ strongly from this step-form, cf. [12, 42].

Concentration dependence of the diffusion coefficient

In a number of previous models of Case II diffusion, a concentration dependent diffusion coefficient has been added to Fick's law Eq. (3.5) to account for the sharp front, cf. [33, 91]. This phenomenological approach does in fact yield a significant change in the concentration profiles but is, however, not sufficient for the description of Case II transport behaviour as it does not account for the wave-like transport at a constant velocity because it neglects the existence of the relaxation process.

For comparison, simulations have been carried out for Fickian diffusion with a concentration dependent diffusion coefficient according to Eq. (3.8) and for the proposed Case II model with a constant diffusion coefficient. In Fig. 3.5, the resulting concentration profiles are depicted at different times that correspond to the same amount of absorbed solvent. Including the concentration dependence in Fick's law changes the predicted concentration profile significantly towards a front-like curve, however, no equilibrium plateau is established behind this front. The dual-phase-lag model with a constant diffusion coefficient predicts a more step-like profile but the front is broad. Neither of these two approaches predicts the sharp fronts of Case II diffusion, these are only modelled by the proposed dual-phase-lag approach with a concentration dependent diffusion coefficient. This considerable difference in the predicted behaviour is attributed to the fact that the concentration dependence of the diffusion coefficient accounts for the change in transport due to the plasticisation of the polymer, while the dual-phase-lag

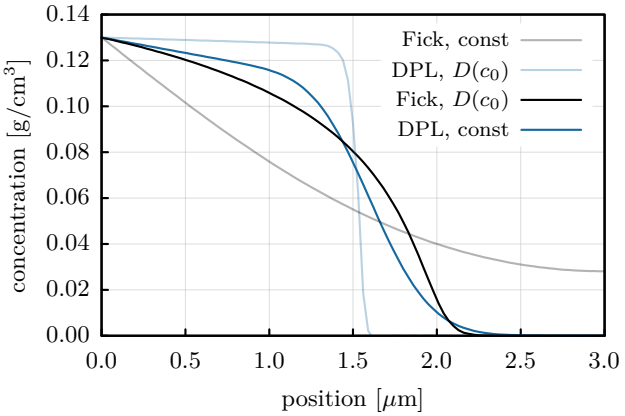

Figure 3.5: Influence of the concentration dependence of the diffusion coefficient. Depicted are the profiles predicted by Fick's laws and the dual-phase-lag model (DPL), each with a constant or a concentration dependent diffusion coefficient. It is obvious that neither adding a concentration dependence to Fick's laws nor neglecting the concentration dependence in DPL is sufficient in modelling Case II behaviour.

approach models molecular interactions and the resulting relaxation times. A full description of Case II diffusion has to incorporate both phenomena as is evident from these results.

3.3 Coupling diffusion with thermoelasticity

To fully describe the process of Case II diffusion not only a suitable diffusion law is needed but the coupling of diffusion, deformation and heat conduction has to be considered. Thus, in the following, the diffusion law derived and examined in Section 3.2 is incorporated into a general framework coupling diffusion and thermomechanics. The modelling approach follows the continuum mechanical framework for Case II diffusion which was proposed in [60] and has been extended to the thermomechanically coupled case in [94]. This approach does not differentiate between the solvent and the polymer but describes the mixture as a continuum.

Formulations for constitutive equations are presented that capture the distinct diffusion kinetics and the induced swelling of Case II. This specialised, multiphysically coupled model is implemented into a finite element code to examine the capabilities of the developed formulation.

The following sections have been partially published in [142] and are reproduced here according to the license agreement.

3.3.1 Governing equations

Based on the fundamental principles outlined in Chapter 2, the governing equations describing the coupling of deformation, diffusion and heat conduction in Case II diffusion are derived from an evaluation of the fundamental balance equations. For further details regarding this derivation, the reader is referred to [60, 94, 95].

Conservation of mass

In Case II diffusion, two mass balances have to be considered. As described in Section 2.2.1, the mass balance for the solid, i.e., the mass of the polymer is

$$\frac{\mathrm{d}}{\mathrm{d}t}\int_{\mathcal{B}} \mathrm{d}m = \frac{\mathrm{d}}{\mathrm{d}t}\int_{\mathcal{B}} \rho\,\mathrm{d}v = 0 \tag{3.17}$$

which, following standard arguments, gives

$$\rho_0 = J\,\rho \qquad \text{with } J = \det\boldsymbol{F}\,. \tag{3.18}$$

For the diffusing species, the balance of mass is formulated in terms of the concentration c_0, which is defined as the mass of solvent per volume of the polymer/solvent mixture. Thus, the localised form of the mass balance for the diffusing species is given by

$$\dot{c}_0 = -\mathrm{Div}\boldsymbol{J} + W\,, \tag{3.19}$$

as described in Section 2.2.1.

Balance of linear and angular momentum

Following the argumentation described in Section 2.2.2, the local form of the balance of linear momentum is formulated as

$$\rho_0\ddot{\boldsymbol{u}} = \mathrm{Div}\boldsymbol{P} + \rho_0\boldsymbol{b}\,, \tag{3.20}$$

where $\boldsymbol{P}$ denotes the first Piola-Kirchhoff stress tensor relating current forces to the reference area. The vector $\boldsymbol{b}$ is the body force vector.

Evaluation of the balance of angular momentum shows that the second Piola-Kirchhoff stress tensor $\boldsymbol{S}$ defined by $\boldsymbol{S} = \boldsymbol{F}^{-1}\cdot\boldsymbol{P}$ is symmetric. Therefore, $\boldsymbol{P}\cdot\boldsymbol{F}^T = \boldsymbol{F}\cdot\boldsymbol{P}^T$.

Balance of internal energy

For the description of a diffusion process, one has to take into account that the solvent entering the system contributes to the internal energy ε of the mixture, i.e., the system is open in contrast to the closed one described in Section 2.2.4.

To take the solvent's contribution into account, an equation of state for the chemical potential of the mixture μ^{mix} of the form

$$\mu^{\mathrm{mix}} = \varphi^{\mathrm{mix}} - T\eta^{\mathrm{mix}} \tag{3.21}$$

is assumed. Here, T is the absolute temperature and φ^{mix} and η^{mix} denote the specific enthalpy and specific entropy contributed to the system by mixing. Only the enthalpic part of the chemical potential contributes to the change in the total internal energy, while the entropic part appears in the balance of entropy. As they are introduced to the system via solvent uptake, these contributions are directly related to the solvent flux over the boundary.

With that, the local balance of internal energy is given by

$$\rho_0 \dot{\varepsilon} = \boldsymbol{P} : \dot{\boldsymbol{F}} - \operatorname{Div}(\underbrace{\boldsymbol{Q} + \varphi^{\mathrm{mix}} \boldsymbol{J}}_{\boldsymbol{Q}_{\mathrm{eff}}}) + \underbrace{\rho_0 r + \varphi^{\mathrm{mix}} W}_{Q_{\mathrm{eff}}} . \tag{3.22}$$

In the following, the contributions of the heat flux $\boldsymbol{Q}$ and the diffusion flux $\boldsymbol{J}$ are condensed to the coupled effective value $\boldsymbol{Q}_{\mathrm{eff}}$. Analogously, the change in internal energy caused by the sources of heat and diffusing species within the body, $\rho_0 r$ and $\varphi^{\mathrm{mix}} W$, are condensed to Q_{eff}.

Balance of entropy

The local form of the balance of entropy with respect to the reference configuration reads

$$\rho_0 \dot{\eta} = -\operatorname{Div}\left(\frac{\boldsymbol{Q}}{T} + \eta^{\mathrm{mix}} \boldsymbol{J}\right) + \frac{\rho_0 \, r}{T} + \eta^{\mathrm{mix}} W + \Gamma_0 \,, \tag{3.23}$$

where $\Gamma_0 \geq 0$ is the dissipation density.

Applying standard arguments and assuming a specific Helmholtz free energy of the form $\psi = \varepsilon - T\eta$ gives the balance of entropy in its Clausius-Duhem form. With the equation of state for the chemical potential Eq. (3.21) and introducing the coupled effective term $\boldsymbol{H}_{\mathrm{eff}} := \frac{1}{T}\boldsymbol{Q} + \eta^{\mathrm{mix}} \boldsymbol{J}$ this formulation reduces to

$$\boldsymbol{P} : \dot{\boldsymbol{F}} - \rho_0 \dot{\psi} - \rho_0 \eta \dot{T} - \boldsymbol{H}_{\mathrm{eff}} \cdot \operatorname{Grad} T - \boldsymbol{J} \cdot \operatorname{Grad} \mu^{\mathrm{mix}} + \mu^{\mathrm{mix}} \dot{c}_0 \geq 0 \,. \tag{3.24}$$

The Helmholtz free energy is chosen to be of the general form $\psi = \psi(\boldsymbol{C}, c_0, T, \boldsymbol{\Xi}; \boldsymbol{X})$. Here, $\boldsymbol{\Xi}$ denotes the set of internal variables.

To obtain the constitutive relations, the balance of entropy (3.24) is examined using the standard Coleman-Noll procedure, yielding

$$\boldsymbol{P} = 2\rho_0 \boldsymbol{F} \cdot \frac{\partial \psi}{\partial \boldsymbol{C}} \,, \quad \mu^{\mathrm{mix}} = \rho_0 \frac{\partial \psi}{\partial c_0}, \quad \eta = -\frac{\partial \psi}{\partial T} \,, \tag{3.25}$$

and the reduced dissipation inequality

$$-\boldsymbol{J} \cdot \operatorname{Grad} \mu^{\mathrm{mix}} - \boldsymbol{H}_{\mathrm{eff}} \cdot \operatorname{Grad} T - \rho_0 \frac{\partial \psi}{\partial \boldsymbol{\Xi}} \cdot \dot{\boldsymbol{\Xi}} \geq 0 \,, \tag{3.26}$$

which is to be satisfied by the constitutive equations.

Temperature evolution

The evolution equation for the temperature is derived from the energy balance in its localised form Eq. (3.22), and the constitutive relations for the entropy density given in Eq. (3.25). Combining these two gives the following relation for the temperature evolution

$$\begin{aligned} -\rho_0 T \frac{\partial^2 \psi}{\partial T^2} \dot{T} = & \; - \boldsymbol{J} \cdot \operatorname{Grad} \mu^{\mathrm{mix}} - \operatorname{Div}(T \boldsymbol{H}_{\mathrm{eff}}) + T H_{\mathrm{eff}} - \rho_0 \frac{\partial \psi}{\partial \boldsymbol{\Xi}} \cdot \dot{\boldsymbol{\Xi}} \\ & + T \frac{\partial}{\partial T} \left[\boldsymbol{P} : \dot{\boldsymbol{F}} + \mu^{\mathrm{mix}} \dot{c}_0 + \rho_0 \frac{\partial \psi}{\partial \boldsymbol{\Xi}} \cdot \dot{\boldsymbol{\Xi}} \right] \end{aligned} \tag{3.27}$$

Table 3.2: Governing equations of Case II diffusion

mass balance	$\dot{c}_0 = -\operatorname{Div} \boldsymbol{J} + W$
linear momentum	$\rho_0 \ddot{\boldsymbol{u}} = \operatorname{Div} \boldsymbol{P} + \rho_0 \boldsymbol{b}$
temperature evolution	$\rho_0 \mathrm{C}_p \dot{T} = -\boldsymbol{J} \cdot \operatorname{Grad} \mu^{\mathrm{mix}} - \operatorname{Div}(T \boldsymbol{H}_{\mathrm{eff}}) + T H_{\mathrm{eff}} - \rho_0 \frac{\partial \psi}{\partial \boldsymbol{\Xi}} \cdot \dot{\boldsymbol{\Xi}} + T \frac{\partial}{\partial T} \left[\boldsymbol{P} : \dot{\boldsymbol{F}} + \mu^{\mathrm{mix}} \dot{c}_0 + \rho_0 \frac{\partial \psi}{\partial \boldsymbol{X} \boldsymbol{i}} \cdot \dot{\boldsymbol{\Xi}} \right]$

with $H_{\mathrm{eff}} := \frac{\rho_0 r}{T} + \eta^{\mathrm{mix}} W$. The specific heat capacity of the material is defined by $\mathrm{C}_p := -T \frac{\partial^2 \psi}{\partial T^2}$.

In Eq. (3.27), the coupled nature of the proposed framework is particularly distinct: The coupling between temperature evolution and deformation which gives rise to the effect of structural heating is incorporated through the thermal derivative of the stress power $\boldsymbol{P} : \dot{\boldsymbol{F}}$, while the effective entropy fluxes and sources, $\boldsymbol{H}_{\mathrm{eff}}$ and H_{eff}, include both thermal and diffusional contributions.

3.3.2 Constitutive model

The framework summarised in Table 3.2 describes a general system in which diffusion, deformation and heat conduction are coupled. In the following, the constitutive equations necessary to apply the general framework to the modelling of Case II diffusion are formulated. Special attention is paid to deriving the free energy of mixing which is responsible for the coupling between diffusion and deformation.

Diffusion

To model the characteristic Case II diffusion kinetics, the new diffusion law developed in Section 3.2 is employed:

$$\boldsymbol{J}(\boldsymbol{X}, t + \tau_j) = -\boldsymbol{D}(c_0, J, T) \cdot \operatorname{Grad} c_0(\boldsymbol{X}, t + \tau_c) \,. \tag{3.28}$$

From this expression of the diffusion flux $\boldsymbol{J}$ it is not obvious that the dissipation inequality Eq. (3.26) is fulfilled. To ascertain that the model produces thermodynamically sound results, the fulfilment of the dissipation inequality is checked for in every quadrature point during calculation, cf. Appendix A.2.

The coupling of the diffusion behaviour to temperature and deformation is accounted for by the diffusion coefficient as a function of concentration, temperature and the determinant of the deformation gradient given by Eq. (3.8):

$$D(c_0, T, J) = D_0 [1 - \nu_s]^2 [1 - 2\chi^{FH} \nu_s] \exp\left(-\frac{E_A}{RT} + \delta \left[\frac{c_0}{c_0^{\mathrm{eq}}} - 0.5 \right] \right) . \tag{3.29}$$

Here, the volume fraction of the solvent is given by $\nu_s = \frac{c_0}{J \rho_0^s}$. A scalar expression is chosen for the diffusion coefficient because the polymer is homogeneous and isotropic.

Helmholtz free energy

Following [60], the Helmholtz free energy is assumed to be additively decomposed into

$$\psi = \psi^{\mathrm{eq}}(\boldsymbol{C}, T) + \psi^{\mathrm{neq}}(\boldsymbol{C}, T, \boldsymbol{\Xi}) + \psi^{\mathrm{mix}}(\boldsymbol{C}, c_0, T)\,, \tag{3.30}$$

where ψ^{eq} is the free energy of an elastic material, ψ^{neq} accounts for non-equilibrium contributions and ψ^{mix} is the free energy of mixing.

To describe the equilibrium thermomechanical material behaviour of the polymer, a Neo-Hookean material model is chosen:

$$\begin{aligned}\rho_0\psi^{\mathrm{eq}} = \frac{\mu}{2}\left[\boldsymbol{C} - \boldsymbol{I}\right] : \boldsymbol{I} + \frac{\lambda}{2}\ln^2 J - \mu \ln J + \rho_0 \mathrm{C}_p \left[T - T_0 - T\ln\frac{T}{T_0}\right] \\ - 3\alpha\left[\lambda + \frac{2}{3}\mu\right]\left[T - T_0\right]\frac{\ln J}{J}\,,\end{aligned} \tag{3.31}$$

with the Lamé constants μ and λ, the thermal expansion coefficient α and the reference temperature T_0.

In accordance with [60], the non-equilibrium contribution of the material behaviour is described by

$$\frac{\partial \psi^{\mathrm{neq}}}{\partial \boldsymbol{C}} = \int_{-\infty}^{t} \beta \exp\left(-\frac{t-s}{\tau_{\mathrm{relax}}(s)}\right)\frac{\mathrm{d}}{\mathrm{d}s}\left[\frac{\partial \psi^{\mathrm{eq}}}{\partial \boldsymbol{C}}(s)\right]\mathrm{d}s\,. \tag{3.32}$$

Here, β is a dimensionless parameter describing the ratio of Young's moduli in the glassy and the rubber-like state and τ_{relax} is the visco-elastic relaxation time of the polymer.

To determine the functional relation of the mixing contribution ψ^{mix}, the Flory-Huggins theory of polymer mixtures, cf., e.g., [50, 51, 54], is applied. The Flory-Huggins model describes the mixing of a low-molecular-weight solvent and polymer on the basis of a theoretical lattice, as shown schematically in Fig. 3.6. One lattice site in this model can only be occupied by a single molecule. To account for the large difference in size and molecular weights between the solvent and the polymer, the polymer is represented by a chain of molecular segments, each occupying one lattice site. These segments are chosen so that the volume occupied by a chain segment is approximately equal to that occupied by a solvent molecule.

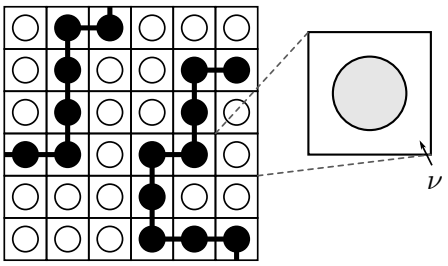

Figure 3.6: Two-dimensional depiction of Flory-Huggins model lattice. Every lattice side is occupied by either a solvent molecule (open circle) or a segment of the polymer chain (filled circle).
Figure reproduced from [142].

In this framework, the entropy of mixing is obtained via statistical considerations following the Boltzmann relation, which relates the change in entropy to the number of possible

arrangements of N_p polymer molecules and N_s solvent molecules in the lattice. From that, the specific entropy of mixing is given by (see [50])

$$\Delta S^{\mathrm{mix}} = -\frac{k_B}{nN_p m_p}\left[N_s \ln\frac{N_s}{N_s+nN_p} + N_p \ln\frac{nN_p}{N_s+nN_p}\right]. \tag{3.33}$$

Here, N_p and N_s denote the number of polymer and solvent molecules, respectively. Furthermore, r is the number of chain segments per polymer molecule (i.e., for most systems approximately the degree of polymerisation), and m_p is the mass of a chain segment, with k_B the Boltzmann constant.

In addition to m_p giving the mass of a polymer chain segment, one can define m_s as the mass of a single solvent molecule. With that, the concentration and the density with respect to the volume in the reference configuration V_0 can be written as

$$c_0 = \frac{N_s m_s}{V_0} \quad \text{and} \quad \rho_0 = \frac{nN_p m_p}{V_0}.$$

Using these relations, Eq. (3.33) is rearranged to

$$\Delta S^{\mathrm{mix}} = -\frac{k_B}{\rho_0}\left[\frac{c_0}{m_s}\ln\left(\frac{c_0}{c_0+\rho_0\frac{m_s}{m_p}}\right) + \frac{\rho_0}{nm_p}\ln\left(\frac{\rho_0}{c_0\frac{m_p}{m_s}+\rho_0}\right)\right]. \tag{3.34}$$

The enthalpy of mixing is given in the framework of the Flory-Huggins model by consideration of the interaction between neighbouring molecules. The change in energy if a solvent-polymer contact is formed is given by

$$\Delta\omega_{ps} = \omega_{ps} - 0.5[\omega_{ss}+\omega_{pp}], \tag{3.35}$$

where ω_{ij} is the energy of a contact i-j. The number of contacts of polymer and solvent is approximately equal to the number of possible contacts of a solvent molecule (i.e., the coordination number z of the lattice) times the probability that the site in question is occupied by a polymer chain segment. This probability is equal to the volume fraction of polymer in the current volume. Therefore, the specific mixing enthalpy is given by

$$\Delta H^{\mathrm{mix}} = \frac{1}{\rho_0 V_0} z N_s \frac{nN_p\nu}{v}\Delta\omega_{ps}. \tag{3.36}$$

Here, ν denotes the volume of a lattice site. As the reference volume V_0 is the volume of the unswollen polymer, the relation $V_0 = nN_p\nu$ holds. With this relation and the identity $v = JV_0$, the probability term is $\frac{nN_p\nu}{v} = \frac{1}{J}$. Furthermore, the dimensionless Flory-Huggins interaction parameter $\chi^{FH} := \frac{z\Delta\omega_{ps}}{k_B T}$ can be introduced. Thus, Eq. (3.36) becomes

$$\Delta H^{\mathrm{mix}} = \frac{1}{\rho_0} k_B T \chi^{FH} \frac{c_0}{m_s}\frac{1}{J}. \tag{3.37}$$

The Gibbs potential of mixing is given by $\Delta G^{\mathrm{mix}} = \Delta H^{\mathrm{mix}} - T\Delta S^{\mathrm{mix}}$.

From the equation of state, Eq. (3.21), it is evident that the chemical potential is a Gibbs potential. As it accounts for the change in Gibbs free enthalpy if an infinitesimal amount of

the solvent is added to the system, μ^{mix} is determined from the above relations by

$$\mu^{\text{mix}} = \frac{\partial \Delta G^{\text{mix}}}{\partial N_s} = \frac{\partial \Delta H^{\text{mix}}}{\partial N_s} - T\frac{\partial \Delta S^{\text{mix}}}{\partial N_s} \,. \tag{3.38}$$

The specific enthalpy and entropy of the solvent as introduced in Eq. (3.21) can thus be determined by $\varphi^{\text{mix}} = \frac{\partial \Delta H^{\text{mix}}}{\partial N_s}$ and $\eta^{\text{mix}} = \frac{\partial \Delta S^{\text{mix}}}{\partial N_s}$, respectively, cf. Appendix A.1.

Evaluating the balance of entropy by the Coleman-Noll procedure yields

$$\mu^{\text{mix}} = \rho_0 \frac{\partial \psi}{\partial c_0} = \rho_0 \frac{\partial \psi^{\text{mix}}}{\partial c_0} \,. \tag{3.39}$$

The mixing contribution to the Helmholtz potential can therefore be derived by integration of the chemical potential which yields

$$\psi^{\text{mix}} = \frac{k_{\text{B}}T}{{\rho_0}^2 V_0}\left[c_0 \chi^{FH}\frac{1}{J} + c_0 \ln\left(\frac{c_0}{c_0 + \rho_0 \frac{m_s}{m_p}}\right) + \rho_0 \frac{m_s}{n m_p}\ln\left(\frac{c_0 + \rho_0 \frac{m_s}{m_p}}{\rho_0 \frac{m_s}{m_p}}\right)\right] + \gamma \,, \tag{3.40}$$

As the chemical potential is a Gibbs potential, the concentration-independent value γ accounts for the difference between the Gibbs and the Helmholtz free energy per amount of solvent. This relates to a change in pressure and temperature upon mixing. At constant pressure, this change is negligible [90]. Thus, in the following we assume $\gamma = 0$.

Heat conduction

The heat conduction in amorphous polymers is considered to be classical and, therefore, is described by Fourier's law

$$\boldsymbol{Q} = -K \operatorname{Grad} T \,, \tag{3.41}$$

with K denoting the material's thermal conductivity. Here, K is a scalar quantity. The amorphous polymer is isotropic, thus, no anisotropies in the heat conduction behaviour arise. The difference in conductivity in the glassy and the rubber-like state is neglected. However, Eq. (3.41) can easily be extended by a concentration dependent heat conductivity to account for these effects.

3.4 Numerical examples

The equations established in the previous sections are solved using a finite element discretisation in space. In time, an implicit Euler scheme is applied. The numerical treatment employed here follows the principles introduced in Section 3.2.3.

The primary fields, i.e., the concentration, the displacement and the temperature, are approximated using linear functions. To interpolate the spatial gradient of the chemical potential μ^{mix} occurring in the temperature evolution equation (3.27) and the dissipation inequality (3.26), a fourth equation is introduced to be fulfilled on the element nodes, relating the specific enthalpy of mixing φ^{mix} to the primary fields according to

$$\varphi^{\text{mix}} = \frac{k_{\text{B}}\,T}{\rho_0\, V_0}\frac{\chi^{FH}}{J} \,, \tag{3.42}$$

Table 3.3: Material parameters for polystyrene and toluene

	symbol	value	source
diffusion			
equilibrium concentration	c_0^{eq}	0.13 g/cm^3	[56]
maximum diffusion coefficient	D_0	$4.50714 \cdot 10^8$ cm^2/min	[56]
activation energy	E_A	1.13 eV	[56]
variation parameter of concentration dependence	δ	5	[141]
Flory interaction parameter	χ^{FH}	0.133	[112]
retardation time (flux)	τ_j	6732.45 min	†
retardation time (gradient)	τ_c	50 min	
deformation			
mass density of the polymer	ρ_0	1.04 g/cm^3	[35]
mass density of the solvent	ρ_0^s	0.8669 g/cm^3	
number of polymer segments	n	3500	[56]
mass polymer chain segment	m_p	$1.73 \cdot 10^{-25}$ kg	
mass solvent molecule	m_s	$1.53 \cdot 10^{-25}$ kg	
Lamé constants (glassy)	λ	2.8 GPa	
	μ	1.2 GPa	
Lamé constants (plasticised)	λ	0.14 GPa	
	μ	0.06 GPa	
viscoelastic relaxation time	τ_{relax}	$5 \cdot 10^3$ min	[60]
thermal expansion coefficient	α	$9.0 \cdot 10^{-5}$ $\frac{1}{\text{K}}$	[35]
heat conduction			
specific heat capacity	C_p	1250 J/(kg K)	
thermal conductivity	K	0.17 W/(m K)	

† estimated from velocity values given in [56] using the Deborah number theory [134]

see Appendix A.1.

Thus, a system of four strongly coupled differential equations is formed. There are a number of approaches and methods to solve such coupled systems that can be differentiated into three general types: field elimination, monolithic or partitioned approaches. Field elimination is only possible for few linear systems and eliminates one or more of the fields by transformations. In monolithic approaches, the whole system is treated as an entity and solved simultaneously, while partitioned approaches aim to separate the system into multiple only lightly coupled systems, cf., [47] for further details. Here and in the whole thesis, monolithic solution schemes are applied, that is all coupled effects and interactions between the equations are taken into account and no simplifying assumptions about the coupled nature are made.

In the following numerical examples, the diffusion of toluene in polystyrene is examined as has been done in the study of the diffusion law in Section 3.2.4. The material parameters used are given in Table 3.3.

The two-way coupling between diffusion and deformation in Case II diffusion arises from the plasticisation of the material by the absorbed solvent. Ahead of the diffusion front, where almost no solvent exists, the polymer remains in its rigid, glassy state. The mixture behind the front, however, is plasticised and, thus, has a different mechanical behaviour - including different Lamé parameters.

In Table 3.3, the Lamé constants for the glassy and the plasticised state are given. For concentrations greater than $0.5\,c_0^{\mathrm{eq}}$, i.e., behind the front, the values for the plasticised state are used. This relates to a decrease in Young's modulus to approximately 1/20-th of the glassy value. The Poisson's ratio remains constant. A further temperature dependence of the mechanical properties is neglected as the plasticisation is the focus of the examination.

In addition to this change in the mechanical behaviour of the material, the coupling is introduced to the system via the dependence of the diffusion coefficient on the volume fraction of the solvent according to Eq. (3.8) and the Helmholtz free energy of mixing, cf. Eq. (3.40).

For the numerical examples, a cuboidal geometry as shown in Fig. 3.2 is examined. The geometry is discretised using linear hexahedral elements. To accurately capture the sharp diffusion front, the mesh is finer in x-direction, resulting in a discretisation with 2,214 degrees of freedom. As the propagation velocity increases with temperature, the timestep size is reduced for higher applied temperatures, thus, ranging from 0.2 min to 12.5 min.

The displacement of the cuboid is constrained on three adjacent faces, for each in the plane's normal direction. Additionally, Dirichlet boundary conditions for the concentration and temperature are applied on only the small one of these three faces, i.e., the yz-plane. The boundary conditions for concentration and temperature are chosen to be the equilibrium concentration c_0^{eq} and a constant temperature above the reference temperature $T_0 = 293.15$ K, respectively. For all surfaces, the concentration and temperature fluxes are assumed to vanish.

3.4.1 Case II diffusion

This setup and an imposed heating to 333.15 K (89.3 % of the polymer's glass transition temperature) on the small face are used to investigate the model's capability to describe Case II behaviour. The results are presented in Figs. 3.7 - 3.10.

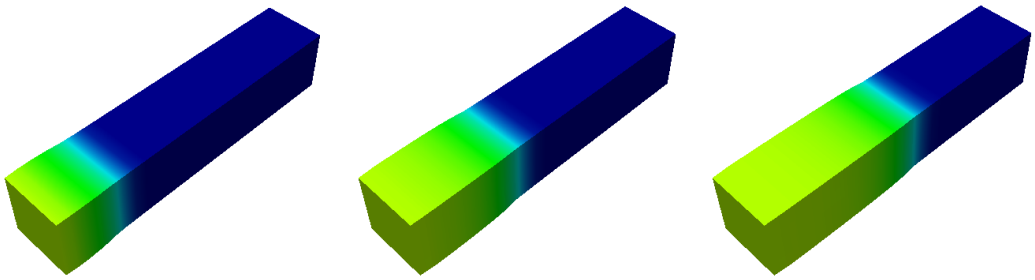

Figure 3.7: Temporal evolution of Case II diffusion. A sharp concentration front moves with constant velocity through the specimen. Behind the front, a constant concentration and an equilibrium state of swelling are established. The severe swelling due to solvent uptake is clearly visible.
Figure reproduced from [142].

Figure 3.7 displays deformation and solvent transport over time. The sharp Case II front is upheld over the whole diffusion time. Behind the front, concentration and swelling are in equilibrium.

Figure 3.8 shows the concentration, temperature and stress fields in the swollen geometry after an exposure of 200 min. Behind the solvent front, the polymer swells considerably while almost no deformation besides thermal expansion occurs in the low-concentration region. In

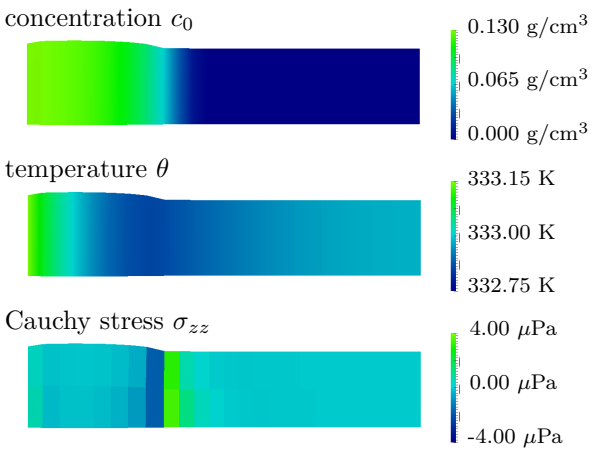

Figure 3.8: Distribution of concentration c, temperature T and the Cauchy stress component σ_{zz} in the swollen sample after an exposure time of 200 minutes.
Figure reproduced from [142].

the temperature field, a heating of a few millikelvin is visible. This is the effect of the heat of mixing as introduced via the chemical potential into the temperature evolution equation (3.27), cf. also Fig. 3.10.

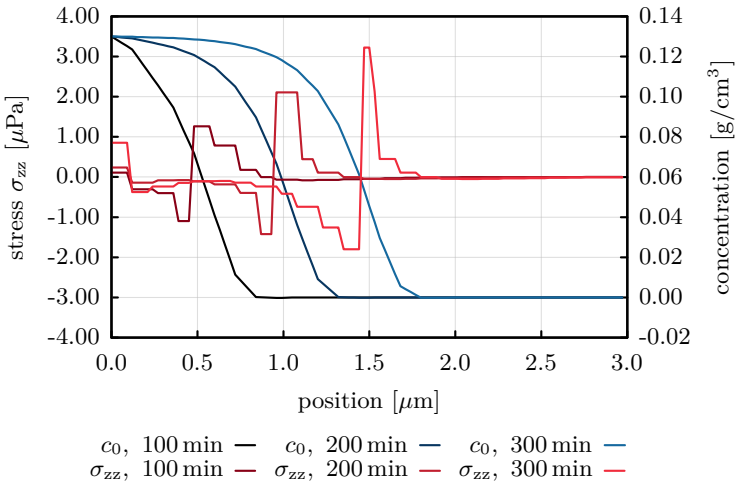

Figure 3.9: Cauchy stress and concentration profiles in x-direction of the undeformed sample at different exposure times. At the concentration front, a jump in the stresses occurs because only the plasticised, high-concentration region swells.

The distinct deformation behaviour results in the occurrence of stresses in the sample. Directly ahead of the front where the polymer is still glassy and unable to deform, tensile stresses arise. In the layer behind the front, the material is subjected to compressive strains because the swelling is restricted by the adjacent glassy region. This behaviour is further illustrated in Fig. 3.9 depicting the Cauchy stress distribution and the step-like concentration profiles in the unconstrained edge of the cuboid for different time steps. The stresses visible at a position of $x = 0$ μm arise from the displacement constraints on the yz-plane.

In Fig. 3.10, the temperature profile over the undeformed specimen is depicted. For Case II diffusion, heat conduction is orders of magnitude faster than the solvent transport. For this reason, the heating of one face leads to a homogeneous temperature of $T = 333.15$ K in the

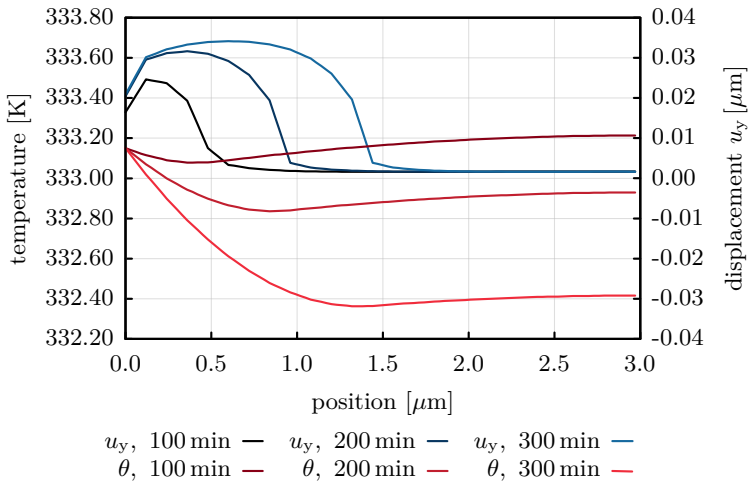

Figure 3.10: Temperature and displacement profiles in x-direction of the undeformed sample at different exposure times. The expanded material cools due to the thermoelastic effect.

whole specimen almost immediately. Further changes in the temperature are caused by two opposing effects, namely the thermoelastic behaviour of the material and the induced heat of mixing. In the beginning, the swelling of the polymer causes structural cooling, which is captured by the term describing the change of the stress power with temperature in Eq. (3.27). Over time, as the solvent concentration increases, the influence of the heat of mixing on the temperature evolution exceeds that of the stress power, causing a heating of the material. Figure 3.10 shows that the maximum of the temperature profile occurs just at the diffusion front.

3.4.2 Investigation of the coupling

As the previous section has demonstrated the capability of the proposed model to fully predict the characteristic properties of Case II diffusion, a further investigation of the effects of coupling diffusion, deformation and temperature is carried out.

To investigate the influence the temperature has on the diffusion kinetics and the swelling, further simulations have been carried out using the same setup as introduced in Fig. 3.2 with different applied temperatures.

In Fig. 3.11, concentration profiles for different applied temperatures are depicted. As the temperature in the material increases, the front velocity increases as well, following an Arrhenius relation as is typical for Case II diffusion because it is a thermally activated process [56, 84]. Furthermore, for higher temperatures, the solvent front widens because the diffusivity in the glassy region increases according to the temperature dependence of the diffusion coefficient in Eq. (3.8). With this rise in the diffusivity, the Fickian precursor becomes less pronounced. For the low temperature profiles, the Fickian precursor as the small region ahead of the front with a low solvent concentration is visible. A higher diffusivity in the glassy region means that more solvent diffuses further into the glassy region, thus, the Fickian precursor widens as well. The broadening of the Fickian precursor and the front indicates the transition of the diffusion behaviour from Case II to Fickian at temperatures above the glass transition that is observed in experiments.

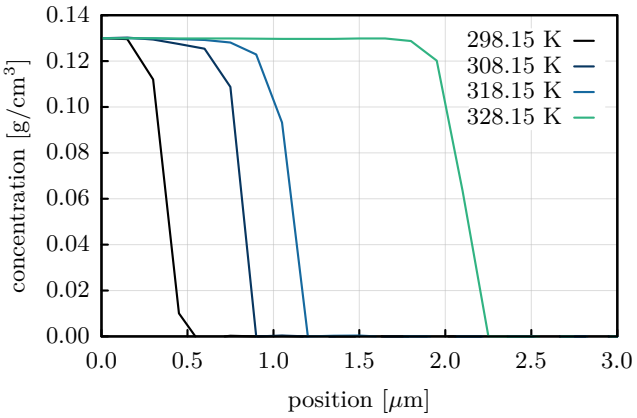

Figure 3.11: Concentration profiles for different applied temperatures at an exposure time of $t = 300$ min. With increasing temperature, the diffusion becomes faster and the front broadens.

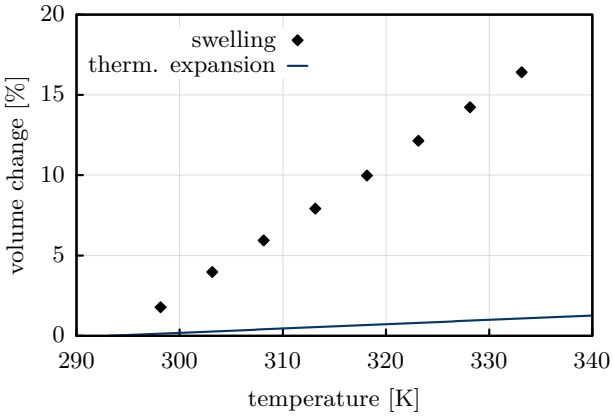

Figure 3.12: Temperature dependence of the volume expansion. The equilibrium degree of swelling increases distinctly more with temperature than the thermal expansion does.

In Fig. 3.12, the equilibrium degree of swelling as a function of temperature is depicted. The volume of the swollen sample increases linearly with the increasing temperature. Thermal expansion only accounts for a minimal percentage of the volume increase.

A pre-deformation of the specimen has only a very small influence on the modelled diffusion behaviour. However, from experiments, e.g., [64], it is known that a considerable pre-deformation causes a transition of the diffusion mechanism from Case II to Fickian behaviour. In its current form, the proposed model only considers the coupling between the deformation state and the diffusion coefficient. To account for the mechanism transition caused by pre-deformation, the model could be extended by a formulation for the generation of free volume during deformation and its influence on the diffusion kinetics.

4 Electroactive polymers

Electroactive polymers or EAPs are polymeric materials characterised by their ability to react to the application of an electric potential difference with reversible deformation, that is, they exhibit electromechanically coupled behaviour that can be utilised in actuators. Some EAPs also exhibit the reverse effect, in which an imposed deformation is translated into an electric signal.

Electromechanical coupling occurs in various material classes with different actuation mechanisms. For example, piezoceramics are known for their fast response time and high mechanical strength. However, they show very small strain amplitudes. Electroactive polymers, by contrast, exhibit actuation strains of about 10 % which are approximately two orders of magnitude larger than those in piezoceramics [113]. Due to these large deformations and their biocompability, EAPs are especially interesting for biomimetic and robotic applications to the point where they sometimes are referred to as "artificial muscles" [11, 16, 115].

Based on their activation mechanism, it is possible to differentiate two basic types of electroactive polymers [10]:

1. **Electronic activation:** This class of EAP includes, among others, electrostrictive, piezo- and ferroelectric polymers. The actuation behaviour in these materials is due to electrostatic forces and reorientation of polarised areas within the polymer that result in deformation of the material. They generally have fast response times but require high activation voltages which means they can only be operated in isolated, completely dry systems.

2. **Ionic activation:** In, e.g., gels, ionomers or conductive polymers, the activation is based on the transport of ions within the polymer network. These ions are either solvated in the polymer ("dry electrolytes") or enter the polymer by dotation or uptake of a liquid electrolyte. In any case, the polymer expands or contracts due to the transport of ions within the applied electric field. Ion transport within a polymer network is, however, comparatively slow, resulting in low response times. In applications that do not depend on fast actuation, the large deformations and low required voltage make up for this disadvantage.

In the following, only the latter kind, ionically activated EAPs, are investigated, yielding a problem of coupled mass transport, electrostatics and deformation to be modelled. Modelling of electronically activated polymer actuators is usually based on the concept of the Maxwell stress which describes the mechanical effect of electric forces. Examples can be found in the literature, for example in [19, 44, 67, 132].

To utilise the actuation behaviour of ionically activated EAPs, they have to be operated in a setup that allows for electric contactation. In many cases, this is realised in form of a layered design of electrodes sandwiching a solid electrolyte that yields a bending motion when

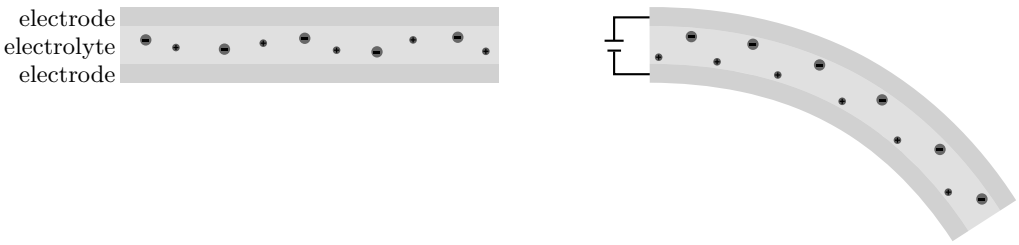

Figure 4.1: Actuator with layer structure of two electrodes sandwiching a solid electrolyte. Upon application of an electric potential, charges in the electrolyte move and induce swelling in the electroactive polymer that translates to bending of the actuator.

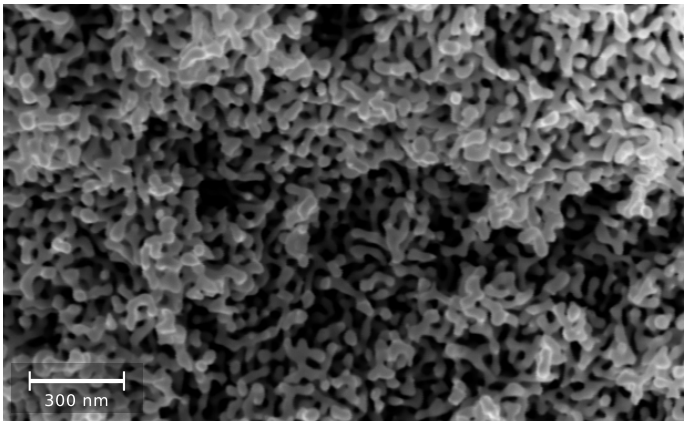

Figure 4.2: Scanning electron micrograph of nanoporous gold showing the interconnected network of pores. The gold ligaments have a diameter of ca. 30 nm.
Image courtesy of Nadiia Mameka at Helmholtz-Zentrum Geesthacht and reproduced from [143].

contacted as depicted in Fig. 4.1. In this setup, the EAP may, depending on its type, be used as either the electrode [45] or the electrolyte [85, 103].

An alternative setup that has been gaining interest recently are nanocomposites, combining nanoscale metals with electroactive polymers [37, 83, 87]. One promising material for the metallic phase are nanoporous metals, which are monolithic materials made up of an interconnected network of nanoscale metal wires or ligaments as visible in the micrograph of nanoporous gold in Fig 4.2. The pores giving the material its name form a continuous network and, thus, yield an exceptionally high surface-to-volume ratio. This high surface-to-volume ratio is known to be responsible for actuation behaviour in response to an applied electric field due to charging of the metal's surface and adsorption of ions from a liquid electrolyte [77, 82, 140].

Recent experiments at the Institute of Materials Physics and Technology at Hamburg University of Technology investigate the possibility of replacing the liquid electrolyte with a solid EAP, thus, forming a bicontinuous, electroactive nanocomposite. Usage of a solid electrolyte would significantly expand the range of possible applications due to the fact that such composites can be operated in air and do not require caring for the possible corrosiveness or flammability of the electrolyte.

However, replacing the liquid electrolyte by a polymer is evidently not a one-to-one substitution, as the polymer affects the mechanical behaviour of the nanoporous metal and even introduces possible new deformation mechanisms [14, 136]. Furthermore, ion transport in

the polymer is much slower than in a liquid and the polymer's behaviour may be affected by the constrained space and the formation of interphase areas. Computational modelling of the composites makes it possible to study such effects and, thus, offer insights into the material behaviour that are inaccessible from experiments, such as the nature of the superposition of the metal's and the polymer's actuation behaviour or the mechanisms involved in ion transport. Therefore, a modelling framework for such nanoporous metal/EAP composites is developed in the following.

Electroactive nanocomposites are a very recent development and, thus, no dedicated models for their behaviour exist as of yet. There are, however, numerous publications on modelling ionomeric polymer/metal composites, also called IPMCs, that are typically realised in the layered bending setup introduced in Fig. 4.1. Here, the ionomeric polymer is utilised as the carrier medium for ions that are introduced to the polymer by soaking it in a liquid electrolyte. This imbued polymer is then sandwiched between metal film electrodes and the bending motion is induced by the formation of space charge regions at the electrodes due to ion transport in an applied electric field. This bending setup is utilised in a number of phenomenological modelling approaches that are based on beam deflection theory and focus on the relationship between applied potential and deformation without explicitly taking the ion transport into account [2, 45, 97].

In [99, 100], a more general approach accounting for the chemo-electromechanical coupling in IPMCs is introduced by coupling ion transport to the induced deformation by introducing a microstructurally informed relation for the electromechanical coupling. This and similar approaches have been used and further extended in a number of works describing actuating [28, 72, 105, 135] behaviour, back relaxation phenomena [111] and sensing [26, 46].

These models introduce many concepts applicable in the description of various types of electroactive polymers. However, the details of the electromechanical coupling mechanisms in different kinds of EAPs vary significantly. In this thesis, dry electrolytes and intrinsically conducting polymers are considered. The complex ion transport behaviour in conjugated polymers, cf., Section 4.2, is modelled in [138] without consideration of electromechanical effects. In [127], a constitutive model is introduced that relates the ion uptake caused by a gradient in chemical potential to the induced strain for polypyrrole. Bay et al. [17] present a multiphysically coupled model examining the thermodynamics of volume change in conducting polymers and point out the importance of osmotic pressure for the actuation behaviour.

Despite this quantity of available modelling approaches, there exists no all-encompassing theory for the description of ionically activated EAPs, because their behaviour tends to be a superposition of many effects that not all are fully understood as of yet. Furthermore, the actuation mechanisms in different types of polymer differ considerably, for example in the presence of a liquid phase, the formation of clusters and the number of mobile ion species in the material. The modelling framework developed here focusses on the description of interface effects in electroactive polymer/metal composites that play a significant role in nanoscale materials such as composites based on nanoporous metals due to their high interface-to-volume ratio.

In the following, a short summary of the fundamentals of electromagnetism is given as the basis for modelling electromechanical coupling. In Section 4.2, different mechanisms of ion transport are outlined and a general theoretical description is presented. Section 4.3 focusses on the development of a general framework to model electromechanical coupling in EAPs.

To account for the effect of electro-adsorption of ions on composite interfaces, the interface elasticity framework is introduced and extended to coupled electro-mechanical behaviour. Based on these concepts, electromechanically coupled models for nanocomposites including a dry polymer electrolyte in Section 4.4 and conjugated polymer in Section 4.5 are established.

Parts of the models and numerical studies presented in this chapter have been published by Wilmers et al. in [143].

4.1 State of the art: Fundamentals of electromagnetism

Electromagnetism describes the interactions of charged particles with electric and magnetic fields. The force exhibited on a moving point charge e with the velocity $\boldsymbol{v}$ by electromagnetic fields is the Lorentz force $\boldsymbol{f} = e\,[\boldsymbol{e} + \boldsymbol{v} \times \boldsymbol{b}]$. Here, $\boldsymbol{e}$ denotes the electric field which is defined by the force it exerts on a stationary point charge and $\boldsymbol{b}$ is the magnetic induction field which exerts force on moving charges. Here and in the following, electromagnetic fields are marked in a sans-serif font.

Within the continuum framework, a distribution of discrete point charges e is "smeared" out to a continuous charge density function $q(\boldsymbol{x})$. With the average velocity of the individual charges $\boldsymbol{v}$, the electric current density $\boldsymbol{i}$ is given by $\boldsymbol{i} = q\,\boldsymbol{v}$.

Within an arbitrary volume V, the charge is a conserved quantity. That is, any change in charge within this volume arises from fluxes across the volume's boundary. Furthermore, charges are neither destroyed nor created. Thus, a further fundamental balance equation in addition to those presented in Section 2.2 is introduced to describe electromagnetic problems

$$\frac{\mathrm{d}}{\mathrm{d}t}\int_{\mathcal{B}} q\,\mathrm{d}v = -\int_{\partial\mathcal{B}} \boldsymbol{i}\cdot\boldsymbol{n}\,\mathrm{d}a\,. \tag{4.1}$$

Localisation of this balance of charge yields the local form

$$\dot{q} = -\mathrm{div}\,\boldsymbol{i}\,. \tag{4.2}$$

In vacuo, these charges are free moving. In condensed matter, however, the total charge density q is made up of these free charges q^f and "bound" charges q^b. The latter arise from dipole moments, i.e., localised separations of positive and negative charges that may be a permanent material characteristic or can be induced by an applied electric field $\boldsymbol{e}$. The dipole moment density in a material is expressed by the polarisation field vector $\boldsymbol{p}$. As information about the bound charges is in many cases of no interest, an auxiliary field, the electric displacement $\boldsymbol{d}$ is introduced with the definition $\boldsymbol{d} := \varepsilon_0\boldsymbol{e} + \boldsymbol{p}$, where ε_0 denotes the constant vacuum permittivity.

Similarly, the magnetisation $\boldsymbol{m}$ within a material is a property tied to matter and is zero in vacuo. Here, the auxilary field to be introduced for separating the effects is the magnetic field $\boldsymbol{h}$ defined by $\boldsymbol{h} := \mu_0^{-1}\boldsymbol{b} - \boldsymbol{m}$, where μ_0 is the constant vacuum permeability.

Using these field vectors, the general, time dependent electromagnetic behaviour in polarisable and magnetisable matter is described by the four Maxwell equations

$$\text{Gauß's law} \qquad \operatorname{div} \boldsymbol{d} = q^f \tag{4.3}$$

$$\text{Gauß's law for magnetism} \qquad \operatorname{div} \boldsymbol{b} = 0 \tag{4.4}$$

$$\text{Faraday's law of induction} \qquad \operatorname{curl} \boldsymbol{e} = -\frac{\partial \boldsymbol{b}}{\partial t} \tag{4.5}$$

$$\text{Ampere's circuital law} \qquad \operatorname{curl} \boldsymbol{h} = \boldsymbol{i}^f + \frac{\partial \boldsymbol{d}}{\partial t}\,. \tag{4.6}$$

Here, the two Gauß's laws relate the fields to their sources, i.e., free charge carriers are the sources of electric fields and the magnetic induction is source free. Faraday's law of induction states that variations in the magnetic induction induce an electric field, while Ampere's circuital law states that the flux of free charge carriers $\boldsymbol{i}^f$ and the displacement current induce magnetic fields. Combining Gauß's and Ampere's law yields the charge balance Eq. (4.2), thus, Maxwell's equations are compatible with this balance equation.

To fully describe a distinct material behaviour, additionally, constitutive equations are required that characterise the connections of the three electric and the three magnetic fields. The simplest and most well-known examples for these constitutive equation are those for a electrically and magnetically linear, isotropic material in which the polarisation $\boldsymbol{p}$ is proportional to the electric field and the magnetisation $\boldsymbol{m}$ is proportional to the magnetic induction. This yields the relations

$$\boldsymbol{d} = \varepsilon_r \varepsilon_0 \boldsymbol{e} \qquad \text{and} \qquad \boldsymbol{h} = \frac{1}{\mu_r \mu_0} \boldsymbol{b}\,, \tag{4.7}$$

with the relative permittivity ε_r and the relative permeability μ_r as material parameters.

Note that all these relations are given with respect to the current configuration. How the Maxwell equations have to be correctly formulated with respect to the reference configuration is subject to discussion in the literature, compare, e.g., [38, 139]. In this thesis, the pull-backs $\boldsymbol{E} = \boldsymbol{F}^T \cdot \boldsymbol{e}$, $\boldsymbol{H} = \boldsymbol{F}^T \cdot \boldsymbol{h}$, $\boldsymbol{D} = J\boldsymbol{F}^{-1} \cdot \boldsymbol{d}$ and $\boldsymbol{B} = J\boldsymbol{F}^{-1} \cdot \boldsymbol{b}$ as presented in [38] and [39] are employed, yielding the following Maxwell equations in the reference configuration:

$$\text{Gauß's law} \qquad \operatorname{Div} \boldsymbol{D} = q_0^f \tag{4.8}$$

$$\text{Gauß's law for magnetism} \qquad \operatorname{Div} \boldsymbol{B} = 0 \tag{4.9}$$

$$\text{Faraday's law of induction} \qquad \operatorname{Curl}\left(\boldsymbol{E} + \boldsymbol{F}^{-1} \cdot \boldsymbol{v} \times \boldsymbol{B}\right) = -\frac{\partial \boldsymbol{B}}{\partial t} \tag{4.10}$$

$$\text{Ampere's circuital law} \qquad \operatorname{Curl}\left(\boldsymbol{H} + \boldsymbol{F}^{-1} \cdot \boldsymbol{v} \times \boldsymbol{D}\right) = \boldsymbol{I}^f + \frac{\partial \boldsymbol{D}}{\partial t} \tag{4.11}$$

where $\boldsymbol{v} = \frac{\partial \boldsymbol{x}}{\partial t}$ is the velocity of a material particle. Furthermore, the pull-back operations for the polarisation and the magnetisation are assumed to be $\boldsymbol{P} = J\boldsymbol{F}^{-1} \cdot \boldsymbol{d}$ and $\boldsymbol{M} = \boldsymbol{F}^T \cdot \boldsymbol{m}$. With that, the definitions of the electric displacement field and the magnetic field in the spatial setting become

$$\boldsymbol{D} = \varepsilon_0 J \boldsymbol{C}^{-1} \cdot \boldsymbol{E} + \boldsymbol{P} \qquad \text{and} \qquad \boldsymbol{H} = \mu_0^{-1} J^{-1} \boldsymbol{C} \cdot \boldsymbol{B} - \boldsymbol{M}\,. \tag{4.12}$$

Note, however, that there are different possible choices for the pull-back of $\boldsymbol{p}$ and $\boldsymbol{m}$ that are equally valid [38].

4.2 State of the art: Ion transport in ionically activated EAPs

The class of ionically activated electroactive polymers can be further distinguished depending on various factors such as the conduction mechanisms, the chemical properties of the polymer or the need for a liquid electrolyte. An extensive overview about various kinds of ion-conducting polymers and polymer electrolytes is given in [63].

In the following, two types of ionically activated EAP will be considered, a "dry" setup and a "wet" one, where the "wet" EAPs operate within a liquid electrolyte. The "dry" EAPs, however, do not require a liquid component and themselves function as an electrolyte by dissolving a salt within the polymer network.

This solvation is facilitated by functional groups along the polymer chains that coordinate the ions and, thus, stabilise them within the network. The oldest and still most prominent example for a dry polymer electrolyte is poly(ethylene oxide) (PEO) which has an ether group in every monomer unit that acts as the stabilising group in ion solvation.

Ion transport in such dry EAPs and, thus, their conductivity is significantly lower than in liquid electrolytes [63] because it depends on conformational motion of the polymer chains. Through such movement of the polymer chain itself, the coordinated ions can be transported along the chain or be transferred from one chain to the next. Figure 4.3 presents a schematic depiction how such a movement between coordinating sites along the chain works. Slight movement of the polymer chain brings previously unoccupied coordinating groups in contact with the ion and, thus, allows the ion to hop from one site to the other and be carried through the polymer network. This mechanism allows for transport along the chain as well as from one chain to another.

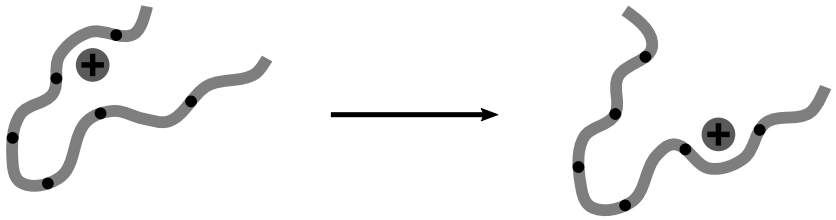

Figure 4.3: Schematic depiction of charge transport in a dry electroactive polymer. A coordinated ion is transported from one coordinating site (marked by black dots) on the chain to the next by movement of the polymer chain. This results in a net transport of the ion along the chain.

Such inter- and intra-chain hopping is only possible if the mobility of the polymer chains is high enough. The necessary molecular mobility is provided by local relaxation of the polymer. Hence, the ion transport is only possible due to relaxation processes [59], a phenomenon also well-known from anomalous diffusion, compare Chapter 3.

The conformational movement of the polymer chains is random. However, the net flux of ions is controlled by steric effects and interactions of the ion charges. Steric effects are related to the space occupied by an atom or molecule and the interaction of molecules with each other. As ions are charged particles, there are repulsive interactions between ions of the same charge and attractive forces between differently charged ions. The latter favours a balancing of the

charges due to the requirement of charge balance in a solid body. If a potential difference is applied to the EAP, the ions will be transported to balance charges arising at the electrodes, thus, forming regions of ion excess and depletion.

As ion transport is facilitated by conformational changes and movement of the base polymer chains, it causes deformation of the material. Further displacement and stresses are induced by the repulsive forces between the ions that cause an extension of the polymer network especially in regions of ion excess. These effects are utilized in actuator applications. Conversely, it is easy to see that a deformation of the polymer may evoke a redistribution of the charges that is measurable as an electric signal.

As no liquid electrolyte is necessary for operating dry EAPs such as PEO derivatives, they are especially useful for applications in which contact with corrodible materials is required or in which a highly flammable organic electrolyte would be a hazard. Furthermore, they can be operated in environments in which a liquid electrolyte would evaporate.

Despite these advantages of the dry setup, most EAPs rely on the presence of a liquid electrolyte to provide ions. In these systems, ions are incorporated into the polymer network by either swelling the polymer in the liquid (gel electrolytes or ionomeric polymers) and relying on classical transport within the electrolyte or by absorption of, possibly hydrated, ions from a surrounding electrolyte.

The latter mechanism is the one occurring in actuators based on electrically conducting polymers such as Polypyrrole (PPy) or Polyaniline (PANI). These are intrinsically conducting due to their characteristic chemical structure, a conjugated system of double bonds allowing for delocalisation of charges.

In the oxidised state, these polymers exhibit positive charges along the chains that facilitate electric conduction in a similar fashion as hole conduction in semiconductors. To maintain electro-neutrality, anions, i.e., negatively charged ions, are incorporated into the polymer network to balance these positive charges [115] which is referred to as “polymer doping”. Applying a reducing potential to this oxidised polymer will cause reduction of the polymer backbone, i.e., the polymer chain gains electrons and the positive charge vanishes. However, as the whole material still has to maintain electroneutrality, the incorporated ions have to be either expelled from the network or their charges have to be balanced by incorporation of ions from the environment, i.e., the electrolyte, thus, causing a net ion transport in reaction to an applied electric field.

This process is depicted schematically in Fig. 4.4. Starting from the oxidised and doped state, two different reduction paths are possible:

(1) $\mathrm{P}^{n+} \cdot n\,\mathrm{A}^- + n\,\mathrm{C}^+ + n\,\mathrm{e}^- \rightleftharpoons \mathrm{P}^0 \cdot n\,\mathrm{A}^- \cdot n\,\mathrm{C}^+$

(2) $\mathrm{P}^{n+} \cdot n\,\mathrm{A}^- + n\,\mathrm{e}^- \rightleftharpoons \mathrm{P}^0 + n\,\mathrm{A}^-$.

Here, P denotes the polymer and A^- and C^+ the anion and the cation, respectively. Note that, here, the simplest case of monovalent ions is chosen only for readability and, in reality, higher and differing valence numbers are possible.

In path (2), the anions are expelled from the polymer network while in path (1) the anions remain distributed in the polymer and their charges are balanced by uptake of cations from the liquid electrolyte. The latter reaction goes along with an increase in volume of the polymer while ejection of ions causes shrinking. Both processes are entirely reversible.

Which process occurs, depends primarily on the mobility of the involved ion species in the polymer. For large, immobile anions, only reaction path (1) is viable, thus, causing swelling

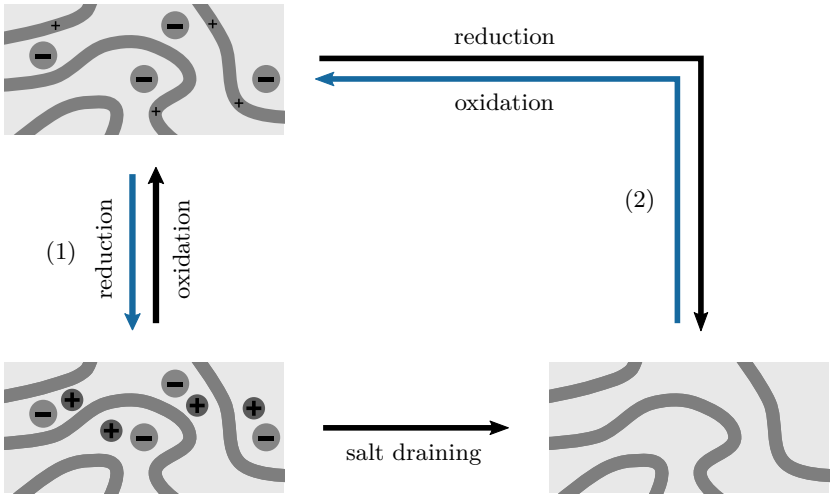

Figure 4.4: Schematic depiction of ion transport in a conjugated polymer. Oxidation induces positive charges along the polymer backbone. To maintain electroneutrality, charges arising during redox reactions are balanced by incorporation or ejection of electrolyte ions into the polymer network, thus, inducing swelling or shrinking of the polymer. Blue arrows denote processes in which the volume increases, black arrows denote decrease in volume.
The two possible redox reactions may occur simultaneously depending on the size and mobility of the ions.

during reduction and shrinking upon subsequent oxidation. If the anions are medium-sized and mobile, both processes may occur simultaneously, influenced further by the applied electric potential and pH. Furthermore, small and mobile ions allow for so-called "salt draining" in which cations and anions bond together to form a neutral salt and diffuse from the polymer, causing contraction. This superposition of multiple mechanisms with opposing effects results in fluctuating actuator responses as visible for example in the cyclic voltametry experiments in [58]. Hence, immobilising either the anion or the cation and, thus, having only a single moving species, is usually desirable for actuator applications [115].

The two types of ionically activated EAPs considered in this thesis exhibit very different mechanisms for both ion transport and actuation. These mechanisms, however, are driven by the same forces as they are reactions to potential differences and concentration distributions. Therefore, they can be described using the same governing principles.

4.2.1 Governing equations

The fundamental balance equation governing the ion transport in electroactive polymers is, as for any mass transport, the balance of mass of the individual ion species i

$$\dot{c}_0^i = -\mathrm{Div}\, \boldsymbol{J}^i + W^i \,, \tag{4.13}$$

see also Eq. (2.10). The sources W^i cannot be neglected here as done in Chapter 3 because chemical reactions are possible in the considered EAPs, leading to, e.g., salt draining.

This equation holds for every ion species. In the simplest case, this yields two equations, one for the anions and one for the cations. However, in reality, multiple species of ions with the same charge may be present, e.g., doped conjugated polymers may be used in electrolytes

providing a different anion and ion exchange between the polymer and the electrolyte might occur.

To describe the electric fields, the Maxwell equations of electrostatics are employed. Reduction to electrostatics is a valid simplification in the case of EAPs as the transport within the polymer network is so slow that any response of the electromagnetic fields can, in comparison, be considered as instantaneous.

Thus, any magnetic fields and effects can be neglected, and Eq. (4.8) and Eq. (4.10) are reduced to

$$0 = -\mathrm{Div}\,\boldsymbol{D} + q_0^f(\boldsymbol{X}) \tag{4.14}$$

$$\boldsymbol{0} = \quad \mathrm{Curl}\,\boldsymbol{E}\,. \tag{4.15}$$

As different charges cancel each other, the free charge density q_0^f is the sum of the charge densities of the different charge types present:

$$q_0^f(\boldsymbol{X}) = F\sum_i z^i\, c_0^i(\boldsymbol{X}) + q_0^p(\boldsymbol{X}). \tag{4.16}$$

Here, F denotes the Faraday constant [C/mol] which gives the charge of 1 mol of elementary charges. With the charge number or valence z^i and the molar concentration c_0^i, this yields the total charge density of all ions of species i. The distribution of charges on the polymer chain is described by $q_0^p(\boldsymbol{X})$. For the dry setup, $q_0^p = 0$ while for the conjugated polymers its spatial distribution is approximately homogeneous.

Equation (4.15) states that the electric field $\boldsymbol{E}$ is irrotational in electrostatics, i.e., it is a conservative field that can be expressed as the gradient of a scalar potential function. This potential is called the electric or electrostatic potential Φ and is defined by $\boldsymbol{E} =: -\mathrm{Grad}\,\Phi$.

4.2.2 Constitutive relations

The set of equations (4.13) - (4.15) is completed with constitutive equations for the ion flux and the electric fields. The transport of ions within electric fields is as described driven by the potential gradient but is also influenced by concentration gradients and any superimposed convective transport. Thus, the flux $\boldsymbol{J}^i$ of ion species i is described by the Nernst-Planck equation [147] as the sum of the fluxes arising from convection, diffusion and migration as

$$\begin{aligned}\boldsymbol{J}^i &= \boldsymbol{J}^{i\,\mathrm{convection}} + \boldsymbol{J}^{i\,\mathrm{diffusion}} \quad + \boldsymbol{J}^{i\,\mathrm{migration}} \\ &= c_0^i\boldsymbol{v}^i \qquad\quad - \boldsymbol{D}^i\cdot\mathrm{Grad}\,c_0^i - c_0^i\frac{z^iF}{RT}\boldsymbol{D}^i\cdot\mathrm{Grad}\,\Phi\end{aligned} \tag{4.17}$$

where $\boldsymbol{v}$ denotes a possible solvent velocity that in general is zero for all kinds of electroactive polymers. Furthermore, $\boldsymbol{D}^i$ is the diffusion coefficient, R the gas constant and T the temperature. Here, the Einstein relation is assumed, relating the diffusivity $\boldsymbol{D}^i$ and mobility $\boldsymbol{m}^i$ of the ions by $\boldsymbol{D}^i/\boldsymbol{m}^i = RT/F$. However, there is discussion about the Einstein relation being valid for the high ion concentrations possible in conjugated polymers [138].

Equation (4.17) describes the ion transport in both, dry EAPs and conjugated polymers. The repulsive and attractive forces between the ions are accounted for in the migration com-

ponent of the flux while chain mobility and transport of ions from an electrolyte as well as the arising steric effects are described by the diffusion component.

The EAPs considered here are homogeneous and can be described as electrically isotropic and linear, cf., Eq. (4.18). In these materials, the polarisation field is parallel and proportional to the electric field, i.e., $\boldsymbol{P} = \chi J \boldsymbol{C}^{-1} \cdot \boldsymbol{E}$. This, in turn, allows to express the definition of the nominal electric displacement field as

$$\boldsymbol{D} = \varepsilon_0 \left[1 + \chi\right] J \boldsymbol{C}^{-1} \cdot \boldsymbol{E} = \varepsilon_0 \varepsilon_r J \boldsymbol{C}^{-1} \cdot \boldsymbol{E} \,, \tag{4.18}$$

introducing the relative permittivity ε_r as 1 plus the electric susceptibility χ.

Equation (4.17) shows that ion transport is driven by a gradient in concentration as typical for mass transport as well as a gradient in the electric potential due to the influence of electric fields on the charged ions, thus, yielding an electrochemically coupled transport problem. Furthermore, as is evident from Eq. (4.18), the electric displacement depends on the deformation.

With this set of coupled governing and constitutive equations, the ion transport within any electroactive polymer is fully described. To take into account the actual actuation behaviour, the mechanisms of electromagnetic coupling have to be investigated.

4.3 Modelling electromechanical coupling in nanoscale EAP/metal composites

The transport of ions in an applied electric field as described in the previous section induces stresses and deformation in the material, i.e., an electromechanical coupling in the bulk polymer. This deformation is reversible and caused by the uptake and ejection of ions from the polymer network in case of conjugated polymers or the build-up of space charges, i.e., ion accumulation in some areas and other areas that are ion-deprived, in dry EAPs. Thus, independent of the underlying mechanism, the arising deformation depends on the ion concentration.

Furthermore, when using EAPs in composites, the migration brings ions into contact with the, here metallic, second phase, where they can be electroadsorbed and, thus, alter the interface properties. Especially in composites of EAPs with nanoporous metals, such effects may have a pronounced influence on the overall behaviour of the composite, as, due to their very high surface-to-volume ratio, seemingly small surface modifications strongly affect their behaviour. For example changes in the surface state induce stresses and strains in the bulk material, leading to macroscopic deformation and, thus, actuation behaviour in nanoporous metals themselves [77]. It has been shown that electrically induced modifications of the nanoporous metal's surface also result in a change of its mechanical properties. For instance, in [89], a compression test is conducted on a nanoporous gold sample immersed in a liquid electrolyte during potential sweeps, showing that the material's stiffness can be increased by up to $\sim 8\,\%$ by surface modification. It stands to reason that these effects occur in EAP/nanoporous metal composites as well, resulting in a considerably more complex actuation behaviour, as the interface effects of the metal and the polymer's deformation are superimposed.

In the following, a modelling framework for the description of electroactive metal/polymer composite is developed that incorporates electromechanical coupling in the bulk as well as

coupling effects arising from modification of the metal/polymer interface. To this end, interface elasticity is combined with a continuum mechanical model coupling the mechanical behaviour of the metal and the polymer with ion transport in an electric field as described in Section 4.2.

The development of this framework as presented here has been published in [143] are reproduced here according to the license agreement.

Classic continuum theories generally do not account for the influence surfaces and interfaces have on the response of the bulk material as these effects are often negligible. However, their role becomes significant if one considers nanoporous materials which are characterised by a large surface-to-volume ratio. In the proposed model, the critical impact of interfaces on the overall functionality of the electroactive composite is described using an extension of the surface elasticity theory of Gurtin and Murdoch [62]. In this theory, surfaces are endowed with their own thermodynamic structure, that is, they have their own free energy and a resulting stress measure which is governed by a balance relation.

A metal/ion-conducting polymer composite can be described as a body consisting of three physical domains that exhibit considerably different behaviour, namely the metal, the polymer, and the metal/polymer interface. In the model, this is represented in a decomposition of a continuum body $\mathscr{B}_0$ in the reference configuration according to $\mathscr{B}_0 = \mathcal{B}_0^m \,\dot\cup\, \mathcal{I}_0 \,\dot\cup\, \mathcal{B}_0^p$, cf. Fig. 4.5, where the disjoint union $\mathcal{B}_0 := \mathcal{B}_0^m \,\dot\cup\, \mathcal{B}_0^p$ represents the bulk and $\mathcal{I}_0$ is the interface. Following the principles described in Section 2, the position of a material point in $\mathscr{B}_0$ is denoted by $\boldsymbol{X}$ and is mapped to the current configuration at time t via the motion $\boldsymbol{\varphi}$ as $\boldsymbol{x} = \boldsymbol{\varphi}(\boldsymbol{X}, t)$. The interface $\mathcal{I}_0$ is assumed to be material and geometrically coherent, i.e., there is no discontinuity in the motion $\boldsymbol{\varphi}$ over the interface and a material point on the interface is denoted by $\overline{\boldsymbol{X}} = \boldsymbol{X}|_{\mathcal{I}_0}$. Here and in the following, interface properties are denoted by an overbar $\overline{\bullet}$. Furthermore, no bulk material is transported over the interface, i.e., every material point $\boldsymbol{X}^m$, $\boldsymbol{X}^p$ and $\overline{\boldsymbol{X}}$ remains in its initial domain.

The deformation gradients in the bulk and on the interface are defined by

$$\boldsymbol{F} := \operatorname{Grad} \boldsymbol{\varphi} \qquad \text{and} \qquad \overline{\boldsymbol{F}} := \overline{\operatorname{Grad}}\, \overline{\boldsymbol{\varphi}}\,,$$

where the interface gradient operator is the projection of the bulk operator to the interface according to $\overline{\operatorname{Grad}}\, \bullet := \operatorname{Grad} \bullet \cdot \overline{\boldsymbol{I}}$ with the rank-deficient second-order interface identity tensor $\overline{\boldsymbol{I}} := \boldsymbol{I} - \overline{\boldsymbol{N}} \otimes \overline{\boldsymbol{N}}$. The interface divergence is defined by $\overline{\operatorname{Div}}\, \bullet := \overline{\operatorname{Grad}}\, \bullet : \overline{\boldsymbol{I}}$. A jump of a quantity $\bullet$ over the interface $\mathcal{I}_0$ is defined by $[\![\bullet]\!] := \bullet|_{\mathcal{I}_0^m} - \bullet|_{\mathcal{I}_0^p}$, where $\mathcal{I}_0^m$ and $\mathcal{I}_0^p$ denote the two sides of the interface.

The extended divergence theorems in the bulk and on the interface are given by

$$\int_{\mathcal{B}_0} \operatorname{Div}(\bullet)\, \mathrm{d}V = \int_{\partial\mathcal{B}_0} \bullet \cdot \boldsymbol{N}\, \mathrm{d}A - \int_{\mathcal{I}_0} [\![\bullet]\!] \cdot \overline{\boldsymbol{N}}\, \mathrm{d}A\,, \tag{4.19a}$$

$$\int_{\mathcal{I}_0} \overline{\operatorname{Div}}(\overline{\bullet})\, \mathrm{d}V = \int_{\partial\mathcal{I}_0} \overline{\bullet} \cdot \widetilde{\boldsymbol{N}}\, \mathrm{d}L + \int_{\mathcal{I}_0} \overline{\operatorname{Div}}\, \overline{\boldsymbol{N}}\, \overline{\bullet} \cdot \overline{\boldsymbol{N}}\, \mathrm{d}A\,, \tag{4.19b}$$

where $\boldsymbol{N}$ and $\widetilde{\boldsymbol{N}}$ are the normal vectors to the body's surface and curve of the interface, respectively. Further details on the derivation are given in [74].

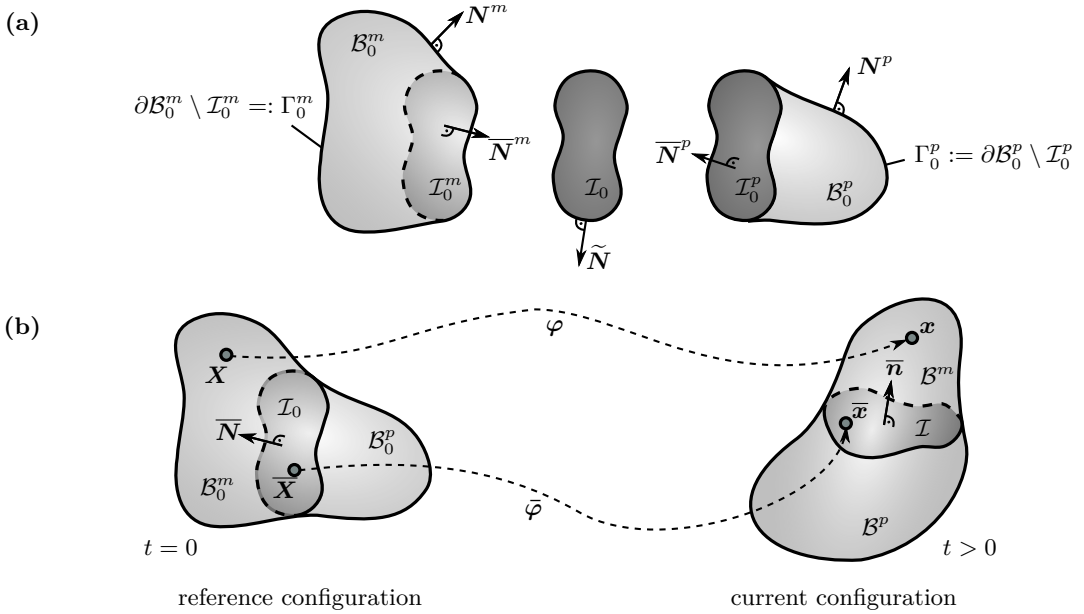

Figure 4.5: Schematic representation of a continuum body $\mathcal{B}_0$ that is separated into two domains $\mathcal{B}_0^m$ and $\mathcal{B}_0^p$ by the coherent interface $\mathcal{I}_0$. (a) Each of the two volumes includes one side of the interface $\mathcal{I}_0$. For the corresponding interface normals the relation $\overline{\boldsymbol{N}}(\boldsymbol{X}) := \overline{\boldsymbol{N}}^p(\boldsymbol{X}) = -\overline{\boldsymbol{N}}^m(\boldsymbol{X})$ holds. (b) Material points are mapped from the reference configuration to the current configuration by the motions $\boldsymbol{\varphi}$ and $\overline{\boldsymbol{\varphi}} = \boldsymbol{\varphi}|_{\mathcal{I}_0}$.
This figure was published in [143], Copyright Elsevier (2017).

Using these definitions and identities, the governing equations for the primary fields, i.e., the displacement, electric potential and ion concentration, in the bulk and on the interface are derived from fundamental balance equations.

4.3.1 Deformation

Following the argumentation presented in, e. g., [76] and extending it to account for inertial effects, the global balance of linear momentum for a continuum body with a coherent interface can be derived from the integral balance:

$$\int_{\mathcal{B}_0} \rho_0 \ddot{\boldsymbol{u}}\,\mathrm{d}V + \int_{\mathcal{I}_0} \overline{\rho}_0 \ddot{\overline{\boldsymbol{u}}}\,\mathrm{d}A = \int_{\partial\mathcal{B}_0} \boldsymbol{P}\cdot\boldsymbol{N}\,\mathrm{d}A + \int_{\partial\mathcal{I}_0} \overline{\boldsymbol{P}}\cdot\widetilde{\boldsymbol{N}}\,\mathrm{d}L + \int_{\mathcal{B}_0} \rho_0\boldsymbol{b}\,\mathrm{d}V + \int_{\mathcal{I}_0} \overline{\rho}_0\overline{\boldsymbol{b}}\,\mathrm{d}A\,. \quad (4.20)$$

Here, ρ_0 $[\frac{\mathrm{kg}}{\mathrm{m}^3}]$ and $\overline{\rho}_0$ $[\frac{\mathrm{kg}}{\mathrm{m}^2}]$ are the mass densities with respect to the reference bulk volume and reference interface area, respectively. The superimposed dots denote time derivatives which are well-defined on the interface as every material point $\overline{\boldsymbol{X}}$ remains in the interface domain during deformation. For details in case of a moving interface, refer to [22].

As the interface is assumed to be mechanically coherent, there is no jump in the displacement over the interface and, hence, $\overline{\boldsymbol{u}} = \boldsymbol{u}|_{\mathcal{I}_0^p} = \boldsymbol{u}|_{\mathcal{I}_0^m}$.

Localising Eq. (4.20) for an arbitrary control region in the bulk that does not include any part of the interface yields the balance of linear momentum in the well known form

$$\rho_0\ddot{\boldsymbol{u}} = \mathrm{Div}\,\boldsymbol{P} + \rho_0\boldsymbol{b} \qquad \text{in } \mathcal{B}_0\,, \quad (4.21)$$

cf. Eq. (3.20).

Using the divergence theorems in the bulk Eq. (4.19a) and on the interface Eq. (4.19b), the balance of linear momentum at a point $\overline{\boldsymbol{X}} \in \mathcal{I}_0$ becomes

$$\frac{\mathrm{D}}{\mathrm{D}t}\left[\int_{\mathcal{B}_0} \rho_0 \dot{\boldsymbol{u}}\,\mathrm{d}V + \int_{\mathcal{I}_0} \overline{\rho}_0 \dot{\overline{\boldsymbol{u}}}\,\mathrm{d}A\right] = \int_{\mathcal{B}_0} \operatorname{Div} \boldsymbol{P}\,\mathrm{d}V - \int_{\mathcal{I}_0} [\![\boldsymbol{P}]\!] \cdot \overline{\boldsymbol{N}}\,\mathrm{d}A + \int_{\mathcal{I}_0} \overline{\operatorname{Div}}\,\overline{\boldsymbol{P}}\,\mathrm{d}A + \int_{\partial\mathcal{I}_0} \overline{\operatorname{Div}}\,\overline{\boldsymbol{N}}[\overline{\boldsymbol{P}} \cdot \overline{\boldsymbol{N}}]\,\mathrm{d}L + \int_{\mathcal{B}_0} \rho_0 \boldsymbol{b}\,\mathrm{d}V + \int_{\mathcal{I}_0} \overline{\rho}_0 \overline{\boldsymbol{b}}\,\mathrm{d}A\,. \tag{4.22}$$

Considering that the interface Piola-Kirchhoff stress $\overline{\boldsymbol{P}}$ is, by definition, a superficial tensor and, therefore, $\overline{\boldsymbol{P}} \cdot \overline{\boldsymbol{N}} = \boldsymbol{0}$, localisation for the case $\mathcal{B}_0 \to \emptyset$ (resp. $\mathscr{B}_0 \to \mathcal{I}_0$) yields

$$\overline{\rho}_0 \ddot{\overline{\boldsymbol{u}}} = \overline{\operatorname{Div}}\,\overline{\boldsymbol{P}} + \overline{\boldsymbol{B}} + [\![\boldsymbol{P}]\!] \cdot \overline{\boldsymbol{N}} \qquad \text{on } \mathcal{I}_0. \tag{4.23}$$

Following a similar argument as presented in [74], the balance of angular momentum yields

$$\boldsymbol{F} \cdot \boldsymbol{P}^T = \boldsymbol{P} \cdot \boldsymbol{F}^T \qquad \text{in } \mathcal{B}_0 \tag{4.24}$$

$$\overline{\boldsymbol{F}} \cdot \overline{\boldsymbol{P}}^T = \overline{\boldsymbol{P}} \cdot \overline{\boldsymbol{F}}^T \qquad \text{on } \mathcal{I}_0\,. \tag{4.25}$$

4.3.2 Electrostatics

For ion-conducting polymers, any changes in the electric fields can be considered instantaneous in comparison to the slow ion transport. Therefore, the development of electric fields upon application of an electric potential is described within the electrostatic (i. e., steady state) framework. Furthermore, magnetic fields are not considered as their influence on ion transport is negligible.

The electrostatic framework is governed by Faraday's and Gauß's laws as detailed in Section 4.2.1. Following the argumentation presented in [24] (an electrostatics framework accounting for surface effects), the electric field on the interface is tangential and, therefore, Faraday's law reduces to it's classical form

$$\begin{aligned} \boldsymbol{0} &= \operatorname{Curl} \boldsymbol{E} && \text{in } \mathcal{B}_0 \\ \boldsymbol{0} &= \overline{\boldsymbol{N}} \times [\![\boldsymbol{E}]\!] && \text{on } \mathcal{I}_0\,. \end{aligned}$$

With these relations, the electric potential can be defined by $\boldsymbol{E} =: -\operatorname{Grad}\Phi$.

Gauß's law relates the electric flux through a closed surface to the enclosed electric charges and can be alternatively derived from temporal integration of the charge balance. For the bulk and the interface, the integral form of Gauß's law is given by

$$0 = -\int_{\partial\mathcal{B}_0} \boldsymbol{D} \cdot \boldsymbol{N}\,\mathrm{d}A - \int_{\partial\mathcal{I}_0} \overline{\boldsymbol{D}} \cdot \widetilde{\boldsymbol{N}}\,\mathrm{d}L + \int_{\mathcal{B}_0} q_0^f\,\mathrm{d}V + \int_{\mathcal{I}_0} \overline{q}_0^f\,\mathrm{d}A\,, \tag{4.26}$$

where the free charge density q_0^f is the sum over all free charges present and, thus, is expressed in terms of the concentrations of the different charge carrier types c_0^i as $q_0^f(\boldsymbol{X}) = F \sum_i z^i c_0^i(\boldsymbol{X})$ with the Faraday constant F and the species valence z^i.

Localisation of Eq. (4.26) using the same arguments employed for the linear momentum balance in Section 4.3.1 and applying the divergence theorems for the bulk Eq. (4.19a) and

the interface Eq. (4.19b) yields

$$0 = -\operatorname{Div} \boldsymbol{D} + q_0^f \qquad \text{in } \mathcal{B}_0 \tag{4.27}$$

$$0 = -\overline{\operatorname{Div}}\, \overline{\boldsymbol{D}} + \overline{\operatorname{Div}}\, \overline{\boldsymbol{N}} \left[\overline{\boldsymbol{D}} \cdot \overline{\boldsymbol{N}}\right] + \overline{q}_0^f - [\![\boldsymbol{D}]\!] \cdot \overline{\boldsymbol{N}} \qquad \text{on } \mathcal{I}_0\,. \tag{4.28}$$

Note that, as the electric displacement field originates from free charges that emit fields in all directions (see Fig. 4.6), $\overline{\boldsymbol{D}}$ is (in contrast to the interface stress and interface flux) not a tangential vector. Thus, the second right-hand-side term in Eq. (4.28) does not vanish as it does in the other interface equations.

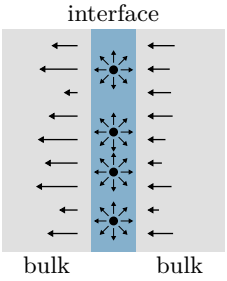

Figure 4.6: Schematic representation of the electric field induced by (positive) interface charges. This figure was published in [143], Copyright Elsevier (2017).

4.3.3 Charge carrier transport

Charge carriers are transported within a body as a reaction to an applied electric field. To describe this transport, the balance of mobile species mass is evaluated, as the charge carrier mass is a conserved quantity. The relations derived in the following are valid for any mass transport phenomenon, e.g., diffusion or advection. To maintain this generality, no assumptions about the continuity of material fluxes or concentrations over the boundary $\mathcal{I}_0$ are made.

The mass balance for the transported species i is expressed in terms of the mass concentration in the bulk c_0^i and on the interface $\overline{c}_0^i$. This yields the mass balance for the system

$$\begin{aligned}\int_{\mathcal{B}_0} \dot{c}_0^i \,\mathrm{d}V + \int_{\mathcal{I}_0} \dot{\overline{c}}_0^i \,\mathrm{d}A = &- \int_{\partial\mathcal{B}_0} \boldsymbol{J}^i \cdot \boldsymbol{N} \,\mathrm{d}A - \int_{\partial\mathcal{I}_0} \overline{\boldsymbol{J}}^i \cdot \widetilde{\boldsymbol{N}} \,\mathrm{d}L \\ &+ \int_{\mathcal{B}_0} W^i \,\mathrm{d}V + \int_{\mathcal{I}_0} \overline{W}^i \,\mathrm{d}A\,.\end{aligned} \tag{4.29}$$

The interface flux $\overline{\boldsymbol{J}}^i$ is a tangential vector that possesses the orthogonality property $\overline{\boldsymbol{J}}^i \cdot \overline{\boldsymbol{N}} = 0$.

Application of the divergence theorems (4.19a) and (4.19b) yields

$$\begin{aligned}\int_{\mathcal{B}_0} \dot{c}_0^i \,\mathrm{d}V + \int_{\mathcal{I}_0} \dot{\overline{c}}_0^i \,\mathrm{d}A = &- \int_{\mathcal{B}_0} \operatorname{Div} \boldsymbol{J}^i \,\mathrm{d}V - \int_{\mathcal{I}_0} [\![\boldsymbol{J}^i]\!] \cdot \overline{\boldsymbol{N}} \,\mathrm{d}A - \int_{\mathcal{I}_0} \overline{\operatorname{Div}}\, \overline{\boldsymbol{J}}^i \,\mathrm{d}A \\ &+ \int_{\mathcal{B}_0} W^i \,\mathrm{d}V + \int_{\mathcal{I}_0} \overline{W}^i \,\mathrm{d}A\,.\end{aligned} \tag{4.30}$$

Localisation of Eq. (4.30) to the bulk and to the interface yields, for every diffusing species i, the general diffusion laws

$$\dot{c}_0^i = -\operatorname{Div} \boldsymbol{J}^i + W^i \qquad \text{in } \mathcal{B}_0\,, \tag{4.31}$$

$$\dot{\overline{c}}_0^i = -\overline{\operatorname{Div}}\, \overline{\boldsymbol{J}}^i + \overline{W}^i - [\![\boldsymbol{J}^i]\!] \cdot \overline{\boldsymbol{N}} \qquad \text{on } \mathcal{I}_0\,. \tag{4.32}$$

Similarily, the diffusion laws with respect to an energetic surface are presented in [95].

The balance equations on the interface as established here are valid for any mass transport mechanism. The nature of the transport is described by the constitutive relations for the diffusion fluxes $\boldsymbol{J}^i$ and $\overline{\boldsymbol{J}}^i$. Furthermore, the behaviour at the interface has to be specified for different transport phenomena.

For the limiting case of a non-permeable interface, such as the one in a metal/ion-conducting polymer composite, $\boldsymbol{J}^i \cdot \overline{\boldsymbol{N}} = 0$ and, thus, any change in the interface concentration solely arises from interface effects according to $\dot{\overline{c}}_0 = -\overline{\operatorname{Div}}\, \overline{\boldsymbol{J}}^i + \overline{W}^i$.

Assuming continuity in the concentration over the interface, i.e., $[\![c_0^i]\!] = 0$, the interface concentration becomes $\overline{c}_0^i = c_0|_{\mathcal{I}_0^m} = c_0^i|_{\mathcal{I}_0^p} = c_0^i|_{\mathcal{I}_0}$. This case could be called a "highly diffusive" interface following the terminology for heat conduction across interfaces, cf., e. g., [74].

4.3.4 Balances of Energy and Entropy

Transport of ions within the polymer network is associated with "mixing" the ions with the polymer chains. As presented in Section 3.3.1, this mixing contributes to the system's internal energy and entropy via the specific enthalpy φ^{mix^i} and the specific entropy η^{mix^i} that together give the chemical potential of mixing $\mu^{\mathrm{mix}^i} = \varphi^{\mathrm{mix}^i} - T\eta^{\mathrm{mix}^i}$.

Furthermore, the charge carried by the ions contributes to the system's energy. In an electrostatic framework, the potential energy per charge is described by the electric potential Φ. Thus, the balance of internal energy of the system includes mechanical, electrical and chemical contributions:

$$\rho_0 \dot{\varepsilon} = \boldsymbol{P} : \dot{\boldsymbol{F}} - \dot{\boldsymbol{D}} \cdot \operatorname{Grad} \Phi - \sum_i \left[\Phi F z^i c_0^i - \varphi^{\mathrm{mix}^i} \dot{c}_0^i + \boldsymbol{J}^i \cdot \operatorname{Grad} \varphi^{\mathrm{mix}^i} \right] \qquad \text{in } \mathcal{B}_0 \tag{4.33}$$

$$\begin{aligned} \overline{\rho}_0 \dot{\overline{\varepsilon}} = {} & \overline{\boldsymbol{P}} : \dot{\overline{\boldsymbol{F}}} - \overline{\Phi} F \sum_i z^i \dot{\overline{c}}_0^i - \dot{\overline{\boldsymbol{D}}} \cdot \overline{\operatorname{Grad} \Phi} \\ & + \sum_i \left[\overline{\varphi}^{\mathrm{mix}^i} \dot{\overline{c}}_0^i - \overline{\boldsymbol{J}}^i \cdot \overline{\operatorname{Grad} \varphi}^{\mathrm{mix}^i} - \left[\varphi^{\mathrm{mix}^i} - \overline{\varphi}^{\mathrm{mix}^i} \right] [\![\boldsymbol{J}^i]\!] \cdot \overline{\boldsymbol{N}} \right] \end{aligned} \qquad \text{on } \mathcal{I}_0\,. \tag{4.34}$$

The derivation of this localised form from the full integral formulation is presented in Appendix B.

Here, a fully isothermal case is considered that, however, can be easily extended to account for thermal effects using the well-known principles of thermoelasticity, see Chapter 2 and [74].

The localised form of the entropy inequality for the isothermal case is

$$\rho_0 \dot{\eta} - \sum_i \left[\eta^{\mathrm{mix}^i} - \boldsymbol{J}^i \cdot \operatorname{Grad} \eta^{\mathrm{mix}^i} \right] \geq 0 \qquad \text{in } \mathcal{B}_0\,, \tag{4.35}$$

$$\overline{\rho}_0 \dot{\overline{\eta}} - \sum_i \left[\overline{\eta}^{\mathrm{mix}^i} - \overline{\boldsymbol{J}}^i \cdot \overline{\operatorname{Grad} \eta}^{\mathrm{mix}^i} \right] \geq 0 \qquad \text{on } \mathcal{I}_0\,, \tag{4.36}$$

Table 4.1: Governing equations in an electroactive composite

	bulk	interface
momentum	$\rho_0 \ddot{\boldsymbol{u}} = \operatorname{Div} \boldsymbol{P} + \rho_0 \boldsymbol{b}$	$\overline{\rho}_0 \ddot{\overline{\boldsymbol{u}}} = \overline{\operatorname{Div}}\, \overline{\boldsymbol{P}} + \overline{\rho}_0 \overline{\boldsymbol{b}} + [\![\boldsymbol{P}]\!] \cdot \overline{\boldsymbol{N}}$
Gauß's law	$0 = -\operatorname{Div} \boldsymbol{D} + q_0^f$	$0 = -\overline{\operatorname{Div}}\, \overline{\boldsymbol{D}} + \overline{\operatorname{Div}}\, \overline{\boldsymbol{N}} \left[\overline{\boldsymbol{D}} \cdot \overline{\boldsymbol{N}}\right] + \overline{q}_0^f - [\![\boldsymbol{D}]\!] \cdot \overline{\boldsymbol{N}}$
diffusion	$\dot{c}_0 = -\operatorname{Div} \boldsymbol{J} + W$	$\dot{\overline{c}}_0 = -\overline{\operatorname{Div}}\, \overline{\boldsymbol{J}} + \overline{W} - [\![\boldsymbol{J}]\!] \cdot \overline{\boldsymbol{N}}$

compare also Appendix B.

Substituting the balances of internal energy into the entropy inequalities and evaluating them using the Coleman-Noll formalism yields the constitutive relations

$$\begin{aligned} \boldsymbol{P} &= \rho_0 \frac{\partial \psi}{\partial \boldsymbol{F}} = 2\,\rho_0 \boldsymbol{F} \frac{\partial \psi}{\partial \boldsymbol{C}}\,, & \overline{\boldsymbol{P}} &= \overline{\rho}_0 \frac{\partial \overline{\psi}}{\partial \overline{\boldsymbol{F}}} = 2\,\overline{\rho}_0 \overline{\boldsymbol{F}} \frac{\partial \overline{\psi}}{\partial \overline{\boldsymbol{C}}}\,, \\ \boldsymbol{E} &= -\operatorname{Grad} \Phi = \rho_0 \frac{\partial \psi}{\partial \boldsymbol{D}}\,, & \overline{\boldsymbol{E}} &= -\overline{\operatorname{Grad}}\, \overline{\Phi} = \overline{\rho}_0 \frac{\partial \overline{\psi}}{\partial \overline{\boldsymbol{D}}}\,, \\ \mu^{\mathrm{mix}^i} &= F z^i \Phi + \rho_0 \frac{\partial \psi}{\partial c_0^i} & \overline{\mu}^{\mathrm{mix}^i} &= F z^i \overline{\Phi} + \overline{\rho}_0 \frac{\partial \overline{\psi}}{\partial \overline{c}_0^i}\,. \end{aligned}$$

as well as the requirements

$$\begin{aligned} &-\sum_i \boldsymbol{J}^i \cdot \operatorname{Grad} \mu^{\mathrm{mix}^i} \geq 0 \qquad \text{and} \\ &-\sum_i \left[\overline{\boldsymbol{J}}^i \cdot \overline{\operatorname{Grad}}\, \overline{\mu}^{\mathrm{mix}^i} + \left[\mu^{\mathrm{mix}^i} - \overline{\mu}^{\mathrm{mix}^i}\right] [\![\boldsymbol{J}^i]\!] \cdot \overline{\boldsymbol{N}}\right] \geq 0\,. \end{aligned} \tag{4.37}$$

For the bulk, these relations are identical to ones previously published for other types of electroactive polymers, compare, e.g., [23, 68].

4.4 Modelling of dry polymer electrolyte composites

The governing equations derived in Section 4.3 form a general framework for the description of the electromechanically coupled behaviour of composites based on ionically activated EAPs. In this and the following section, this framework is utilised in modelling composites of nanoporousgold and EAP.

Here, a dry polymer electrolyte such as polyethylene oxide is considered in which one ion species is immobile due to being covalently bond to the polymer chain. The counterion, however, is free to move, that is, the considered polymer is a dry single-ion-conducting polymer electrolyte [63], chosen here because of the straight-forward and controlled deformation behaviour resulting from only one mobile ion species. This setup is considered because it may be a possible transference of the actuation behaviour of nanoporous gold in a liquid electrolyte studied in [89] to a completely dry setup.

The contents of this section are reproduced here from [143].

4.4.1 Constitutive description

The governing equations describing the system are summarised in Table 4.1. In the following, the constitutive equations describing the different kinds of material behaviour observed in the dry polymer electrolyte, the metal and on the interface are presented.

Polymer electrolyte

The specific Helmholtz free energy is considered to be additively decomposed into a part describing the polymer's purely mechanical behaviour and two parts accounting for the electrically and ionically induced behaviour:

$$\psi(\boldsymbol{C}, c_0) = \psi^{\mathrm{mech}}(\boldsymbol{C}) + \psi^{\mathrm{electro}}(\boldsymbol{C}, \boldsymbol{D}) + \psi^{\mathrm{chem}}(\boldsymbol{C}, c_0)\,. \tag{4.38}$$

The purely mechanical part is modelled by a Neo-Hookean material model

$$\rho_0 \psi^{\mathrm{mech}}(\boldsymbol{C}) = \frac{\mu}{2}\left[\boldsymbol{C} - \boldsymbol{I}\right] : \boldsymbol{I} + \frac{\lambda}{2}\ln^2 J - \mu \ln J\,, \tag{4.39}$$

where μ and λ denote the Lamé parameters.

The electrical part of the free energy for an isotropic and electrically linear material is, following [23], given by

$$\rho_0 \psi^{\mathrm{electro}}(\boldsymbol{C}, \boldsymbol{D}) = \frac{1}{2\varepsilon_r \varepsilon_0} \frac{\boldsymbol{C} : \boldsymbol{D} \otimes \boldsymbol{D}}{J}\,. \tag{4.40}$$

The chemical contribution to the Helmholtz free energy density comprises a term accounting for the chemomechanically coupled behaviour and a classical expression for the mixing contribution:

$$\rho_0 \psi^{\mathrm{chem}}(\boldsymbol{C}, c_0^{\mathrm{mobile}}) = -\frac{1}{z^{\mathrm{mobile}}} k\, q_0^f \ln J + RT \left[\ln\left(\frac{c_0^{\mathrm{mobile}}}{c_0^{\mathrm{initial}}}\right) c_0^{\mathrm{mobile}} - c_0^{\mathrm{mobile}}\right]\,. \tag{4.41}$$

Here, k is a proportionality constant and c_0^{intial} denotes the mobile ion concentration in the initial state without any loads or potential differences applied. The first term on the right hand side of Eq. (4.41) describes changes in the free energy due to the coupled behaviour as arising from changes in the free charge density in the material q_0^f that is for the considered case of a single-ion-conducting dry electrolyte given by

$$q_0^f = F\left[z^{\mathrm{mobile}} c_0^{\mathrm{mobile}} + z^{\mathrm{immobile}} c_0^{\mathrm{immobile}}\right]\,, \tag{4.42}$$

and, thus, reflects changes in the concentration of mobile ions. This formulation is adapted from considerations in [100] in which the electrochemomechanical coupling in a ionomeric polymer is described based on micromechanical considerations. Note, that this formulation for the chemical or ionically induced part of the Helmholtz free energy is limited to the fundamental processes in the material as the focus of this work is the development of a model accounting for interface elasticity effects in electromechanical coupling. More complicated formulations could, for example, take size effects into account, cf. [18, 80].

With this Helmholtz free energy, the first Piola-Kirchhoff stress tensor $\boldsymbol{P}$ is decomposed into a purely mechanical, an electromechanical and a chemomechanical contribution as well:

$$\begin{aligned}\boldsymbol{P} = 2\boldsymbol{F}\cdot\frac{\partial\rho_0\psi}{\partial\boldsymbol{C}} =& \mu\boldsymbol{F} + [\lambda\ln J - \mu]\,\boldsymbol{F}^{-T} \\ &+ \frac{1}{J\varepsilon_r\varepsilon_0}\left[-0.5[\boldsymbol{C}:\boldsymbol{D}\otimes\boldsymbol{D}]\cdot\boldsymbol{F}^{-T} + \boldsymbol{F}\cdot\boldsymbol{D}\otimes\boldsymbol{D}\right] - \frac{1}{z}k\,q_0^f\boldsymbol{F}^{-T}\,.\end{aligned} \tag{4.43}$$

Note that, from here on, the superscript mobile is dropped for better readability.

The electromechanical coupling arises from two contributions, namely the purely electrically induced nominal Maxwell stress (e.g. [23, 44]) accounting for the stresses arising from forces induced during polarisation of the material and the ionically induced stress. The latter, $\boldsymbol{P}^{\text{chem}} = -1/zk\,q_0^f\boldsymbol{F}^{-T}$, is an extension of the relation given in [100] that also accounts for the mobile species valance z such that it is independent of the kind of mobile ion species and, thus, valid for various types of ion-conducting polymers. This coupling solely arises from stresses induced by the repulsive forces and molecular interactions arising in regions of high or low charge carrier concentration.

From the electrically induced part of the Helmholtz free energy it follows that the electric field is

$$\boldsymbol{E} = \frac{\partial\rho_0\psi}{\partial\boldsymbol{D}} = \frac{1}{J\varepsilon_r\varepsilon_0}\boldsymbol{C}\cdot\boldsymbol{D}\,. \tag{4.44}$$

This is identical to the classical expression for $\boldsymbol{D}$ in a polymer exhibiting isotropic and linear electric behaviour as given in Section 4.2. Recalling that the electric potential Φ is defined by $\boldsymbol{E} = -\text{Grad}\,\Phi$, Eq. (4.27) can, thus, be written as

$$0 = \text{Div}\,(\varepsilon_0\varepsilon_r\,J\boldsymbol{C}^{-1}\cdot\text{Grad}\,\Phi) + q_0^f\,.$$

The chemical potential of mixing is given by

$$\mu_s = \Phi F z + \frac{\partial\rho_0\psi}{\partial c_0} = Fz[\Phi - k\ln J] + RT\ln\left(\frac{c_0}{c_0^{\text{initial}}}\right)\,. \tag{4.45}$$

For the ion flux, the constitutive requirement $-\boldsymbol{J}\cdot\text{Grad}\,\mu_s \geq 0$ has to be fulfilled. Consequently, a formulation for the flux vector could be obtained from a relation such as $\boldsymbol{J} = -\boldsymbol{M}(\boldsymbol{C},\boldsymbol{D},c_0)\cdot\text{Grad}\,\mu_s$. However, here, the formulation for the ion flux is chosen by considering the driving forces of the ion transport in the polymer, i.e., the gradients in concentration and electric potential. Thus, the flux $\boldsymbol{J}$ of the mobile ion species is described by the Nernst-Planck equation (4.17) as the sum of the fluxes arising from diffusion and migration as

$$\boldsymbol{J} = -\boldsymbol{D}\cdot\text{Grad}\,c_0 - c_0\frac{zF}{RT}\boldsymbol{D}\cdot\text{Grad}\,\Phi\,, \tag{4.46}$$

which is consistent with classical models for charge transport, compare Section 4.2.2. This formulation is also obtainable from the gradient of the chemical potential when any contributions from deformational or pressure effects are neglected, cf., Appendix B.3.

Taking into account that no ions can be produced or destroyed within the material, this yields the diffusion law

$$\dot{c}_0 = \mathrm{Div}\,(\boldsymbol{D} \cdot \mathrm{Grad}\, c_0) + \frac{zF}{RT}\mathrm{Div}\,(c_0 \boldsymbol{D} \cdot \mathrm{Grad}\,\Phi) \tag{4.47}$$

for the mobile ions and a constant, homogeneous concentration distribution for the immobilised ions.

Metal

In a bulk metal, the charge carrier and electric potential distributions are perfectly homogeneous for all phenomena occurring in this application case. Any charge building up in the metal is strictly localised to the interface, thus, it is described by the interface model. Hence, no further information would be gained from modelling electrostatics or ion transport within the metal parts of the composite. Therefore, the modelling of the metal domain is limited to solving the momentum balance Eq. (4.24). As the processes in the actuator are fully reversible, only the elastic behaviour of the metal, in this case gold, in considered, using a Neo-Hookean constitutive relation for the Helmholtz free energy:

$$\rho_0 \psi(\boldsymbol{C}) = \frac{\mu}{2}\left[\boldsymbol{C} - \boldsymbol{I}\right] : \boldsymbol{I} + \frac{\lambda}{2}\ln^2 J - \mu \ln J\,. \tag{4.48}$$

Thus, the first Piola-Kirchhoff stress is given by

$$\boldsymbol{P} = 2\boldsymbol{F} \cdot \frac{\partial \rho_0 \psi}{\partial \boldsymbol{C}} = \mu \boldsymbol{F} + \left[\lambda \ln J - \mu\right] \boldsymbol{F}^{-T}\,. \tag{4.49}$$

Interface

As both bulk materials exhibit a Neo-Hookean mechanical behaviour, the interface between them does as well. To account for the interface modification that occurs due to either capacitive charging or ion adsorption on the interface, the Helmholtz free energy of the interface has to include a contribution depending on the charge density at the interface $\overline{q}_0^f$. To characterise the electro-elastic coupling in nanoporous gold immersed in a liquid electrolyte, the coupling parameter $\overline{\xi}$ has been introduced in [89] as the derivative of the surface elastic excess constant with respect to the surface charge density. Extending this definition to the interface Helmholtz free energy yields the definition

$$\overline{\xi}\,\overline{\boldsymbol{\mathcal{I}}} := -\frac{\partial^3 \overline{\rho}_0 \overline{\psi}}{\partial \overline{\boldsymbol{F}}^2 \partial \overline{q}_0^f}\,, \tag{4.50}$$

with $\overline{\boldsymbol{\mathcal{I}}}$ being the fourth-order interface identity tensor.

Electromechanical coupling at the interface arises from two different mechanisms that are connected to the two different kinds of charge carriers present in the composite. The mobile ions in the polymer can be adsorbed onto the interface, while on the metal side, an interface charge which balances the space charge in the polymer is build up by a shift of the electron concentration at the interface, see Fig. 4.7.

During electroadsorption, the monolayer of ions directly located at the polymer side of the interface $\overline{q}_0 = q_0|_{\mathcal{I}_0^p}$ is chemically adsorbed to the electrode and, thus, alters the interface

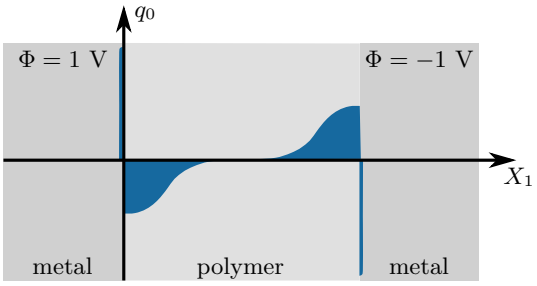

Figure 4.7: Charge density distribution in an electrochemical cell consisting of two metal electrodes with an ion-conducting polymer electrolyte sandwiched in between. In the polymer, ions accumulate in a broad area at the metal/polymer interface. This charge accumulation induces a balancing charge in the metal surface by causing an increased or lowered electron concentration. Both kinds of charge are involved in the electromechanical coupling.
Figure reproduced from [143].

energy. To describe this process, it is necessary to transfer the bulk concentration information to the interface using the relation $\overline{c}_0 = c_0 \frac{\overline{V}_0}{\overline{A}_0}$, where $\overline{A}_0$ denotes the reference interface area and $\overline{V}_0$ the polymer volume affecting the interface which, here, is considered to have a thickness of 2 nm in which all mobile ions are assumed to be electroadsorbed to the interface.

The build-up of an interface charge in response to an applied electric field in a metallic conductor is described by the interface electrostatic equation (4.28). Furthermore, the classic interface condition for electric fields $\overline{\boldsymbol{N}} \times [\![\boldsymbol{E}]\!] = 0$ holds (see also [24]), i.e., the tangential component of the electric field is continuous across the interface. In a metallic conductor $\boldsymbol{E} = \boldsymbol{0}$, thus, it follows that the electric potential distribution is perfectly homogeneous along the interface (in fact, in the subsequent numerical implementation the electric potential is applied as a boundary condition on the interface). Hence, no separate interface effects occur and Eq. (4.28) on the interface reduces to the classical interface relation in electrostatics

$$0 = \overline{q}_0^f - [\![\boldsymbol{D}]\!] \cdot \overline{\boldsymbol{N}} \,. \tag{4.51}$$

With this, the electromechanically coupled interface Helmholtz free energy is expressed as

$$\begin{aligned} \overline{\rho}_0 \overline{\psi}(\overline{\boldsymbol{F}}, \overline{q}_0^f) = & \frac{1}{2}\overline{\lambda} \ln^2 \overline{J} + \frac{1}{2}\overline{\mu}\left[\overline{\boldsymbol{F}} : \overline{\boldsymbol{F}} - 2 - 2\ln \overline{J}\right] - \frac{1}{2}\overline{\xi}\, \overline{q}_0^f \overline{\boldsymbol{F}} : \overline{\boldsymbol{F}} \\ & + R\overline{T}\left[\ln\left(\frac{\overline{c}_0}{\overline{c}_0^{\text{initial}}}\right)\overline{c}_0 - \overline{c}_0\right] , \end{aligned} \tag{4.52}$$

yielding an interface stress

$$\overline{\boldsymbol{P}} = \overline{\mu}\overline{\boldsymbol{F}} + \left[\overline{\lambda}\ln\overline{J} - \overline{\mu}\right]\overline{\boldsymbol{F}}^{-T} - \overline{\xi}\,\overline{q}_0^f \overline{\boldsymbol{F}} \,. \tag{4.53}$$

The charge carriers in a metal are electrons. Their transport along the interface is described by Eq. (4.32) which requires a constitutive expression for the diffusion flux $\overline{\boldsymbol{J}}$ that obeys the requirement Eq. (4.37b).

Table 4.2: Bulk material parameters and constants

	symbol	value	source
Faraday constant	F	96485.337 C/mol	
vacuum permittivity	ε_0	$8.854 \cdot 10^{-12}$ F/m	
polymer			
mass density	ρ_0	1.47 g/cm^3	[88]
Lamé parameters	λ	1.13 GPa	[128]
	μ	0.75 GPa	
relative permittivity	ε_r	$1 \cdot 10^3$	[6]
valence mobile species	z	-1	
mobile ion concentration	c_0	1200 mol/m^3	[106]
diffusivity	D	$10 \cdot 10^{-11}$ m^2/s	[106]
electromechanical coupling parameter	k	50 J/C	[100]
gold			
mass density	ρ_0	19.3 g/cm^3	
Lamé parameters	λ	198.6 GPa	[8]
	μ	27.08 GPa	

Here, a non-permeable interface is considered, so that $[\![\boldsymbol{J}]\!] \cdot \overline{\boldsymbol{N}} = 0$. Hence, Eq. (4.37b) reduces to the equivalent of the requirement for the bulk flux law:

$$-\overline{\boldsymbol{J}} \cdot \overline{\operatorname{Grad} \mu}^{\mathrm{mix}} \geq 0\,. \tag{4.54}$$

To ensure this, the flux is assumed to be of the general form $\overline{\boldsymbol{J}} = -\overline{\boldsymbol{M}}(\boldsymbol{C}, c_0^{\mathrm{el}}) \cdot \overline{\operatorname{Grad} \mu}^{\mathrm{mix}}$, where $\overline{\boldsymbol{M}}(\overline{\boldsymbol{C}}, \overline{c}_0^{\mathrm{el}})$ is a general mobility constant. With $\overline{\boldsymbol{D}} = R\overline{T}\frac{1}{\overline{c}_0^{\mathrm{el}}}\overline{\boldsymbol{M}}$ and the chemical potential

$$\overline{\mu}^{\mathrm{mix}} = Fz^{\mathrm{el}}\overline{\Phi} + \overline{\rho}_0 \frac{\partial \overline{\psi}}{\partial \overline{c}_0^{\mathrm{el}}} = Fz\overline{\Phi} + R\overline{T} \ln\left(\frac{\overline{c}_0^{\mathrm{el}}}{\overline{c}_0^{\mathrm{el,initial}}}\right)\,, \tag{4.55}$$

this yields the classic flux law (see Section 3.2.1)

$$\overline{\boldsymbol{J}} = -\overline{\boldsymbol{D}} \cdot \overline{\operatorname{Grad} c_0^{\mathrm{el}}}\,. \tag{4.56}$$

Note, that this expression only has a diffusive component, as gradients in the potential or convective transport do not occur in a metal/ion-conducting polymer interface.

4.4.2 Numerical studies

In the following, a structure consisting of a dry, single-ion-conducting polymer sandwiched inbetween two gold electrodes similar to the layered actuator in Fig. 4.1 is considered as a benchmark example for a nanoporous metal/polymer composite to elucidate the theory developed in the previous sections. This sandwich structure is rigidly clamped on the bottom face and a potential difference of 1 V is applied as a boundary condition on the electrode surfaces, see Fig. 4.7. This setup highlights the different coupling mechanisms by having two differently charged interfaces. The material parameters used for the bulk and the interface are summarised in Tables 4.2 and 4.3, respectively.

Table 4.3: Interface material parameters

	symbol	value	source
Lamé parameters	$\overline{\lambda}$	-2.0 N/m	†
	$\overline{\mu}$	3.5 N/m	†
electromech. coupling parameter (electroadsorption)	$\overline{\xi}^{\text{ion}}$	12 J/C	‡
electromech. coupling parameter (interface charge)	$\overline{\xi}^{\text{el}}$	30 J/C	‡
diffusivity	$\overline{D}$	$5 \cdot 10^{-8}$ m^2/s	

† based on the surface parameters computed in [43]
‡ provided by N. Mameka at Helmholtz-Zentrum Geesthacht based on [89]

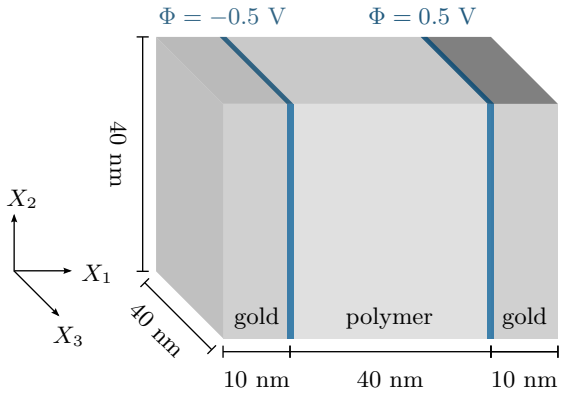

Figure 4.8: Sketch of the gold-polymer sandwich structure. The block's bottom face is rigidly clamped and the potential difference is imposed as a boundary condition on the interface.
This figure was published in [143], Copyright Elsevier (2017).

Implementation

To solve the highly non-linear and strongly coupled system of equations, the finite element method is applied within an in-house code using the finite element library `deal.II` [9]. Temporal discretisation is performed using a backward Euler finite difference scheme, cf. also Section 3.2.3. An iterative Newton scheme is used to linearise and solve the resulting residual equations.

The interface is represented by a two-dimensional manifold that is embedded in the surrounding three-dimensional volume. The nodes of the interface mesh coincide with the respective nodes of the bulk mesh, thus, ensuring geometrical coherency in the solution. The `deal.II` library provides a number of routines and methods which calculate derivatives of fields on $n-1$-manifolds, thus, enabling a straightforward implementation of the interface operators.

This implementation builds on the surface-elasticity framework presented in [75] and [93] that has been extended to interfaces already in [32]. These works, however, deal with uncoupled mechanics problems, i.e., the only degrees of freedom considered are the displacement components, which are continuous over the interface due to material and geometrical coherency. The metal/polymer composite modelled here exhibits electromechanical coupling and, thus, the framework had to be extended to a multiphysical one including electric potential and charge carrier concentration fields.

Furthermore, the fields differ between the three domains metal, polymer and interface. In the bulk metal, no electric fields or differences in the electron concentration occur. Thus, it is sufficient to model only the displacement in the metal domain, while both the interface and the polymer require information about the electric potential and, respectively, the electron and ion concentrations. To account for this coupling of different physical fields in different domains, an approach that extends these fields by zero over the entire problem domain is employed.

In addition, special care has to be taken in mapping information from the bulk to the interface because the interface equations are coupled to bulk values, for example in the jumps of fields over the interface or in determining the ion concentration at the interface.

Effects of the interface

An interface has a distinct influence on the overall behaviour of a composite. This is usually neglected in classic continuum models which is reasonable for materials where the bulk dominates the behaviour. However, in nanomaterials, interface effects cannot be neglected. The introduction of an interface with its own constitutive behaviour addresses this shortcoming. Figure 4.9 illustrates the role of the interface by comparison of simulations of bulk electromechanical coupling in the sandwich structure without the interface and including the purely mechanic behaviour of the interface.

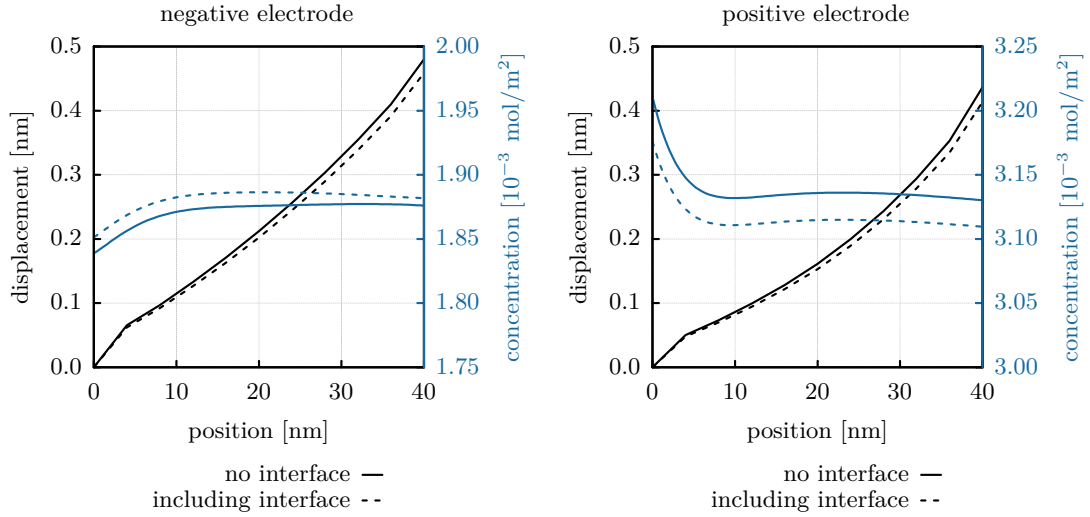

Figure 4.9: Difference between the deformation and ion concentration at the interface if interface elasticity is neglected or taken into account.

It is visible that when considering the stiffness of the interface, the interface resists the bending imposed by the polymer bulk, yielding a smaller deformation of the gold electrode. As the electric fields depend on the deformation of the composite, there is also a pronounced difference in the ion distribution visible. Modification of the interface's behaviour, thus, modifies the behaviour of the whole composite.

This is further visible in Fig. 4.10, depicting the deformed bulk and interface in case of full chemoelectromechanical coupling. Chemoelectromechanical coupling on the interface results in a curving of both interfaces. This influence of the electromechanical coupling on the interface is investigated further in the following.

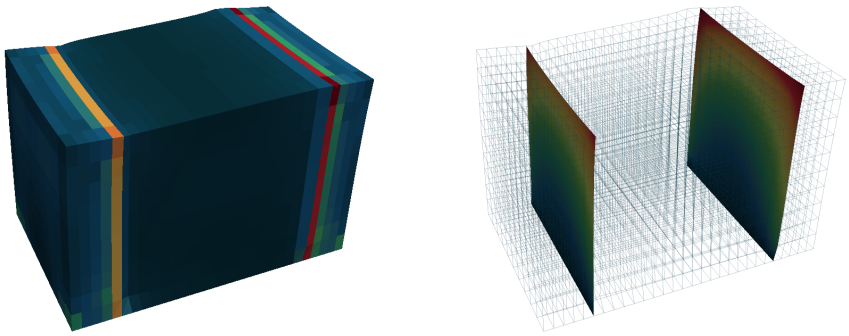

Figure 4.10: Deformed bulk and interfaces. The colour map of the bulk specimen illustrates the norm of the stress tensor while for the interface the displacement perpendicular to the interface is shown. Electromechanical coupling on the interface causes curving of the interfaces.
This figure was published in [143], Copyright Elsevier (2017).

In addition to the mechanical influence, the interface exhibits charge carrier transport. Interface charges arise from electric fields in the bulk which are deformation dependent and, thus, the charge distribution on the interface is not homogeneous. However, as charge carriers diffuse along the interface, ultimately a uniform charge distribution is established on the interface, cf. Fig. 4.11.

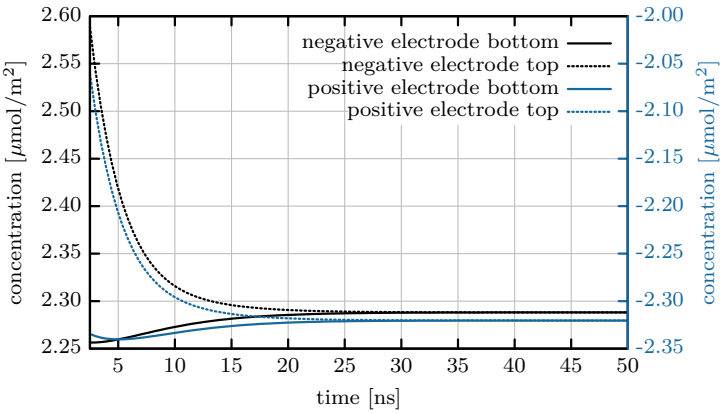

Figure 4.11: Variation of the interface electron concentration for two points at the bottom and the top of the specimen for both interfaces. The initial difference due to the deformed geometry is balanced by diffusion along the interface.

Effects of electromechanical coupling

Four different mechanisms cause chemoelectromechanical coupling in the metal/ion-conducting polymer composite. In the bulk polymer, coupled behaviour arises due to polarisation (compare Eq. (4.40)) and differences in the ion concentration (compare Eq. (4.41)) while on the interface, both interface charges and electroadsorption of ions influence the mechanical response.

The latter two mechanisms are separated in the sandwich setup employed here as it has two differently charged interfaces. On the “positive” electrode on which the positive electric

potential is applied, the negative mobile anions of the polymer are electroadsorbed. The "negative" electrode has a negative interface charge (i.e., a high electron concentration $\bar{c}_0^{\mathrm{el}}$).

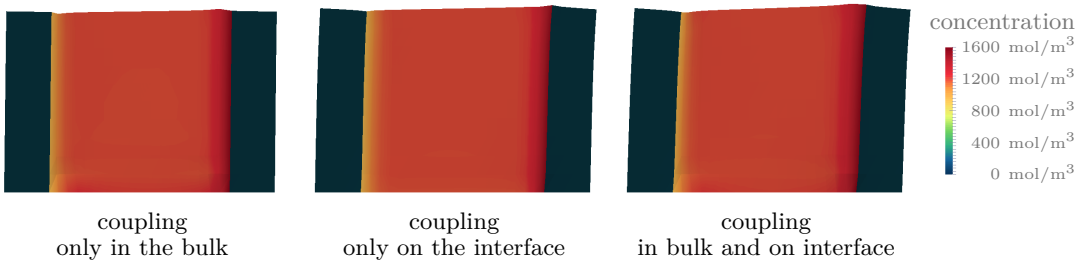

Figure 4.12: Comparison of deformation states caused by different electromechanical coupling mechanisms. In the bulk polymer, expansion occurs at the "positive" electrode due to ion excess and contraction arises in regions of reduced ion concentration. If only interface coupling mechanisms are considered, the "negative" electrode contracts due to the interface charge while the "positive" electrode expands upon electroadsorption. These effects are superimposed if chemoelectromechanical coupling in the bulk and on the interface are modelled.
This figure was published in [143], Copyright Elsevier (2017).

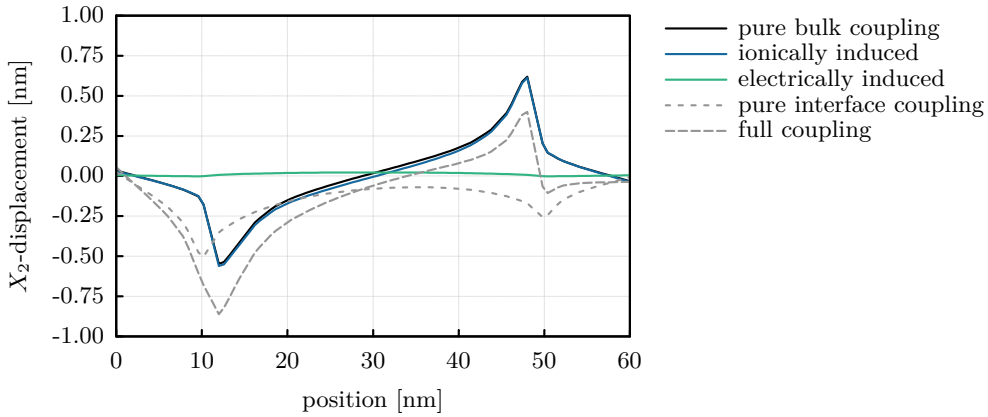

Figure 4.13: Displacement at the top of the specimen as induced by the different coupling mechanisms. The electrically induced deformation caused by polarisation of the material occurs over the whole polymer volume while the ionically induced deformation is localised to the regions close to the electrodes. The bulk coupling is a superposition of both mechanisms.
This figure is reproduced from [143].

Figure 4.12 depicts the deformed sandwich structure with the electromechanical coupling activated either in the bulk or on the interface as well as the case in which the electromechanical coupling in the bulk interacts with the electromechanical coupling on the interface. Electromechanical coupling in the bulk causes the polymer to swell in the region close to the "positive" electrode where there is an ion excess and to contract in regions of reduced ion concentration, causing a bending deformation of the composite block. A negative interface charge results in a contraction of the interface as it increases the bonding strength between surface atoms while electroadsorption of anions causes an expansion of the interface. If all coupling mechanisms are superimposed, the interface coupling effects amplify the bulk deformation in this setup.

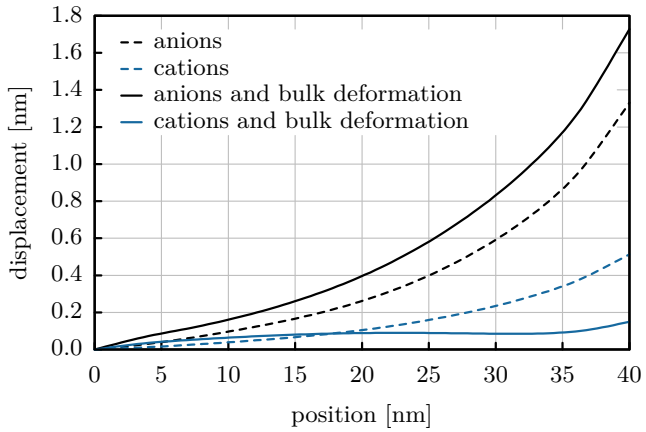

Figure 4.14: Norm of the interface displacement vector $\overline{\boldsymbol{u}}$ for electroadsorption of differently charged ions. The displacements arising from electroadsorption of anions and cations only differ in magnitude, while the superposition of bulk and interface behaviour results in a more complex deformation in case of cation adsorption, in which the two coupling mechanisms counteract each other.

The electromechanical coupling in the polymer bulk arises due to two different mechanisms as depicted in Fig. 4.13. Polarisation induces a volumetric expansion of the polymer upon application of a potential difference. In contrast, deformation due to ion migration occurs in the regions close to the electrodes in which space charges arise. This type of coupling is responsible for the bending deformation visible in Fig. 4.12 and is strongly influenced by the superposition of the interface coupling effects which may counteract or amplify the deformation.

The effect the superposition of different coupling mechanisms has on the displacement of the interface is further illustrated in Fig. 4.14. Here, the norm of the interface displacement vector $\overline{\boldsymbol{u}}$ is shown over the X_2-length of the interface. As the charge concentration is almost homogeneous along the interface, it deforms evenly for the cases of electromechanical coupling through electroadsorption of anions and cations. If the coupling on the interface and in the bulk act in the same direction as they do for anion adsorption, the interface deformation remains even. However, for adsorption cations on the "positive" electrode, interface and bulk coupling are opposing effects and the resulting deformation state is more complex.

4.5 Modelling of conjugated polymer composite

In this section, another possible second phase for nanoporous metal/polymer composites is considered, namely a conjugated polymer such as polypyrrole or polyaniline. As described in Section 4.2, these polymers are electrically conducting and show actuation due to ingress of ions from a liquid electrolyte. While this setup does not have the advantage of being completely dry as the one described in Section 4.4, it offers a variety of possible actuation reactions because of the dependence on varied ion transport paths that can be influenced by the choice of electrolyte and doping ions. Therefore, the transport mechanisms and the resulting deformation behaviour are the focus in modelling the composite's behaviour in the following.

4.5.1 Constitutive description

The composite described here consists of four distinct domains with differing physical behaviour: the polymer, the liquid electrolyte, the nanoporous metal and the polymer/metal interface. Due to their differing physical nature, different fields have to be considered in each domain.

The general set of governing equations and modelling principles described in Section 4.3 is applied here, cf. also Table 4.1 for a summary of the governing equations. Establishing the chosen constitutive relations also follows the general principles presented in Sections 4.3 and 4.4, so that, in the following, only the chosen relations for the transport law, the stresses and the nominal electric displacement field are presented.

Conjugated polymer

In the conjugated polymer, ions are transported via diffusion and migration. As in the previous section, this behaviour is modelled by the Nernst-Planck relation Eq. (4.17) for the mass flux. No convection occurs in the setting used here, thus,

$$\boldsymbol{J}^i = -\boldsymbol{D}^i \cdot \operatorname{Grad} c_0^i - c_0^i \frac{z^i F}{RT} \boldsymbol{D}^i \cdot \operatorname{Grad} \Phi \,. \tag{4.57}$$

Furthermore, the differently charged mobile ion species may bond to form a neutral salt according to

$$m\,\mathrm{A}^{\mathrm{n}-} + n\,\mathrm{C}^{\mathrm{m}+} \underset{r_d}{\overset{r_a}{\rightleftharpoons}} \mathrm{A}_{\mathrm{m}}\mathrm{C}_{\mathrm{n}} \,. \tag{4.58}$$

Here r_a and r_d are the rates of association and dissociation, respectively. Equation (4.58) states that m anions and n cations together form one salt molecule in a reversible reaction. In general, the equilibrium state for this reaction lies somewhere in between complete dissociation (only ions) and full association (only salt) depending on the rates. This continuous creation and destruction of salt molecules is described by the source term W^i in Eq. (4.31):

$$W^{\mathrm{salt}} = C_0^{\mathrm{salt}} \left[r_a \left[\frac{c_0^+}{C_0^{\mathrm{salt}}} \right]^n \left[\frac{c_0^-}{C_0^{\mathrm{salt}}} \right]^m - r_d \frac{c_0^{\mathrm{salt}}}{C_0^{\mathrm{salt}}} \right] . \tag{4.59}$$

Here, C_0^{salt} denotes the maximum possible salt concentration and is used to normalise the concentrations. The expression $\left[\frac{c_0^+}{C_0^{\mathrm{salt}}}\right]^n \left[\frac{c_0^-}{C_0^{\mathrm{salt}}}\right]^m$ is the probability of the necessary number of ions "meeting" and, thus, enabling formation of a salt molecule. An increase in salt concentration naturally decreases the concentration of the ions, therefore, $n\,W^+ = m\,W^- = -W^{\mathrm{salt}}$.

These expressions for the sources and Eq. (4.57) inserted into the mass balance Eq. (4.13) yield a system of coupled reaction-diffusion-migration equations describing the transport of

ions in the polymer:

$$\dot{c}_0^+ = -\boldsymbol{D}^+ \cdot \operatorname{Grad} c_0^+ - c_0^+ \frac{z^+ F}{RT} \boldsymbol{D}^+ \cdot \operatorname{Grad} \Phi - n\, W^{\text{salt}}\,, \tag{4.60a}$$

$$\dot{c}_0^- = -\boldsymbol{D}^- \cdot \operatorname{Grad} c_0^- - c_0^- \frac{z^- F}{RT} \boldsymbol{D}^- \cdot \operatorname{Grad} \Phi - m\, W^{\text{salt}}\,, \tag{4.60b}$$

$$\dot{c}_0^{\text{salt}} = -\boldsymbol{D}^{\text{salt}} \cdot \operatorname{Grad} c_0^{\text{salt}} \qquad\qquad + W^{\text{salt}}\,. \tag{4.60c}$$

Note that the salt is not charged and, thus, not affected by potential gradients. Hence, Eq. (4.60c) has no migration component.

In addition to the ions, electrons are transported in conjugated polymers as described in Section 4.2. As [81] shows that the ion transport is significantly slower than the electron transport in the polymer and that the resistance for ions to cross the polymer-solution interface is negligible, this work focusses on the modelling of the ion transport and the electron charge contribution is simplified to a homogeneous charge density q_0^p that vanishes over time upon application of a potential. Thus, the charge density in the polymer is given by:

$$q_0^f(\boldsymbol{X}, t) = F\left[z^+ c_0^+(\boldsymbol{X}, t) + z^- c_0^-(\boldsymbol{X}, t)\right] + q_0^p(t)\,. \tag{4.61}$$

Here, the superscript + and − denote the cation and the anion, respectively. For a study that explicitly models the electron transport, see [138].

Furthermore, as in the previous section, the polymer is assumed to be homogeneous and electrically linear:

$$\boldsymbol{D} = -\varepsilon_0 \varepsilon_r J \boldsymbol{C}^{-1} \cdot \operatorname{Grad} \Phi\,. \tag{4.62}$$

Just as in Section 4.4.1, the first Piola-Kirchhoff stress is additively decomposed into a purely mechanical contribution and an electromechanically induced stress

$$\boldsymbol{P}(\boldsymbol{C}, c_0^i) = \boldsymbol{P}^{\text{mech}}(\boldsymbol{C}) + \boldsymbol{P}^{\text{electromech}}(\boldsymbol{C}, c_0^i)\,. \tag{4.63}$$

As the discussion in the previous section has shown that the Maxwell stress contribution is negligible, only stresses induced by changes in the ion and salt concentrations are considered here. Again, a Neo-Hookean material model is used to describe the purely mechanical contribution:

$$\boldsymbol{P}^{\text{mech}}(\boldsymbol{C}) = \mu \boldsymbol{F} + [\lambda \ln J - \mu]\, \boldsymbol{F}^{-T} \tag{4.64}$$

To describe the ionically induced stress, the model proposed in Section 4.4.1 (Eq. (4.41)) is adapted here to account for different ion species contributing to the stress due to differences in their concentration instead of charge denstity, thus, yielding the expression

$$\boldsymbol{P}^{\text{electromech}}(\boldsymbol{C}, c_0^i) = -F \sum_i k^i \Delta c_0^i \boldsymbol{F}^{-T}\,, \tag{4.65}$$

where $\Delta c_0^i = c_0^i(t) - c_0^i(0)$ denotes the difference in concentration of species i between the current and the initial state and k^i is a proportionality constant expressing the energy intro-

duced to the system per charge. The proportionality constant is expressed per unit charge to keep the general structure introduced in Section 4.4.

Liquid electrolyte

The principles of salt formation and ion transport are the same in the liquid as they are in the conjugated polymer. Hence, Eq. (4.59) and Eq. (4.60) are used to model the flux and sources in the liquid as well. Here, no convective contribution to the transport in the liquid is assumed but the expression Eq. (4.60) can be easily extended to account for such effects for example to describe a stirred electrolyte, cf. also Eq. (4.17). Furthermore, the liquid electrolyte exhibits electrically linear behaviour that is modelled by Eq. (4.62). The difference between the two media is captured by the material parameters, that is, the diffusion coefficients and association and dissociation rates as well as the dielectric constants.

Any mechanical interactions between the liquid domain and the solids is considered to be negligible, i.e., the liquid does not impose any pressure on the solids and their deformation does not induce any pressure differences in the liquid.

Metal

The nanoporous metal is considered to be a perfect conductor, thus, no discontinuities in the electron concentration or electric potential arise within the material.

The actuation strains in nanoporous metals is fully reversible [140]. Hence, only the elastic behaviour of the material is considered which is described by the same Neo-Hookean material model as in Section 4.4.1:

$$\boldsymbol{P} = \mu \boldsymbol{F} + [\lambda \ln J - \mu]\, \boldsymbol{F}^{-T} . \tag{4.66}$$

Interface

As the conjugated polymer is inherently electrically conducting, the interface between polymer and metal does not develop a charge. Instead, electrons are free to move from one material to the other and only on the polymer surface a surface charge is established. Thus, no interface charge transport is modelled. As the metal side of the interface is an ideal conductor, no inhomogeneities of the electric potential occur along the interface, cf. Section 4.4.1. Thus, for the electrostatic framework, the constitutive relations are

$$\overline{\boldsymbol{D}} = \boldsymbol{0} \qquad \text{and} \qquad \overline{q}_0^f = 0 .$$

The stress on the interface is additively decomposed into a purely mechanical and an electrically induced part just as it is for the bulk polymer:

$$\overline{\boldsymbol{P}}(\overline{F}, \overline{c}_0^i) = \overline{\boldsymbol{P}}^{\mathrm{mech}}(\overline{F}) + \overline{\boldsymbol{P}}^{\mathrm{electromech}}(\overline{F}, \overline{c}_0^i) . \tag{4.67}$$

As for both bulk materials, the purely mechanical part is given by a Neo-Hookean relation

$$\overline{\boldsymbol{P}}^{\mathrm{mech}}(\overline{F}) = \overline{\mu}\overline{\boldsymbol{F}} + \left[\overline{\lambda} \ln \overline{J} - \overline{\mu}\right] \overline{\boldsymbol{F}}^{-T} , \tag{4.68}$$

see also [75] and Section 4.4.1.

The electromechanical coupling on the interface arises from electrosorption of ions. This is modelled with a phenomenological expression using the electroelastic coupling parameter $\overline{\xi}^i$ as introduced in [89]:

$$\overline{\boldsymbol{P}}^{\text{electromech}}(\overline{\boldsymbol{F}}, \overline{c}_0^i) = -\overline{\xi}^i \, \overline{q}_0^f \overline{\boldsymbol{F}} \, . \tag{4.69}$$

Here, the interface charge density $\overline{q}_0^f = F \sum_i z^i \, \overline{c}_0^i$ is determined from the bulk charge density and transferred to the interface by evaluating a 0.1 nm-thickness layer of polymer that is assumed to influence the interface.

4.5.2 Numerical studies

To study the proposed model, an electric cell setup as presented in Fig. 4.15 is modelled. The interconnected pore network of the nanoporous gold is represented by the channels in the gold domain. Complete filling of the pores with polymer and perfect contact are assumed.

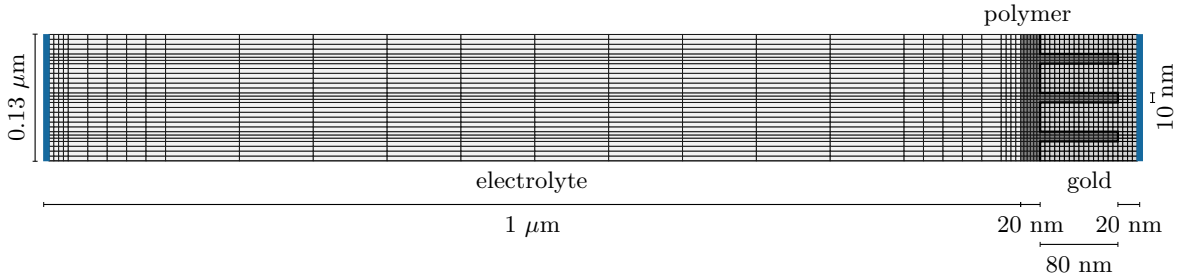

Figure 4.15: Meshed geometry of the electric cell using an electroactive polymer/gold composite electrode. The pore channels in the gold have a diameter of 10 nm and are completely filled with polymer. The electrolyte domain has a width of 1 μm. On the left-hand coloured side and the interface, potential boundary conditions are applied while on the right hand side, the displacement of the electrode is fully constrained.

A potential difference is applied over the geometry by imposing constant potential boundary conditions on the side of the electrolyte domain and the metal/polymer interface. The displacement of the electrode is constrained on one side. All other surfaces are flux and traction free. The material properties used here are summarised in Table 4.4 and do not represent a specific material as the goal in the following is to illustrate the general capabilities of the proposed framework. Furthermore, slightly exaggerated values for the relative permittivities are used to allow avoid an unreasonably fine mesh, compare [138].

The model is implemented into a finite element code utilising the `deal.ii` library. The non-linear system of equations is solved using a monolithic scheme, thus, all coupling effects are accounted for.

Ion transport

In conjugated polymers, the transport of multiple ion species and the associated salts with very different mobilities is possible. As all of these induce deformation in the material, the superimposed deformation behaviour is not easily predictable. Therefore, special attention in modelling the EAP/metal nanocomposite is paid to the ion transport here.

Table 4.4: Material parameters of the conjugated polymer composite system

	symbol	value	source
conjugated polymer			
mass density	ρ_0	1.47 g/cm^3	[88]
Lamé parameters	λ	0.346 GPa	[52]
	μ	0.231 GPa	
relative permittivity	ε_r	10000.	[6]
valence anion	z^-	-1	
valence cation	z^+	1	
anion concentration	c_0^-	1500 mol/m^3	
cation concentration	c_0^+	0 mol/m^3	
cation diffusivity	D^+	$10 \cdot 10^{-10}$ m^2/s	
anion coupling parameter	k^-	5 J/C	
cation coupling parameter	k^+	2.5 J/C	
salt coupling parameter	k^{salt}	$0.75\,\lvert z^+\rvert k^- + \lvert z^-\rvert k^+$	
salt association rate	r_a	10 1/ms	
salt dissociation rate	r_d	5 1/ms	
electrolyte			
relative permittivity	ε_r	8000.	
anion concentration	c_0^-	500 mol/m^3	
cation concentration	c_0^+	500 mol/m^3	
cation diffusivity	D^+	$1 \cdot 10^{-10}$ m^2/s	
salt association rate	r_a	0 1/ms	
salt dissociation rate	r_d	100 1/ms	
gold			
mass density	ρ_0	19.3 g/cm^3	
Lamé parameters	λ	198.6 GPa	[8]
	μ	27.08 GPa	
interface			
Lamé parameters	$\overline{\lambda}$	-2 N/m	†
	$\overline{\mu}$	3.5 N/m	
electromechanical coupling parameter	$\overline{\xi}^{\text{ion}}$	30 J/C	‡

† based on the surface parameters computed in [43]
‡ provided by N. Mameka at Helmholtz-Zentrum Geesthacht based on [89]

First, a system in which anions and cations have the same mobility, expressed by the diffusion coefficient D^+, cf. Table 4.4, is considered. Despite transport in liquids being generally faster than in a polymer, the diffusivity of both ion species is assumed to be the same in the electrolyte as in the polymer. The diffusion coefficient of the salt is set to $D^{\text{salt}} = 0.5\,D^-$. For the reduction, an initial homogeneous concentration of 1.5 mol/L is assumed in the polymer, while oxidisation starts with an ion-free polymer.

To study the effect the different transport mechanisms have on the actuation behaviour of the polymer, different mobilities of the anions and cations are compared in Fig. 4.16 for the case of an applied reducing potential. In the case of faster anion transport, the diffusivities are chosen to be $D^- = 0.5\,D^+ = 5 \cdot 10^{-10}$ m^2/s in the polymer the electrolyte. For the case of mobile anions and cations, shrinking of the composite occurs due to salt and unbound

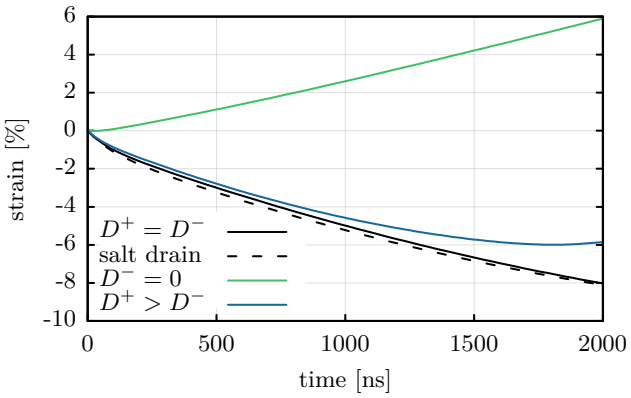

Figure 4.16: Strain over time for different ion mobilities. When both anions and cations are mobile, salt draining occurs. Due to the salt and unbound anions leaving the polymer, the composite contracts. If the anion is immobile ($D^- = 0$), no shrinking occurs, yielding a steady volume increase.

anions leaving the polymer. When the anions are slower than the cations, the shrinking is considerably decreased as it is over time balanced by the faster ingress of cations, resulting in renewed volume increase. Immobilising the anion on the other hand, yields steady swelling of the composite. This case might be preferable in many application cases as it does not exhibit changes in the actuation direction over time, cf. [115]. By variation of the mobility and the species of the ions, thus, the actuation behaviour of the composite can be tailored to different specifications.

Size effects

As described above, the composite electrode exhibits an almost homogeneous electric potential. This is, in part, due to the small pore size that favours balancing of potential differences over the build-up of space charges. To illustrate this, a setup with a singular large pore has been modelled. In Fig. 4.17, the results for multiple nanoscale pores and one large pore are compared. Both cases exhibit their maximum cation concentrations at the parts of the polymer/metal interface closest to the electrolyte. Due to the small pore diameter and the therefore more homogeneous electric potential distribution, the cations diffuse into the pores in the multiple pore setup. In contrast, the large pore allows for potential variations over its diameter, thus, yielding stronger electric fields at the interface close to the electrolyte. Migration in this electric field is dominant over the diffusional transport into the pore space, thus, yielding an increased cation concentration along the pore walls.

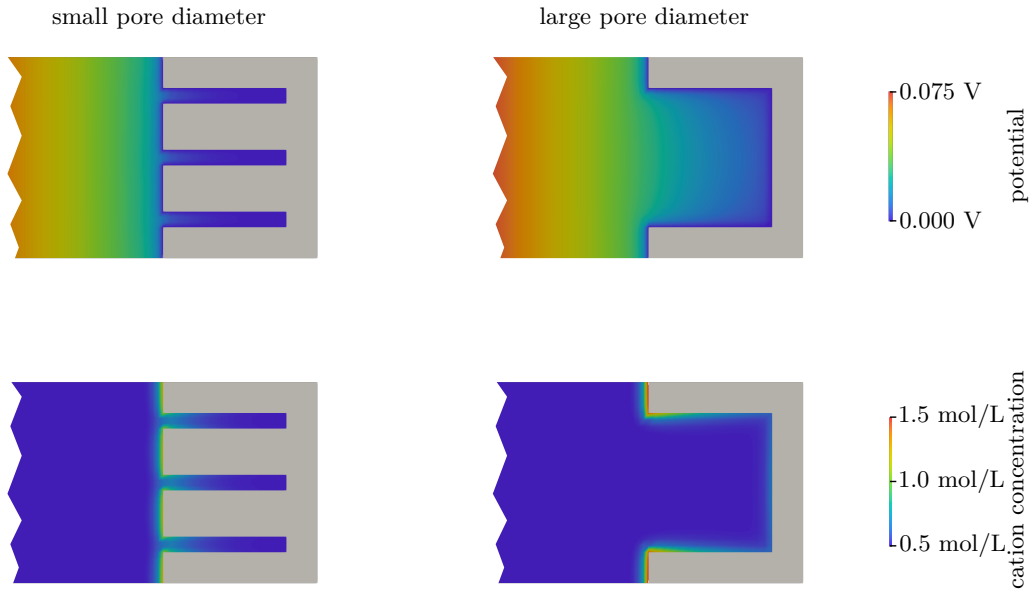

Figure 4.17: Effect of the pore diameter on the electric potential and the cation concentration. The large pore has a diameter that is 9 times larger than the diameter of a small pore. Due to the small pore diameters, the electric potential distribution is more even on the left hand side, allowing for diffusional transport into the pores, while for one large pore the migration to the gold surface is dominant.

5 Conclusions

Models describing the multiphysically coupled behaviour associated with mass transport in polymeric materials have been developed for two example cases, namely, Case II diffusion and ionically activated electroactive polymers. A physically motivated modelling approach has been employed in which fundamental balance principles are examined to identify the governing equations for the different coupled fields.

Using this approach, a general framework for modelling coupled mass transport phenomena is established that allows for the description of all occurring processes and is easily adapted and extended to phenomena other than the example cases described in this thesis. This is due to the fact that independently of the precise mechanism at play, the obeyed balance principles are the same for different phenomena. For example, during Case II diffusion, a fluid moves through free volume in the material, while in some electroactive polymers ions are transported by conformational motion of the surrounding polymer chains, but both, the fluid and the ions, have to obey a mass balance that yields a formally identical transport law.

The specific material behaviour is described by the constitutive relations that, in this thesis, have been identified from the Helmholtz free energy following the Coleman-Noll procedure. To model the distinct kinetics of Case II diffusion that involve formation of a sharp front and wave-like transport, a novel flux law based on the dual-phase lag concept was proposed and tested numerically. Subsequently, this diffusion model has been coupled to thermomechanics, yielding a model that predicts transport and swelling behaviour that is in good qualitative agreement with experimental results and, further, offers insights into the strong temperature dependence of Case II transport as shown in numerical studies.

In the considered electroactive polymers, ion transport is coupled to electric fields and deformation and the governing equations are again derived from fundamental principles as before. In this thesis, composites of electroactive polymers and nanoporous gold are investigated. The characteristically large surface-to-volume area of nanoporous metals and the resulting bicontinous nature of the polymer/gold composite introduce interface effects that cannot be captured using classical continuum mechanical theories. These interface effects are visible in purely mechanical problems and are of great importance in the electromechanically coupled behaviour of the nanoporous metal, which is entirely due to changes of the interface energy caused by adsorption of ions and the formation of interface charges. To account for these effects, the interface elasticity framework has been utilised in this thesis. The governing equations for charge carrier transport, deformation and electric fields were established and completed with constitutive equations that account for the electromechanical coupling in the bulk and on the interface. This novel interface-enhanced framework has been implemented into a finite element code and employed to carry out numerical studies modelling nanocomposites of porous gold with two different types of electroactive polymer. These highlight the influence of the interface and investigate the effects of the different mechanisms of chemo-electromechanical coupling that are at play in these composites. Here, one important feature

of computational modelling of multiphysically coupled phenomena is especially visible: Modelling allows to separate the different, superimposed mechanisms and, thus, gives insight into processes that are inaccessible to experiments.

The numerical studies presented here show the capability of the proposed models to capture and predict the characteristic behaviour of the investigated phenomena. However, they have been carried out for rather simple structures. While for Case II experiments, the considered setup is often used similarly in experimental studies, the geometries studied for the nanocomposite do not represent a realistic polymer-filled nanoporous metal. To model more realistic structures would, therefore, be a natural next step. As this is bound to be computationally expensive due to the complicated structure of the material and the amount of degrees of freedom arising from the multiphysical coupling, it would be valuable to investigate, e.g., optimised discretisation and parallelisation techniques.

More realistic simulations require, furthermore, experimental identification of material properties. While most of the material parameters used in this thesis can be found in the literature for many material systems, especially the mechanical characterisation of different electroactive polymers and identification of transport constants have not received a lot of attention so far. With more realistic structures and material properties, the quantitative agreement of the model with experiments could be investigated.

The general nature of the proposed physics-based modelling approach allows for easy extension to account for further effects, such as ion size effects or the presence of hydration shells in electroactive polymers. The Case II diffusion model could be extended using damage models to predict the crazing and cracking often observed due to the sharp front and large deformations associated with the transport. Moreover, the general governing equations and principles presented in this thesis could be utilised in modelling other coupled mass transport phenomena such as controlled release drugs or environmentally induced corrosion or embrittlement in metals.

Bibliography

[1] T. Alfrey, E. F. Gurnee, and W. G. Lloyd (1966): *Diffusion in glassy polymers*, Journal of Polymer Science Part C: Polymer Symposia 12(1), 249–261.

[2] G. Alici, G. M. Spinks, J. Madden, Y. Wu, and G. G. Wallace (2008): *Response characterization of electroactive polymers as mechanical sensors*, IEEE/ASME Transactions on Mechatronics 13(2), 187 –196.

[3] H. Almeida, M. H. Amaral, and P. Lobao (2012): *Temperature and pH stimuli-responsive polymers and their applications in controlled and selfregulated drug delivery*, Journal of Applied Pharmaceutical Science 2, 2231–3354.

[4] N. M. Ames, V. Srivastava, S. A. Chester, and L. Anand (2009): *A thermo-mechanically coupled theory for large deformations of amorphous polymers. Part II: Applications*, International Journal of Plasticity 25(8), 1495–1539.

[5] L. Anand, N. M. Ames, V. Srivastava, and S. A. Chester (2009): *A thermo-mechanically coupled theory for large deformations of amorphous polymers. Part I: Formulation*, International Journal of Plasticity 25(8), 1474–1494.

[6] M. Aureli, W. Lin, and M. Porfiri (2009): *On the capacitance-boost of ionic polymer metal composites due to electroless plating: Theory and experiments*, Journal of Applied Physics 105(10), 104911.

[7] S. Baek and A. R. Srinivasa (2004): *Diffusion of a fluid through an elastic solid undergoing large deformation*, International Journal of Non-Linear Mechanics 39(2), 201–218.

[8] T. J. Balk, C. Eberl, Y. Sun, K. J. Hemker, and D. S. Gianola (2009): *Tensile and compressive microspecimen testing of bulk nanoporous gold*, JOM 61(12), 26–31.

[9] W. Bangerth, R. Hartmann, and G. Kanschat (2007): *deal.II – a general purpose object oriented finite element library*, ACM Transactions on Mathematical Software 33(4), 24/1–24/27.

[10] Y. Bar-Cohen (2004): *EAP history, current status, and infrastructure*, in Y. Bar-Cohen (editor), *Electroactive Polymer (EAP) Actuators as Artificial Muscles. Reality, Potential, and Challenges*, SPIE Press, 2nd edition.

[11] Y. Bar-Cohen (2010): *8 - Electroactive polymers as actuators*, in K. Uchino (editor), *Advanced Piezoelectric Materials*, Woodhead Publishing, Woodhead Publishing Series in Electronic and Optical Materials, 287 – 317.

[12] A. A. Barba, M. d'Amore, S. Chirico, G. Lamberti, and G. Titomanlio (2009): *Swelling of cellulose derivative (HPMC) matrix systems for drug delivery*, Carbohydrate Polymers 78, 469–474.

[13] S. Bargmann, A. T. McBride, and P. Steinmann (2011): *Models of solvent penetration in glassy polymers with an emphasis on Case II diffusion. A comparative review*, Applied Mechanics Reviews 64(1), 010803–1–010803–13.

[14] S. Bargmann, C. Soyarslan, E. Husser, and N. Konchakova (2016): *Materials based design of structures: Computational modeling of the mechanical behavior of gold-polymer nanocomposites*, Mechanics of Materials 94, 53 – 65.

[15] K.-J. Bathe (2006): *Finite element procedures*, Prentice-Hall.

[16] R. H. Baughman (2003): *Muscles made from metal*, Science 300(5617), 268–269.

[17] L. Bay, T. Jacobsen, S. Skaarup, and K. West (2001): *Mechanism of actuation in conducting polymers: Osmotic expansion*, The Journal of Physical Chemistry B 105(36), 8492–8497.

[18] I. Borukhov, D. Andelman, and H. Orland (2000): *Adsorption of large ions from an electrolyte solution: a modified poisson-boltzmann equation*, Electrochimica Acta 46(2-3), 221 – 229.

[19] R. Bustamante and K. R. Rajagopal (2013): *On a new class of electroelastic bodies. I*, Proceedings of the Royal Society of London A: Mathematical, Physical and Engineering Sciences 469(2149), 1–16.

[20] G. Camera-Roda and G. C. Sarti (1990): *Mass transport with relaxation in polymers*, AIChE Journal 36(6), 851–860.

[21] C. Cattaneo (1948): *Sulla conduzione del calore*, Università di Modena. Facoltà di scienze matematiche, fisiche e naturali, Modena, 83–101.

[22] P. Cermelli, E. Fried, and M. E. Gurtin (2005): *Transport relations for surface integrals arising in the formulation of balance laws for evolving fluid interfaces*, Journal of Fluid Mechanics 544, 339–351.

[23] Y. Cha and M. Porfiri (2014): *Mechanics and electrochemistry of ionic polymer metal composites*, Journal of the Mechanics and Physics of Solids 71, 156 – 178.

[24] G. Chatzigeorgiou, A. Javili, and P. Steinmann (2014): *Surface electrostatics: theory and computations*, Proceedings of the Royal Society of London A: Mathematical, Physical and Engineering Sciences 470(2164), 20130628.

[25] J. K. Chen, J. E. Beraun, and D. Y. Tzou (1999): *A dual-phase-lag diffusion model for interfacial layer growth in metal matrix composites*, Journal of Materials Science 34(24), 6183–6187.

[26] Z. Chen, X. Tan, A. Will, and C. Ziel (2007): *A dynamic model for ionic polymer-metal composite sensors*, Smart Materials and Structures 16(4), 1477.

[27] B. D. Coleman and W. Noll (1963): *The thermodynamics of elastic materials with heat conduction and viscosity*, Archive for Rational Mechanics and Analysis 13(1), 167–178.

[28] P. J. Costa Branco and J. A. Dente (2006): *Derivation of a continuum model and its electric equivalent-circuit representation for ionic polymer-metal composite (IPMC) electromechanics*, Smart Materials and Structures 15(2), 378.

[29] J. Crank (1975): *The Mathematics of Diffusion*, Oxford Science Publications, Clarendon Press, 2nd edition.

[30] J. Crank and G. S. Park (1949): *An evaluation of the diffusion coefficient for chloroform in polystyrene from simple absorption experiments*, Transactions of the Faraday Society 45(0), 240–249.

[31] J. Crank and G. S. Park (1951): *Diffusion in high polymers: some anomalies and their significance*, Transactions of the Faraday Society 47(0), 1072–1084.

[32] D. Davydov, E. Voyiatzis, G. Chatzigeorgiou, S. Liu, P. Steinmann, M. C. Böhm, and F. Müller-Plathe (2014): *Size effects in a silica-polystyrene nanocomposite: Molecular dynamics and surface-enhanced continuum approaches*, Soft Materials 12, S142–S151.

[33] D. De Kee, Q. Liu, and J. Hinestroza (2005): *Viscoelastic (non-fickian) diffusion*, The Canadian Journal of Chemical Engineering 83(6), 913–929.

[34] K. Debrabant (2011): *Numerische Behandlung linearer und semilinearer partieller differentiell-algebraischer Systeme mit Runge-Kutta-Methoden*, Logos-Verlag.

[35] P. T. Delassus and N. F. Whiteman (1999): *Physical and mechanical properties of some important polymers*, in J. Brandrup, E. H. Immergut, and E. A. Grulke (editors), *Polymer Handbook*, Wiley: New York, 4th edition, V/159 – V/169.

[36] K. Derrien and P. Gilormini (2006): *Interaction between stress and diffusion in polymers*, Defect and Diffusion Forum 258-260, 447–452.

[37] E. Detsi, P. Onck, and J. De Hosson (2013): *Metallic muscles at work: High rate actuation in nanoporous gold/polyaniline composites*, ACS Nano 7(5), 4299–4306.

[38] A. Dorfmann and R. W. Ogden (2005): *Nonlinear electroelasticity*, Acta Mechanica 174(3-4), 167–183.

[39] A. L. Dorfmann and R. W. Ogden (2014): *Nonlinear Theory of Electroelastic and Magnetoelastic Interactions*, Springer US.

[40] J. L. Duda, J. S. Vrentas, S. T. Ju, and H. T. Liu (1982): *Prediction of diffusion coefficients for polymer-solvent systems*, AIChE Journal 28(2), 279–285.

[41] C. J. Durning and M. Tabor (1986): *Mutual diffusion in concentrated polymer solutions under a small driving force*, Macromolecules 19(8), 2220–2232.

[42] A. K. Ekenseair, R. A. Ketcham, and N. A. Peppas (2012): *Visualization of anomalous penetrant transport in glassy poly(methyl methacrylate) utilizing high-resolution X-ray computed tomography*, Polymer 53(3), 776–781.

[43] B. Elsner, S. Müller, S. Bargmann, and J. Weissmüller (2017): *Surface excess elasticity of gold: Ab initio coefficients and impact on the effective elastic response of nanowires*, Acta Materialia 124, 468 – 477.

[44] J. Ericksen (2007): *Theory of elastic dielectrics revisited*, Archive for Rational Mechanics and Analysis 183(2), 299–313.

[45] Y. Fang, X. Tan, Y. Shen, N. Xi, and G. Alici (2008): *A scalable model for trilayer conjugated polymer actuators and its experimental validation*, Materials Science and Engineering: C 28(3), 421 – 428. Proceedings from the Advanced Processing of Biomaterials Symposium, Materials Science and Technology Conference and Exhibition.

[46] K. Farinholt and D. J. Leo (2004): *Modeling of electromechanical charge sensing in ionic polymer transducers*, Mechanics of Materials 36(5 - 6), 421 – 433. Coupled Chemo-Mechanical Phenomena.

[47] C. A. Felippa, K. Park, and C. Farhat (2001): *Partitioned analysis of coupled mechanical systems*, Computer Methods in Applied Mechanics and Engineering 190(24 - 25), 3247 – 3270. Advances in Computational Methods for Fluid-Structure Interaction.

[48] A. Fick (1855): *Ueber diffusion*, Annalen der Physik 170(1), 59–86.

[49] D. Fink, J. Vacik, J. Cervena, V. Hnatowicz, Y. Kobayashi, S. Hishita, S. Ghosh, and R. Klett (1998): *On the uptake of aqueous tracer solutions by pristine and ion-irradiated peek*, Nuclear Instruments and Methods in Physics Research Section B: Beam Interactions with Materials and Atoms 134(1), 61–72.

[50] P. Flory (1942): *Thermodynamics of high polymer solutions*, Journal of Chemical Physics 10, 51–61.

[51] P. J. Flory (1970): *Fifteenth Spiers Memorial Lecture. Thermodynamics of polymer solutions*, Discussions of the Faraday Society 49, 7–29.

[52] J. Foroughi, S. R. Ghorbani, G. Peleckis, G. M. Spinks, G. G. Wallace, X. L. Wang, and S. X. Dou (2010): *The mechanical and the electrical properties of conducting polypyrrole fibers*, Journal of Applied Physics 107(10), 103712.

[53] J. B. J. Fourier (1822): *Théorie analytique de la chaleur*, Paris.

[54] J. Fried (2003): *Conformation, solutions, and molecular weight*, in *Polymer Science and Technology*, Pearson Education, chapter 3.

[55] T. Z. Fu and C. J. Durning (1993): *Numerical simulation of Case II transport*, AIChE Journal 39(6), 1030–1044.

[56] T. P. Gall and E. J. Kramer (1991): *Diffusion of deuterated toluene in polystyrene*, Polymer 32(2), 265 – 271.

[57] M. O. Gallyamov (2013): *Sharp diffusion front in diffusion problem with change of state*, The European Physical Journal E 36(8), 1–13.

[58] M. Gandhi, P. Murray, G. Spinks, and G. Wallace (1995): *Mechanism of electromechanical actuation in polypyrrole*, Synthetic Metals 73(3), 247 – 256.

[59] D. Golodnitsky, E. Strauss, E. Peled, and S. Greenbaum (2015): *On order and disorder in polymer electrolytes*, Journal of the Electrochemical Society 162(14), A2551–A2566.

[60] S. Govindjee and J. C. Simo (1993): *Coupled stress-diffusion: Case II*, Journal of the Mechanics and Physics of Solids 41(5), 863–887.

[61] R. Greve (2003): *Kontinuumsmechanik*, Springer.

[62] M. E. Gurtin and A. I. Murdoch (1975): *A continuum theory of elastic material surfaces*, Archive for Rational Mechanics and Analysis 57(4), 291–323.

[63] D. T. Hallinan and N. P. Balsara (2013): *Polymer electrolytes*, Annual Review of Materials Research 43(1), 503–525.

[64] J. P. Harmon, S. Lee, and J. C. M. Li (1987): *Methanol transport in PMMA: The effect of mechanical deformation*, Journal of Polymer Science Part A: Polymer Chemistry 25(12), 3215–3229.

[65] G. S. Hartley (1949): *Diffusion and swelling of high polymers. Part III. - anisotropic swelling in oriented polymer film*, Transactions of the Faraday Society 45(0), 820–832.

[66] G. A. Holzapfel (2000): *Nonlinear Solid Mechanics*, John Wiley & Sons, 1st edition.

[67] W. Hong (2011): *Modeling viscoelastic dielectrics*, Journal of the Mechanics and Physics of Solids 59(3), 637 – 650.

[68] W. Hong, X. Zhao, and Z. Suo (2010): *Large deformation and electrochemistry of polyelectrolyte gels*, Journal of the Mechanics and Physics of Solids 58(4), 558 – 577.

[69] H. B. Hopfenberg and H. L. Frisch (1969): *Transport of organic micromolecules in amorphous polymers*, Journal of Polymer Science Part B: Polymer Letters 7(6), 405–409.

[70] I. Hopkinson, R. A. L. Jones, S. Black, D. M. Lane, and P. J. McDonald (1997): *Fickian and Case II diffusion of water into amylose: A stray field NMR study*, Carbohydrate Polymers 34(1–2), 39–47.

[71] K. Hori, H. Matsuno, and K. Tanaka (2011): *Sorption kinetics of methanol in thin poly(methyl methacrylate) films studied by optical reflectivity*, Soft Matter 7(21), 10319–10326.

[72] M. Hosseinipour and M. Elahinia (2013): *Kinematically stable bipedal locomotion using ionic polymer-metal composite actuators*, Smart Materials and Structures 22(8), 085021.

[73] K. Hutter and Y. Wang (2003): *Phenomenological thermodynamics and entropy principles*, in A. Greven, G. Keller, and G. Warnecke (editors), *Entropy*, Princeton University Press, 57–77.

[74] A. Javili, A. McBride, and P. Steinmann (2013): *Thermomechanics of solids with lower-dimensional energetics: On the importance of surface, interface, and curve structures at the nanoscale. A unifying review*, Applied Mechanics Reviews 65, 010802–010802–31.

[75] A. Javili, A. McBride, P. Steinmann, and B. Reddy (2014): *A unified computational framework for bulk and surface elasticity theory: a curvilinear-coordinate-based finite element methodology*, Computational Mechanics 54(3), 745–762.

[76] A. Javili and P. Steinmann (2010): *On thermomechanical solids with boundary structures*, International Journal of Solids and Structures 47(24), 3245 – 3253.

[77] H.-J. Jin and J. Weissmüller (2010): *Bulk nanoporous metal for actuation*, Advanced Engineering Materials 12(8), 714–723.

[78] D. D. Joseph and L. Preziosi (1989): *Heat waves*, Reviews of Modern Physics 61(1), 41–73.

[79] D. D. Joseph and L. Preziosi (1990): *Addendum to the paper "Heat waves"*, Reviews of Modern Physics 62(2), 375–391.

[80] M. S. Kilic, M. Z. Bazant, and A. Ajdari (2007): *Steric effects in the dynamics of electrolytes at large applied voltages. II. Modified Poisson-Nernst-Planck equations*, Phys. Rev. E 75, 021503.

[81] T. Komura, S. Goisihara, T. Yamaguti, and K. Takahasi (1998): *Electron and ion transport in polypyrrole/polystyrenesulfonate composite films*, Journal of Electroanalytical Chemistry 456(1 - 2), 121 – 129.

[82] D. Kramer, R. N. Viswanath, and J. Weissmüller (2004): *Surface-stress induced macroscopic bending of nanoporous gold cantilevers*, Nano Letters 4(5), 793–796.

[83] X. Lang, L. Zhang, T. Fujita, Y. Ding, and M. Chen (2012): *Three-dimensional bicontinuous nanoporous Au/polyaniline hybrid films for high-performance electrochemical supercapacitors*, Journal of Power Sources 197, 325 – 329.

[84] R. C. Lasky, E. J. Kramer, and C.-Y. Hui (1988): *Temperature dependence of Case II diffusion*, Polymer 29(6), 1131 – 1136.

[85] J.-W. Lee, Y.-T. Yoo, and J. Y. Lee (2014): *Ionic polymer/metal composite actuators based on triple-layered polyelectrolytes composed of individually functionalized layers*, ACS Applied Materials & Interfaces 6(2), 1266–1271.

[86] S. Liu, M. Jiang, S. Ye, X. Xu, P. Lu, and J. Dong (2012): *Biodegradable poly(glycerin citrate) and its application to controlled release of theophylline*, Journal of Applied Polymer Science 124(5), 3633–3640.

[87] Z. Liu, L. Zhang, S. Poyraz, and X. Zhang (2013): *Conducting polymer - metal nanocomposites synthesis and their sensory applications*, Current Organic Chemistry 12, 2256 – 2267.

[88] J. J. Lòpez Cascales and T. F. Otero (2004): *Molecular dynamic simulation of the hydration and diffusion of chloride ions from bulk water to polypyrrole matrix*, The Journal of Chemical Physics 120(4), 1951–1957.

[89] N. Mameka, J. Markmann, H.-J. Jin, and J. Weissmüller (2014): *Electrical stiffness modulation–confirming the impact of surface excess elasticity on the mechanics of nanomaterials*, Acta Materialia 76(0), 272 – 280.

[90] J. E. Mark and Burak (2007): *Rubberlike Elasticity: A Molecular Primer*, Cambridge University Press.

[91] L. Masaro and X. Zhu (1999): *Physical models of diffusion for polymer solutions, gels and solids*, Progress in Polymer Science 24, 731–775.

[92] J. C. Maxwell (1867): *On the dynamical theory of gases*, Philosophical Transactions of the Royal Society of London 157, 49–88.

[93] A. McBride, A. Javili, P. Steinmann, and B. D. Reddy (2015): *A finite element implementation of surface elasticity at finite strains using the deal.II library* ArXiv:1506.01361.

[94] A. T. McBride, S. Bargmann, and P. Steinmann (2011): *Geometrically Nonlinear Continuum Thermomechanics Coupled to Diffusion: A Framework for Case II Diffusion*, Springer Berlin Heidelberg, volume 59 of *Lecture Notes in Applied and Computational Mechanics*, chapter 5, 89–107.

[95] A. T. McBride, A. Javili, P. Steinmann, and S. Bargmann (2011): *Geometrically nonlinear continuum thermomechanics with surface energies coupled to diffusion*, Journal of the Mechanics and Physics of Solids 59(10), 2116–2133.

[96] P. J. Mills and E. J. Kramer (1989): *Debonding of photoresist caused by Case II diffusion*, Journal of Materials Science 24(2), 439–446.

[97] R. Mutlu, G. Alici, X. Xiang, and W. Li (2014): *Electro-mechanical modelling and identification of electroactive polymer actuators as smart robotic manipulators*, Mechatronics 24(3), 241 – 251.

[98] P. Nardinocchi, M. Pezzulla, and L. Placidi (2011): *Thermodynamically based multiphysic modeling of ionic polymer metal composites*, Journal of Intelligent Material Systems and Structures 22(16), 1887–1897.

[99] S. Nemat-Nasser (2002): *Micromechanics of actuation of ionic polymer-metal composites*, Journal of Applied Physics 92(5), 2899–2915.

[100] S. Nemat-Nasser and J. Y. Li (2000): *Electromechanical response of ionic polymer-metal composites*, Journal of Applied Physics 87(7), 3321–3331.

[101] W. Ogieglo, H. Wormeester, M. Wessling, and N. E. Benes (2013): *Temperature-induced transition of the diffusion mechanism of n-hexane in ultra-thin polystyrene films, resolved by in-situ spectroscopic ellipsometry*, Polymer 54(1), 341–348.

[102] G. S. Park (1951): *The diffusion of some organic substances in polystyrene*, Transactions of the Faraday Society 47(0), 1007–1013.

[103] I.-S. Park, S.-M. Kim, D. Pugal, L. Huang, S.-W. Tam-Chang, and K. J. Kim (2010): *Visualization of the cation migration in ionic polymer-metal composite under an electric field*, Applied Physics Letters 96(4), 043301.

[104] N. A. Peppas and J. J. Sahlin (1989): *A simple equation for the description of solute release. III. Coupling of diffusion and relaxation*, International Journal of Pharmaceutics 57(2), 169 – 172.

[105] D. Pugal, K. J. Kim, and A. Aabloo (2011): *An explicit physics-based model of ionic polymer-metal composite actuators*, Journal of Applied Physics 110(8), 084904.

[106] D. Pugal, P. Solin, K. J. Kim, and A. Aabloo (2012): *Modeling ionic polymer-metal composites with space-time adaptive multimesh hp-FEM*, Communications in Computational Physics 11(1), 249 – 270.

[107] R. Quintanilla and R. Racke (2006): *A note on stability in dual-phase-lag heat conduction*, International Journal of Heat and Mass Transfer 49(7–8), 1209–1213.

[108] O. Rahmanian, C.-F. Chen, and D. L. DeVoe (2012): *Microscale patterning of thermoplastic polymer surfaces by selective solvent swelling*, Langmuir 28(35), 12923–12929.

[109] P. L. Ritger and N. A. Peppas (1987): *A simple equation for description of solute release I. Fickian and non-fickian release from non-swellable devices in the form of slabs, spheres, cylinders or discs*, Journal of Controlled Release 5(1), 23 – 36.

[110] P. L. Ritger and N. A. Peppas (1987): *A simple equation for description of solute release II. Fickian and anomalous release from swellable devices*, Journal of Controlled Release 5(1), 37 – 42.

[111] D. Schicker and T. Wallmersperger (2013): *Modeling and simulation of the chemo-electro-mechanical behavior of ionic polymer-metal composites*, Journal of Applied Physics 114(16), 163709.

[112] N. Schuld and B. Wolf (1999): *Polymer-solvent interaction parameter*, in J. Brandrup, E. H. Immergut, and E. A. Grulke (editors), *Polymer Handbook*, Wiley: New York, 4th edition.

[113] M. Shahinpoor, Y. Bar-Cohen, J. O. Simpson, and J. Smith (1998): *Ionic polymer-metal composites (IPMCs) as biomimetic sensors, actuators and artificial muscles - a review*, Smart Materials and Structures 7(6), R15.

[114] B. Singh and L. Pal (2012): *Sterculia crosslinked PVA and PVA-poly(AAm) hydrogel wound dressings for slow drug delivery: Mechanical, mucoadhesive, biocompatible and permeability properties*, Journal of the Mechanical Behavior of Biomedical Materials 9(0), 9–21.

[115] E. Smela (2003): *Conjugated polymer actuators for biomedical applications*, Advanced Materials 15, 481–494.

[116] D. Stamatialis, M. Sanopoulou, and I. Raptis (2002): *Swelling and dissolution behavior of poly(methylmethacrylate) films in methyl ethyl ketone/methyl alcohol mixtures studied by optical techniques*, Journal of Applied Polymer Science 83, 2823–2834.

[117] D. F. Stamatialis, M. Sanopoulou, and J. H. Petropoulos (2002): *Investigation of Case II diffusion behavior. 2. study of the poly(methylmethacrylate) methyl alcohol system by two-beam microinterferometry*, Macromolecules 35, 1021–1027.

[118] P. Steinmann, A. T. McBride, S. Bargmann, and A. Javili (2012): *A deformational and configurational framework for geometrically non-linear continuum thermomechanics coupled to diffusion*, Int J Non Linear Mech 47(2), 215–227.

[119] E. B. Tadmor, R. E. Miller, and R. S. Elliott (2012): *Continuum Mechanics and Thermodynamics*, Cambridge University Press.

[120] N. Thomas and A. H. Windle (1978): *Transport of methanol in poly(methyl methacrylate)*, Polymer 19(3), 255–265.

[121] N. L. Thomas and A. H. Windle (1980): *A deformation model for Case II diffusion*, Polymer 21(6), 613–619.

[122] N. L. Thomas and A. H. Windle (1982): *A theory of Case II diffusion*, Polymer 23(4), 529–542.

[123] V. Triani, C. Papenfuss, V. A. Cimmelli, and W. Muschik (2008): *Exploitation of the second law: Coleman–Noll and Liu procedure in comparison*, Journal of Non-Equilibrium Thermodynamics 33(1), 47–60.

[124] D. Y. Tzou (1995): *The generalized lagging response in small-scale and high-rate heating*, International Journal of Heat and Mass Transfer 38(17), 3231–3240.

[125] D. Y. Tzou (1995): *A unified field approach for heat conduction from macro- to micro-scales*, Journal of Heat Transfer 117(1), 8–16.

[126] K. Umezawa, W. M. Gibson, J. T. Welch, K. Araki, G. Barros, and H. L. Frisch (1992): *A study of Case II diffusion of a fluorinated hydrocarbon in poly(styrene) by resonance nuclear reaction analysis*, Journal of Applied Physics 71(2), 681–684.

[127] V. Venugopal, H. Zhang, R. Northcutt, and V. B. Sundaresan (2014): *A thermodynamic chemomechanical constitutive model for conducting polymers*, Sensors and Actuators B: Chemical 201(0), 293 – 299.

[128] T. V. Vernitskaya and O. N. Efimov (1997): *Polypyrrole: a conducting polymer; its synthesis, properties and applications*, Russian Chemical Reviews 66(5), 443.

[129] P. Vernotte (1958): *Les paradoxes de la théorie continue de l'équation de la chaleur*, CR Acad. Sci 246(22), 3154–3155.

[130] P. K. Vijalapura and S. Govindjee (2003): *Numerical simulation of coupled-stress Case II diffusion in one dimension*, Journal of Polymer Science Part B: Polymer Physics 41(18), 2091–2108.

[131] P. K. Vijalapura and S. Govindjee (2005): *An adaptive hybrid time-stepping scheme for highly non-linear strongly coupled problems*, International Journal for Numerical Methods in Engineering 64(6), 819–848.

[132] F. Vogel, S. Göktepe, P. Steinmann, and E. Kuhl (2014): *Modeling and simulation of viscous electro-active polymers*, European Journal of Mechanics - A/Solids 48, 112 – 128. Frontiers in Finite-Deformation Electromechanics.

[133] J. S. Vrentas and J. L. Duda (1977): *Diffusion in polymer–solvent systems. III. Construction of Deborah number diagrams*, Journal of Polymer Science: Polymer Physics Edition 15(3), 441–453.

[134] J. S. Vrentas, C. M. Jarzebski, and J. L. Duda (1975): *A Deborah number for diffusion in polymer-solvent systems*, AIChE Journal 21(5), 894–901.

[135] T. Wallmersperger, D. J. Leo, and C. S. Kothera (2007): *Transport modeling in ionomeric polymer transducers and its relationship to electromechanical coupling*, Journal of Applied Physics 101(2), 024912.

[136] K. Wang and J. Weissmüller (2013): *Composites of nanoporous gold and polymer*, Advanced Materials 25(9), 1280–1284.

[137] T. Wang, Q. Shen, L. Wen, and J. Liang (2012): *On the thrust performance of an ionic polymer-metal composite actuated robotic fish: Modeling and experimental investigation*, Science China Technological Sciences 55(12), 3359–3369.

[138] X. Wang, B. Shapiro, and E. Smela (2009): *Development of a model for charge transport in conjugated polymers*, The Journal of Physical Chemistry C 113(1), 382–401.

[139] D. S. Weile, D. A. Hopkins, G. A. Gazonas, and B. M. Powers (2014): *On the proper formulation of Maxwellian electrodynamics for continuum mechanics*, Continuum Mechanics and Thermodynamics 26(3), 387–401.

[140] J. Weissmüller, R. N. Viswanath, D. Kramer, P. Zimmer, R. Würschum, and H. Gleiter (2003): *Charge-induced reversible strain in a metal*, Science 300(5617), 312–315.

[141] J. Wilmers and S. Bargmann (2014): *Simulation of non-classical diffusion in polymers*, Heat and Mass Transfer 50, 1543–1552.

[142] J. Wilmers and S. Bargmann (2015): *A continuum mechanical model for the description of solvent induced swelling in polymeric glasses: Thermomechanics coupled with diffusion*, European Journal of Mechanics - A/Solids 53, 10 – 18.

[143] J. Wilmers, A. McBride, and S. Bargmann (2017): *Interface elasticity effects in polymer-filled nanoporous metals*, Journal of the Mechanics and Physics of Solids 99, 163 – 177.

[144] J. C. Wu and N. A. Peppas (1993): *Modeling of penetrant diffusion in glassy polymers with an integral sorption Deborah number*, Journal of Polymer Science Part B: Polymer Physics 31(11), 1503–1518.

[145] J. C. Wu and N. A. Peppas (1993): *Numerical simulation of anomalous penetrant diffusion in polymers*, Journal of Applied Polymer Science 49(10), 1845–1856.

[146] O. Zienkiewicz, R. Taylor, and J. Zhu (2013): *The Finite Element Method: Its Basis and Fundamentals*, Butterworth-Heinemann, seventh edition.

[147] C. G. Zoski (editor) (2007): *Handbook of Electrochemistry*, Elsevier B.V.

A Case II diffusion: Comments on thermodynamical relations

A.1 Chemical Potential

As outlined in Section 3.3.2, the equation of state for the chemical potential is $\mu^{\text{mix}} = \varphi^{\text{mix}} - T\eta^{\text{mix}}$. Furthermore, the chemical potential describes the change in the Gibbs free enthalpy of the system when an infinitesmial amount of solvent is added to the solvent/polymer mixture. Hence,

$$\mu^{\text{mix}} = \frac{\partial \Delta G^{\text{mix}}}{\partial N_s} = \frac{\partial \Delta H^{\text{mix}}}{\partial N_s} - T\frac{\partial \Delta S^{\text{mix}}}{\partial N_s}\,.$$

Therefore, the specific enthalpy φ^{mix} and the specific entropy η^{mix} contribution of the solvent can be obtained from the results of the Flory-Huggins theory by examining the specific mixing enthalpy Eq. (3.36) and the specific entropy of mixing Eq. (3.33), according to

$$\begin{aligned}
\varphi^{\text{mix}} &= \frac{\partial \Delta H^{\text{mix}}}{\partial N_s} = \frac{k_{\text{B}}\,T}{\rho_0\,V_0}\frac{\chi}{J} \\
\eta^{\text{mix}} &= \frac{\partial \Delta S^{\text{mix}}}{\partial N_s} = -\frac{k_{\text{B}}}{\rho_0\,V_0}\left[\ln\frac{N_s}{N_s+nN_p} + \left[1-\frac{1}{n}\right]\frac{nN_p}{N_s+nN_p}\right] \\
&= -\frac{k_{\text{B}}}{\rho_0\,V_0}\left[\ln\frac{c_0}{c_0+\rho_0\frac{m_s}{m_p}} + \left[1-\frac{1}{n}\right]\frac{\rho_0\frac{m_s}{m_p}}{c_0+\rho_0\frac{m_s}{m_p}}\right].
\end{aligned}$$

Thus, yielding the expression

$$\mu^{\text{mix}} = \frac{k_{\text{B}}\,T}{\rho_0\,V_0}\left[\frac{\chi}{J} + \ln\frac{c_0}{c_0+\rho_0\frac{m_s}{m_p}} + \left[1-\frac{1}{n}\right]\frac{\rho_0\frac{m_s}{m_p}}{c_0+\rho_0\frac{m_s}{m_p}}\right]$$

for the chemical potential. Integration of this expression over the concentration allows to determine the mixing contribution of the Helmholtz free energy, because $\mu^{\text{mix}} = \rho_0\frac{\partial\psi^{\text{mix}}}{\partial c_0}$. This integration yields Eq. (3.40).

A.2 Evaluation of the reduced dissipation inequality

A thermodynamically consistent formulation needs to fulfill the reduced dissipation inequality which in its most general formulation is given in Eq. (3.26). For the considered constitutive relations without history variables $\boldsymbol{\Xi}$ and including the equation of state for the chemical potential, Eq. (3.26) reduces to

$$-\boldsymbol{J}\cdot[\operatorname{Grad}\varphi^{\text{mix}} - T\operatorname{Grad}\eta^{\text{mix}}] - \frac{1}{T}\boldsymbol{Q}\cdot\operatorname{Grad}T \geq 0\,. \tag{A.1}$$

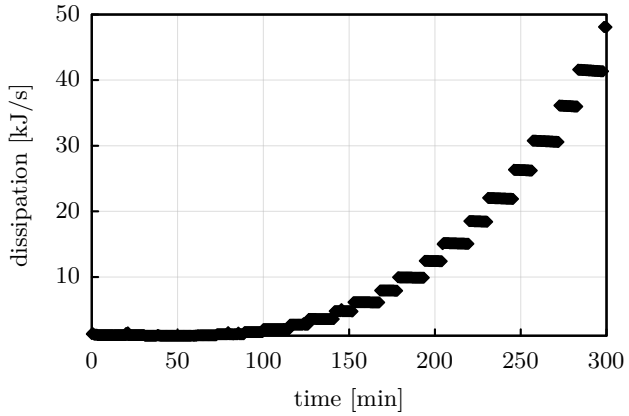

Figure A.1: Dissipation of the whole system for the completely coupled case. As the dissipation density is positive in every time step, the dissipation inequality is fulfilled. The jumps in the curve are a product of the jump in the elasticity constants upon plasticisation.

As $\boldsymbol{Q} = -\boldsymbol{K} \cdot \operatorname{Grad} T$ with $\boldsymbol{K}$ being non-negative, the second term in Eq. (A.1) is always positive.

To account for the characteristic Case II kinetics, the diffusive flux is given by

$$\boldsymbol{J}(\boldsymbol{X}, t + \tau_j) = -\boldsymbol{D}(c_0) \cdot \operatorname{Grad} c_0(\boldsymbol{X}, t + \tau_c) \,,$$

compare Section 3.3.2. With this relation, it is not obvious whether the term including the diffusion flux is greater or equal to zero. This is tested during simulations by calculating the dissipation density given by Eq. (A.1) in every quadrature point.

Exemplarily, the results for the completely coupled case with a boundary temperature of 333.15 K are depicted in Fig. A.1, which shows that the integrated dissipation density for the whole system is positive in every time step. This requirement is not only fulfilled for the whole system but in fact in every quadrature point.

B Electroactive Polymers: Balances of energy and entropy

B.1 Balance of energy

The work performed on an electroactive body can be partioned into a mechanical, an electrical and a chemical contribution, see for example [68] and [98] for discussions of the work performed on polyelectrolyte gels and ionic polymers, respectively. Thus, the balance of energy is of the form

$$\dot{\mathcal{E}} = \mathcal{P}^{\text{mechanical}} + \mathcal{P}^{\text{electrical}} + \mathcal{P}^{\text{chemical}}\,, \tag{B.1}$$

where $\mathcal{E}$ denotes the system's total energy and $\mathcal{P}$ denotes a power, cf. also Section 2.2.4.

In the electroactive nanocomposites described in Chapter 4, the metal/polymer interface is modelled as energetic, i.e., it has its own energetic behaviour. Thus, the total energy for an electroactive body $\mathcal{B}_0$ with an energetic interface $\mathcal{I}_0$ is given by

$$\mathcal{E} = \mathcal{E}_{\mathcal{B}_0} + \overline{\mathcal{E}}_{\mathcal{I}_0} = \int_{\mathcal{B}_0} \left[\rho_0 \varepsilon + \frac{1}{2}\rho_0 \dot{\boldsymbol{u}} \cdot \dot{\boldsymbol{u}}\right] \mathrm{d}V + \int_{\mathcal{I}_0} \left[\overline{\rho}_0 \overline{\varepsilon} + \frac{1}{2}\overline{\rho}_0 \dot{\overline{\boldsymbol{u}}} \cdot \dot{\overline{\boldsymbol{u}}}\right] \mathrm{d}A\,. \tag{B.2}$$

The mechanical power in the volume and on the interface is expressed in terms of the stresses $\boldsymbol{P}$ and $\overline{\boldsymbol{P}}$ and the specific body forces $\boldsymbol{b}$ and $\overline{\boldsymbol{b}}$ according to

$$\begin{aligned} \mathcal{P}^{\text{mechanical}} = &\int_{\partial\mathcal{B}_0} \dot{\boldsymbol{u}} \cdot \boldsymbol{P} \cdot \boldsymbol{N}\, \mathrm{d}A + \int_{\mathcal{B}_0} \rho_0 \dot{\boldsymbol{u}} \cdot \boldsymbol{b}\, \mathrm{d}V \\ &\int_{\partial\mathcal{I}_0} \dot{\overline{\boldsymbol{u}}} \cdot \overline{\boldsymbol{P}} \cdot \overline{\boldsymbol{N}}\, \mathrm{d}L + \int_{\mathcal{I}_0} \overline{\rho}_0 \dot{\overline{\boldsymbol{u}}} \cdot \overline{\boldsymbol{b}}\, \mathrm{d}A\,. \end{aligned} \tag{B.3}$$

The electric power in the system arises from changes in the free charge distribution as characterised by the electric displacement field $\boldsymbol{D}$ and external sources of electric energy such as batteries that provide or consume electrons resulting in a change in the electron charge density q_0^{el}:

$$\begin{aligned} \mathcal{P}^{\text{electrical}} = &- \int_{\partial\mathcal{B}_0} \Phi\, \dot{\boldsymbol{D}} \cdot \boldsymbol{N}\, \mathrm{d}A + \int_{\mathcal{B}_0} \Phi\, \dot{q}_0^{\text{el}}\, \mathrm{d}V \\ &- \int_{\partial\mathcal{I}_0} \overline{\Phi} \cdot \dot{\overline{\boldsymbol{D}}} \cdot \overline{\boldsymbol{N}}\, \mathrm{d}L + \int_{\mathcal{I}_0} \overline{\Phi}\, \dot{\overline{q}}_0^{\text{el}}\, \mathrm{d}A\,. \end{aligned} \tag{B.4}$$

Furthermore, the mass transport within the system contributes to the internal energy of the system as discussed in Section 3.3.1, yielding

$$\begin{aligned}\mathcal{P}^{\text{chemical}} = &- \sum_i \int_{\partial\mathcal{B}_0} \varphi^{\text{mix}^i}\, \boldsymbol{J}^i \cdot \boldsymbol{N}\, \mathrm{d}A + \sum_i \int_{\mathcal{B}_0} \varphi^{\text{mix}^i}\, W^i\, \mathrm{d}V \\ &- \sum_i \int_{\partial\mathcal{I}_0} \overline{\varphi}^{\text{mix}^i} \cdot \dot{\overline{\boldsymbol{J}}}^i \cdot \overline{\boldsymbol{N}}\, \mathrm{d}L + \sum_i \int_{\mathcal{I}_0} \overline{\varphi}^{\text{mix}^i}\, \overline{W}^i\, \mathrm{d}A\,,\end{aligned} \tag{B.5}$$

where φ_s^i and $\overline{\varphi}^{\text{mix}^i}$ denote the specific enthalpy of mixing of ions and polymer in the volume and on the interface, respectively.

Application of the divergence theorems Eq. (4.19a) and Eq. (4.19b) while keeping in mind the tangential nature of $\overline{\boldsymbol{P}}$ and $\overline{\boldsymbol{J}}^i$ as well as the assumptions of mechanical and electrical coherence stating that $\overline{\boldsymbol{u}} = \boldsymbol{u}|_{\mathcal{I}_0}$ and $\overline{\Phi} = \Phi|_{\mathcal{I}_0}$, compare Section 4.3, yields

$$\begin{aligned}\mathcal{P}^{\text{mechanical}} = &\int_{\mathcal{B}_0} \left[\dot{\boldsymbol{u}} \cdot \operatorname{Div} \boldsymbol{P} + \rho_0 \dot{\boldsymbol{u}} \cdot \boldsymbol{b} + \boldsymbol{P} : \operatorname{Grad} \dot{\boldsymbol{u}}\right] \mathrm{d}V \\ &+ \int_{\mathcal{I}_0} \left[\dot{\overline{\boldsymbol{u}}} \cdot [\![\boldsymbol{P}]\!] \cdot \overline{\boldsymbol{N}} + \dot{\overline{\boldsymbol{u}}} \cdot \overline{\operatorname{Div}}\, \dot{\overline{\boldsymbol{P}}} + \overline{\boldsymbol{P}} \cdot \overline{\operatorname{Grad}}\, \dot{\overline{\boldsymbol{u}}} + \overline{\rho}_0 \dot{\overline{\boldsymbol{u}}} \cdot \overline{\boldsymbol{b}}\right] \mathrm{d}A\end{aligned} \tag{B.6}$$

$$\begin{aligned}\mathcal{P}^{\text{electrical}} = &\int_{\mathcal{B}_0} \left[-\Phi \operatorname{Div} \dot{\boldsymbol{D}} - \Phi\, \dot{q}_0^{\text{el}} + \Phi\, \dot{\boldsymbol{D}} \cdot \operatorname{Grad} \Phi\right] \mathrm{d}V \\ &+ \int_{\mathcal{I}_0} \Big[-\overline{\Phi}\, [\![\dot{\overline{\boldsymbol{D}}}]\!] \cdot \overline{\boldsymbol{N}} - \overline{\Phi}\, \overline{\operatorname{Div}}\, \dot{\overline{\boldsymbol{D}}} + \overline{\Phi}\, \overline{\operatorname{Div}}\, \overline{\boldsymbol{N}} \left[\dot{\overline{\boldsymbol{D}}} \cdot \overline{\boldsymbol{N}}\right] \\ &\qquad - \dot{\overline{\boldsymbol{D}}} \cdot \overline{\operatorname{Grad}}\, \overline{\Phi} + \overline{\Phi}\, \dot{\overline{q}}_0^{\text{el}}\Big] \mathrm{d}A\end{aligned} \tag{B.7}$$

$$\begin{aligned}\mathcal{P}^{\text{electrical}} = &\sum_i \int_{\mathcal{B}_0} \left[-\varphi^{\text{mix}^i} \operatorname{Div} \boldsymbol{J}^i + \varphi^{\text{mix}^i}\, W^i - \boldsymbol{J}^i \cdot \operatorname{Grad} \varphi^{\text{mix}^i}\right] \mathrm{d}V \\ &+ \sum_i \int_{\mathcal{I}_0} \Big[-\varphi^{\text{mix}^i} [\![\boldsymbol{J}^i]\!] \cdot \overline{\boldsymbol{N}} - \overline{\varphi}^{\text{mix}^i} \overline{\operatorname{Div}}\, \overline{\boldsymbol{J}}^i - \overline{\boldsymbol{J}}^i \cdot \overline{\operatorname{Grad}}\, \overline{\varphi}^{\text{mix}^i} \\ &\qquad + \overline{\varphi}^{\text{mix}^i}\, W^i\Big] \mathrm{d}A\end{aligned} \tag{B.8}$$

The balances of linear momentum (Eq. (4.21) and Eq. (4.23)), Gauß's law (Eq. (4.27) and Eq. (4.28)) and the balances of the transported species mass (Eq. (4.31) and Eq. (4.32)) can be inserted into these expressions, as well as the relation $q_0^f = q_0^{\text{ion}} + q_0^{\text{el}} = F \sum_i z^i c_0^i + q_0^{\text{el}}$. Finally, application of the divergence theorems and localisation of the balance law yield

$$\rho_0 \dot{\varepsilon} = \boldsymbol{P} : \dot{\boldsymbol{F}} - \dot{\boldsymbol{D}} \cdot \operatorname{Grad} \Phi - \sum_i \left[\Phi F z^i \dot{c}_0^i - \varphi^{\text{mix}^i} \dot{c}_0^i + \boldsymbol{J}^i \cdot \operatorname{Grad} \varphi^{\text{mix}^i}\right] \qquad \text{in } \mathcal{B}_0 \tag{B.9}$$

$$\begin{aligned}\overline{\rho}_0 \dot{\overline{\varepsilon}} = &\overline{\boldsymbol{P}} : \dot{\overline{\boldsymbol{F}}} - \overline{\Phi} F \sum_i z^i \dot{c}_0^i - \dot{\overline{\boldsymbol{D}}} \cdot \overline{\operatorname{Grad}}\, \overline{\Phi} \\ &+ \sum_i \left[\overline{\varphi}^{\text{mix}^i} \dot{\overline{c}}_0^i - \overline{\boldsymbol{J}}^i \cdot \overline{\operatorname{Grad}}\, \overline{\varphi}^{\text{mix}^i} - \left[\varphi^{\text{mix}^i} - \overline{\varphi}^{\text{mix}^i}\right] [\![\boldsymbol{J}^i]\!] \cdot \overline{\boldsymbol{N}}\right]\end{aligned} \qquad \text{on } \mathcal{I}_0\,. \tag{B.10}$$

B.2 Balance of entropy

Ion transport is associated with mixing of ions and polymer. Hence, the transport induces changes of the system's entropy. This is, as discussed before in Section 3.3.1, described using the specific entropy contributions η^{mix^i} in the volume and $\overline{\eta}^{\text{mix}^i}$ on the interface. Thus, the

balance of entropy for the isothermal case is

$$\begin{aligned}\frac{\mathrm{D}}{\mathrm{D}t}\left[\int_{\mathcal{B}_0}\rho_0\eta\,\mathrm{d}V+\int_{\mathcal{I}_0}\overline{\rho}_0\overline{\eta}\,\mathrm{d}A\right]=&-\sum_i\int_{\partial\mathcal{B}_0}\eta^{\mathrm{mix}^i}\,\boldsymbol{J}^i\cdot\boldsymbol{N}\,\mathrm{d}A+\sum_i\int_{\mathcal{B}_0}\eta^{\mathrm{mix}^i}\,W^i\,\mathrm{d}V\\&-\sum_i\int_{\partial\mathcal{I}_0}\overline{\eta}^{\mathrm{mix}^i}\,\overline{\boldsymbol{J}}^i\cdot\boldsymbol{N}\,\mathrm{d}L+\sum_i\int_{\mathcal{I}_0}\overline{\eta}^{\mathrm{mix}^i}\,\overline{W^i}\,\mathrm{d}A\\&+\int_{\mathcal{B}_0}\Gamma_0\,\mathrm{d}V+\int_{\mathcal{I}_0}\overline{\Gamma}_0\,\mathrm{d}A\,.\end{aligned}\tag{B.11}$$

Here, Γ_0 and $\overline{\Gamma}_0$ denote the entropy production rates in the bulk and on the interface, respectively. Both entropy production terms are non-negative, thus, ensuring that the second law of thermodynamics is obeyed in both domains as well as in the whole system, cf. also [74].

Localisation and application of the divergence theorems for the bulk and the interface give

$$\rho_0\dot{\eta}=\sum_i\left[\eta^{\mathrm{mix}^i}-\boldsymbol{J}^i\cdot\mathrm{Grad}\,\eta^{\mathrm{mix}^i}\right]+\Gamma_0\qquad\text{in }\mathcal{B}_0\,,\tag{B.12}$$

$$\overline{\rho}_0\dot{\overline{\eta}}=\sum_i\left[\overline{\eta}^{\mathrm{mix}^i}-\overline{\boldsymbol{J}}^i\cdot\overline{\mathrm{Grad}}\,\overline{\eta}^{\mathrm{mix}^i}\right]+\overline{\Gamma}_0\qquad\text{on }\mathcal{I}_0\,.\tag{B.13}$$

The Helmholtz free energy on the interface is of the form $\overline{\psi}=\overline{\varepsilon}-\overline{T}\,\overline{\eta}$, where $\overline{T}$ denotes the absolute temperature on the interface which is, in the considered isothermal case, identical to the temperature T in the body. Using this expression and it's analogous counterpart $\psi=\eta-T\,\eta$ in the bulk, compare Section 3.3.1, the entropy balance equations (B.12) and (B.13) can be rearranged to

$$\begin{aligned}&\boldsymbol{P}:\dot{\boldsymbol{F}}-\rho_0\dot{\psi}-\dot{\boldsymbol{D}}\cdot\mathrm{Grad}\,\Phi\\&\quad+\sum_i\left[\mu^{\mathrm{mix}^i}\dot{c}_0^i-\Phi F z^i\dot{c}_0^i-\boldsymbol{J}^i\cdot\mathrm{Grad}\,\mu^{\mathrm{mix}^i}\right]\geq 0\,,\qquad\text{in }\mathcal{B}_0\end{aligned}\tag{B.14}$$

$$\begin{aligned}&\overline{\boldsymbol{P}}:\dot{\overline{\boldsymbol{F}}}-\overline{\rho}_0\dot{\overline{\psi}}-\dot{\overline{\boldsymbol{D}}}\cdot\overline{\mathrm{Grad}}\,\overline{\Phi}+\sum_i\left[\overline{\mu}^{\mathrm{mix}^i}\dot{\overline{c}}_0^i-\overline{\Phi}F z^i\dot{\overline{c}}_0^i\right.\\&\quad\left.-\overline{\boldsymbol{J}}^i\cdot\overline{\mathrm{Grad}}\,\overline{\mu}^{\mathrm{mix}^i}-\left[\mu^{\mathrm{mix}^i}-\overline{\mu}^{\mathrm{mix}^i}\right]\llbracket\boldsymbol{J}^i\rrbracket\cdot\overline{\boldsymbol{N}}\right]\geq 0\end{aligned}\qquad\text{on }\mathcal{I}_0\,,\tag{B.15}$$

where μ^{mix^i} and $\overline{\mu}^{\mathrm{mix}^i}$ denote the chemical potential of ion species i in the polymer matrix.

The Helmholtz free energies in the bulk and on the interface are assumed to be functions $\psi(\boldsymbol{F},\boldsymbol{D},c_0^i)$ and $\overline{\psi}(\overline{\boldsymbol{F}},\overline{\boldsymbol{D}},\overline{c}_0^i)$ for $i=1,2...n$ denoting the different ion and salt species. Thus, examining Eq. (B.14) and Eq. (B.15) following the principle of Coleman-Noll yields the constitutive relations

$$\boldsymbol{P}=\rho_0\frac{\partial\psi}{\partial\boldsymbol{F}}=2\,\rho_0\boldsymbol{F}\frac{\partial\psi}{\partial\boldsymbol{C}}\,,\qquad\overline{\boldsymbol{P}}=\overline{\rho}_0\frac{\partial\overline{\psi}}{\partial\overline{\boldsymbol{F}}}=2\,\overline{\rho}_0\overline{\boldsymbol{F}}\frac{\partial\overline{\psi}}{\partial\overline{\boldsymbol{C}}}\,,$$

$$\boldsymbol{E}=-\mathrm{Grad}\,\Phi=\rho_0\frac{\partial\psi}{\partial\boldsymbol{D}}\,,\qquad\overline{\boldsymbol{E}}=-\overline{\mathrm{Grad}}\,\overline{\Phi}=\overline{\rho}_0\frac{\partial\overline{\psi}}{\partial\overline{\boldsymbol{D}}}\,,$$

$$\mu^{\mathrm{mix}^i}=Fz^i\Phi+\rho_0\frac{\partial\psi}{\partial c_0^i}\qquad\overline{\mu}^{\mathrm{mix}^i}=Fz^i\overline{\Phi}+\overline{\rho}_0\frac{\partial\overline{\psi}}{\partial\overline{c}_0^i}\,.$$

Furthermore, to satisfy the entropy inequalities the requirements

$$-\sum_i \boldsymbol{J}^i \cdot \operatorname{Grad} \mu^{\mathrm{mix}^i} \geq 0 \qquad \text{and} \qquad -\sum_i \left[\overline{\boldsymbol{J}}^i \cdot \overline{\operatorname{Grad}}\, \overline{\mu}^{\mathrm{mix}^i} + \left[\mu^{\mathrm{mix}^i} - \overline{\mu}^{\mathrm{mix}^i} \right] [\![\boldsymbol{J}^i]\!] \cdot \overline{\boldsymbol{N}} \right] \geq 0$$

must be met.

B.3 Constitutive relation for the ion flux

In the bulk, the requirement $-\sum_i \boldsymbol{J}^i \cdot \operatorname{Grad} \mu^{\mathrm{mix}^i} \geq 0$ has to be met to not violate the entropy inequality. The simplest, however, not the only, way to ensure this is to introduce a constitutive formulation for the ion flux vector that is proportional to the negative gradient of the chemical potential, that is,

$$\boldsymbol{J}^i = -\boldsymbol{M}^i(\boldsymbol{C}, \boldsymbol{D}, c_0^i) \cdot \operatorname{Grad} \mu^{\mathrm{mix}^i} . \tag{B.16}$$

With the chemical potential of mixing used in Section 4.4, i.e., Eq. (4.45):

$$\mu^{\mathrm{mix}^i} = \Phi F z + \frac{\partial \rho_0 \psi}{\partial c_0^i} = F z^i [\Phi + k^i \ln J] + RT \ln \left(\frac{c_0^i}{c_0^{i\ \mathrm{initial}}} \right) , \tag{B.17}$$

this yields

$$\boldsymbol{J}^i = -\boldsymbol{D}(c_0^i) \left[\operatorname{Grad} c_0^i + \frac{F}{RT} c_0^i \operatorname{Grad} \Phi + \frac{F}{RT} k^i \frac{c_0^i}{J} \operatorname{Grad} J \right] , \tag{B.18}$$

with $\boldsymbol{D}(c_0^i) = {}^{RT}/_{c_0^i} \boldsymbol{M}^i$.

This expression is up to the last right-hand-side term identical to the convection-free Nernst-Planck equation as presented in Section 4.2.2. The additional term introduces a dependence of the flux on the deformation state, that is neglected in this work in favour of following the classical approach. Generally, it is possible to numerical check whether the requirement Eq. (B.16) is met during calculation, compare Appendix A.2.

Lebenslauf

Name	Wilmers
Vorname	Jana
Geburtsdatum	15.11.1988
Geburtsort, -land	Bochum, Germany

08.1995 - 06.1999	Gemeinschaftsgrundschule Buschhoven
08.1999 - 07.2007	St. Josef Gymnasium in Rheinbach
10.2007 - 09.2010	Studium B.Sc. Chemie mit Materialwissenschaft Hochschule Bonn-Rhein-Sieg
10.2010 - 09.2012	Studium M.Sc. Materialwissenschaft Universität des Saarlandes
12.2012 - heute	Wissenschaftlicher Mitarbeiter Helmholtz-Zentrum Geesthacht